AN UNMANNED AERIAL SYSTEMS EVALUATION CHAMBER FOR BRIDGE INSPECTION

by

José Vicente Capa Salinas

A Thesis

Submitted to the Faculty of Purdue University

In Partial Fulfillment of the Requirements for the degree of

Master of Science in Civil Engineering

Lyles School of Civil Engineering

West Lafayette, Indiana

August 2021

THE PURDUE UNIVERSITY GRADUATE SCHOOL
STATEMENT OF COMMITTEE APPROVAL

Dr. Robert Connor, Chair
Lyles School of Civil Engineering

Dr. Mark Bowman
Lyles School of Civil Engineering

Dr. Ayman Habib
Lyles School of Civil Engineering

Approved by:
Dr. Dulcy Abraham

To my little sister Nataly, who inspires me to work harder and always manages to put a smile on my face, and to my mom and dad, Aura and Marcelo, for always being there for me, for loving me unconditionally and for working hard to provide us with what we needed.

ACKNOWLEDGMENTS

I would like to start thanking my advisor and friend, Dr. Robert Connor, for his continued support during the development of this research project, and for always going above and beyond with his advice and help whenever I needed him the most. He always provided me a new approach, a new idea or encouraged me to work harder and smarter in the ideas that I presented to him. But also, for his academic, research, and personal guidance during my life in graduate school.

My second acknowledgment goes to my committee members: Dr. Mark Bowman, for always having time to meet with me to discuss my progress and for providing great ideas to improve my ideas, and Dr. Ayman Habib, for his guidance and support during our group meetings, but also for always being available whenever I needed a camera, a drone, or a plotter printer.

Thanks to my friend Thomas Bradt, M.S.E., for helping me torching, cutting, moving elements for the testing chamber, but also for teaching me with patience and technique how to use the tools at Bowen Laboratory and S-BRITE. Thanks to Dr. Kinsey Skillen, from Texas A&M University, for his help and guidance during his time at Purdue, but also for his advice and support during this research. And thanks to all my friends and colleagues at Bowen Laboratory.

I would also like to thank Dr. John Mott, for providing his direction and criteria from the aviation side of the project, but also for the drone and pilots that made possible the trials and tests. Thanks to: Jack Green, M.S., for the countless hours of indoor and outdoor flights, and to Kristoffer Borgen, M.S., for his braveness to test this project since his first day and his valuable feedback.

This research was funded as a Transportation Pooled Fund Program with Lead Agency the Indiana Department of Transportation, and the Department of Transportation of California, Delaware, Georgia, Illinois, Michigan, Minnesota, Pennsylvania, Utah, and Virginia.

And thanks to the Fulbright Program and the Department of State of the United States, for making this entire journey possible.

TABLE OF CONTENTS

LIST OF TABLES

LIST OF FIGURES

ABSTRACT

Civil engineering structures must provide an adequate and safe performance during their time of service, and the owners of these structures must have a reliable inspection strategy to ensure time-dependent damage does not become excessive. Visual inspection is the first step in every structural inspection; however, many elements in the majority of structures are difficult to access and require specialized personal and equipment. In an attempt to reduce the risk of the inspector and the cost of additional equipment, the use of Unmanned Aircraft Systems (UAS) has been increasing in the last years. The absence of standards and regulations regarding the use of UAS in inspection of structures has allowed the market to widely advertise Unmanned Aerial Vehicles (UAV) without protocols or qualifications that prove their effectiveness, leaving the owners of the structures to solely rely on claims of the vendors before deciding which technology suits their particular inspection needs. Focusing primarily on bridge inspection, this research aimed to address the lack of performance-based evaluation and standards for UAS, developing a validation criterion to evaluate a given UAS based on a repeatable test that resembles typical conditions in a structure.

Current applications of UAS in inspection of structures along with its advantages and limitations were studied to determine the current status of UAS technologies. A maximum typical rotor-tip-to-rotor-tip distance of an UAV was determined based on typical UAVs used in bridge inspection, and two main parameters were found to be relevant when flying close to structures: proximity effects in the UAV and availability of visual line of sight. Distances where proximity effects are relevant were determined based on several field inspections and flights close to structures. In addition, the use of supplementary technologies such as Global Positioning System (GPS) and Inertial Measurement Units (IMU) was studied to understand their effect during inspection.

Following the analysis, the author introduces the idea of a series of obstacles and elements inside an enclosed space that resemble components of bridge structures to be inspected using UAVs, allowing repeatability of the test by controlling outside parameters such as lighting condition, wind, precipitation, temperature, and GPS signal. Using distances based on proximity effects, maximum typical rotor-tip-to-rotor-tip distance, and a gallery of bridges and situations when flying close to bridge structures, a final arrangement of elements is presented as the evaluation chamber.

Components inside the evaluation chamber include both “real” steel and concrete specimens as well as those intended to simulate various geometric configurations on which other features are mounted. Pictures of damages of steel and concrete elements have been placed in the internal faces of the obstacles that can be assessed either in real-time flight or in post-processing work. A detailed comparison between the objectives of this research project and the results obtained by the evaluation chamber was performed using visual evaluation and resolution charts for the images obtained, the availability of visual line of sight during the test, and the absence of GPS signal.

From the comparison and analysis conducted and based on satisfactory flight results as images obtained during flights, the evaluation chamber is concluded to be a repeatable and reliable tool to apply to any UAS prior to inspect bridges and other structures, and the author recommends to refrain from conducting an inspection if the UAS does not comply with the minimum requirements presented in this research work. Additionally, this research provided a clearer understanding of the general phenomenon presented when UAVs approach structures and attempts to fill the gap of knowledge regarding minimum requirements and criterion for the use of UAS technologies in inspection of structures.

1. INTRODUCTION

1.1 Non-destructive Testing in Structures

Civil engineering structures must provide adequate and safe performance during their time of service. Even though the designer will consider parameters and factors to help ensure a specific period of life of the structure, they may also provide guidance regarding the necessary maintenance during this time. Having a reliable inspection strategy will also assist the owner in ensuring time-dependent damage does not become excessive. Further, inspections will also avoid possible failure, collapses or loss of the investment.

Inspection of the structure should be performed in a consistent way that is tailored to the use of the structure, its age, and to identify damage due to unforeseen events that the structure could have experienced: collision, earthquakes, floods, inclement weather, and so on. Ideally, the inspection methods should not interfere with its performance, or if possible, with the service that the structure is providing to the community.

The primary method of non-destructive testing utilized in the inspection of highway bridges is "visual inspection" (VT). Other forms of non-destructive testing are also used regularly, such as magnetic particle testing (MT), dye penetrant testing (DP), ultrasonic testing (UT), ground penetrating radar (GPF), etc. Generally, these more advanced methods are used following a visual inspection to confirm a finding or simply to enhance the overall inspection. In order to choose an appropriate NDT method, five performance measures should be considered: accuracy, precision/repeatability, speed, ease of use, and cost (Gucunski et al., 2013).

1.1.1 Visual Inspection

As stated, visual inspection is the first step in every inspection of a structure. Obviously, since visual inspection is the first step in any inspection process used in highway bridges, the reliability of collected data is critical. It does not require the purchase of any additional equipment with the exception of simple tools such as a flashlight or magnifying glass, etc. (Cawley, 2001). However, visual inspection does require a combination of experience, skills, and sensorial activity. In visual

inspection, the inspector will approach the structure and will gather information to make an assessment and provide recommendations using previous knowledge, past experiences, or current references. Not all defects require immediate action, but detailed documentation of the findings will help ensure additional examination in future inspections.

Visual inspection, like any form of inspection, also requires that the inspector has a reasonable understanding of the damage modes associated with the material, component and structure type (Tenžera et al., 2012). The inspector must discriminate between the levels of damage in the structure to determine the need of a detailed assessment in specific areas. Often, further analysis is required, using other non-destructive tests or a more aggressive measure with destructive testing.

In some cases, the inspector will be able to access the structure to perform a sufficiently detailed inspection. While some inspection may be done from the ground, others require close access, either by choice or when required such as for "fracture critical members" (American Association of State Highway and Transportation Officials, 2019). Unfortunately, for the majority of structures, many of the details are difficult to access and require the use of specialized personal and equipment such as industrial climbers, snooper trucks or large under-bridge units (Hallermann & Morgenthal, 2013). For complex and large structures, the addition of the specialized equipment undoubtedly increases the cost of the inspection and imply a greater risk for both the public and inspector.

In an attempt to reduce the need to physically place the inspector at the location of interest, the use of Unmanned Aircraft System applications to bridge inspection have been increasing in the last years. In fact, authors such as Keshmiri et al. (2018) state that the growing applications of Unmanned Aircraft Systems will force the U.S. to adapt a "hybrid national airspace (manned and unmanned)" as the use of such devices increases.

1.2 Unmanned Aircraft Systems

An Unmanned Aircraft System (UAS) is a system capable of flying under the control of an operator who is not present in the vehicle itself. In the context of this study, UAS typically include a payload of a high resolution digital camera and/or additional sensors (M. N. Gillins et al., 2016). It is important to recognize that the term UAS does not only describe the vehicle or platform used to

collect data. In fact, an Unmanned Aircraft System involves the vehicle, the sensors (e.g., GPS, camera), the person performing the flight operations: the pilot, and any additional features to collect information or improve the assessment. The vehicle and the pilot will be briefly discussed in the next paragraphs to discuss their role in inspection of structures, and additional details are presented in Chapter 2.

1.2.1 Unmanned Aerial Vehicles

UAVs, commonly referred as drones, are aircrafts remotely controlled by a computer, a navigator on the ground or a combination of both, and do not require a pilot to be physically present on the UAV when flying (Hallermann & Morgenthal, 2014). A simple UAV would be able to take off, fly, and land. While flying, the UAV can also take pictures, deliver materials, carry elements, or in general, perform activities flying in high elevations and locations that may be difficult or dangerous for a human being. UAVs come in different sizes, weights, heights, and functionalities, adapted to what the owner requires, and they all need to be taken into account when performing UAS inspections. Today, UAVs with considerable capability of a wide variety are readily available in the marketplace and have become quite affordable as compared to just five to ten years ago.

1.2.2 Pilots of UAVs

The pilot is the human element in the system, controlling the UAV to fly and perform different tasks during takeoff, landing, and throughout the mission (i.e., inspection). In modern applications, the pilot can preplan a route in advance, so the UAV performs the desired activities with autonomy (Kwak & Sung, 2018). In both cases the pilot must monitor the UAV at all times, to react and maneuver avoiding crashes (Kopyt & Żugaj, 2020), implying that a pilot must meet certain criteria or minimum qualifications to fly an UAV during inspection. To have a better understanding on what the minimum qualifications might look like, the next section presents a brief description of the challenges encountered while performing UAS inspection. Further details are explored in Chapter 2.

1.2.3 UAS Applications in Visual Inspection

For visual inspection, the inspector relies on their senses, mainly vision, to perform the assessment of the structure. However, with current technology, the inspector does not have to be up close to the element being inspected. An UAS may be used to gain access, albeit in a virtual sense, to provide the needed inspection data. The UAV becomes the 'eyes' of the inspector so to speak. While the approach may appear straight forward initially, there are obvious challenges in the actual implementation of conducting inspections with UAS, explored in the next paragraphs.

Elements in a structure are not always planar or easy to access. Hence, the UAS will have to be able to fly close to elements of different sizes, shapes, and forms. Failure to do so would negatively impact the inspection by providing incomplete visual information that could lead to incorrect conclusions of the real condition of the structure.

A second challenge is related to the ability to obtain high-quality images, whether still images or video. The camera resolution, focus, ability to rotate, and optical zoom would determine the level of detail that can be captured. Natural and artificial lighting conditions will also play an important role in the data quality. Sun light, shadows, and glare will reduce the quality of the pictures or hide defects that could be seen in different lighting conditions (Andert et al., 2010).

A short time of flight is the third challenge in the inspection with UAS. The battery life might not allow an inspector to collect information in one flight; therefore, the pilot must return the UAV to the original position and execute a change of battery. The battery life is also reduced when additional sensors or other devices are included in the UAV, increasing the duration time of the inspection (Galkin et al., 2019).

Finally, weather conditions also affect UAS inspection. The controller and UAV batteries are susceptible to considerable reduction of energy when exposed to high and low temperatures (when close to the limits provided by the manufacturer). High wind speed will also increase battery-power consumption life due to the additional maneuver of the UAV to perform a flight (Kundu & Matis, 2017).

Challenges above, as well as others presented in Chapter 2, obviously raise concerns regarding the use of UAS in inspection. Specifically, different UAS will have different capabilities resulting in different conclusions from a given inspection. To help ensure that inspection data obtained from UAS are consistent and meet some minimal level of quality, the author proposes that minimum standards must be developed for UAS compliance before a given UAS is used to perform inspection of structures. Further, such criteria should be implemented before UAS are utilized on a large scale for bridge inspection in the US.

While limited existing qualifications for the pilot, the inspector, and parts of the UAV exist, they are relative minimal and disjointed. These will be discussed in the following section and in detail in Chapter 2. In the next section, a general summary of what is currently provided in national standards is presented. Further, recommendations on what additional criteria or requirements should be implemented are also discussed.

1.3 Qualifications in Inspection of Structures

In the inspection of civil engineering structures, all the elements participating in the inspection comply with certain criteria regulated by Federal Agencies or National Standards. In the context of this section, the term "elements" is used loosely to refer to individuals performing the inspection, but also the structure itself. Some of these are explored in this section. However, as will be shown, qualifications for inspection using UAS are not complete, do not cover important challenges or they provide unclear guidance.

1.3.1 Qualifications of Bridge Inspectors

The Code of Federal Regulations, Title 23, Part 650, Subpart C, Section 650.309 (23 CFR 650.309) present minimum requirements that the bridge inspector have to comply before inspecting bridge structures (Federal Highway Administration et al., 2012). These requirements are described in the next paragraph and they show the qualifications an individual must possess before assessing any structure. As shown, they are clear in terms of what is needed and expected for an inspector.

The Program Manager must comply with:

- Be a registered Professional Engineer, or have ten years of bridge inspection engineering.
- Successfully complete a Federal Highway Administration approved comprehensive bridge inspection training course.

The team leader must comply with at least one of the following:

- Qualifications for the Program Manager.
- Five years of bridge inspection and successfully complete the FHWA-approved comprehensive training course.
- Level III or IV Bridge Safety Inspector under the National Certification in Engineering Technologies (NICET) and successfully complete the FHWA-approved comprehensive training course.
- Have:
    - A bachelor's degree from a college or university accredited by the Accreditation Board for Engineering and Technology.
    - Passed the National Council of Examiners for Engineering and Surveying Fundamentals of Engineering examination.
    - Two years of bridge inspection experience.
    - Successfully complete a Federal Highway Administration approved comprehensive bridge inspection training course.
- Have:
    - An associate's degree in engineering or engineering technology from a college or university accredited by the Accreditation Board for Engineering and Technology.
    - Four years of bridge inspection experience.
    - Successfully complete a Federal Highway Administration approved comprehensive bridge inspection training course.

1.3.2 Standard Methods to Collect and Report Data from Bridge Inspections

Once qualified, an inspector must follow guidelines regarding how the inspection data are reported, recorded, and how condition is defined. The AASHTO Manual for Bridge Inspection (American Association of State Highway and Transportation Officials, 2019) as well as other "state"

inspection manuals provide such guidance. Once collected, the data are reported to the Federal Highway Administration, following their guidelines and procedures (Federal Highway Administration, 2014). Additionally, FHWA has provided the Bridge Inspector's Reference Manual applicable with program, procedures, and techniques for inspecting and evaluating a variety of in-service highway bridges, culverts, fracture critical members, cable-stayed bridges, prestressed segmental bridges, among others, as another standard tool to collect and report data (Federal Highway Administration et al., 2012). In other words, after an inspector is deemed qualified for the job, there are a number of resources provided by federal agencies which govern in the inspection of structures.

The inspector may decide that additional in-depth testing is required to collect some specific bit of information. For example, an inspector may determine that magnetic particle testing of a weld is needed to confirm the presence of crack that may be suspected based on the visual inspection. A quick review of the literature shows that every destructive and non-destructive test method has a specification that must be followed to perform the test to ensure repeatability and consistency. For example, the Standard Test Method for Obtaining and Testing Drilled Cores and Sawed Beams of Concrete (ASTM, 2003) is used in the evaluation of concrete samples. The ACI Report on Nondestructive Test Methods for Evaluation of Concrete in Structures (American Concrete Institute, 2013) is also available in the case of non-destructive evaluation.

The above simply confirm that in addition to the qualifications for the individual performing the inspection, there are other requirements in place when performing the inspection, collecting the data, and recording the data.

1.3.3 Qualifications of an UAV Pilot

While not specific to bridge inspection applications, the FAA requires the pilot of any UAV to comply with four basic requirements (Federal Aviation Administration, 2020b):

- Must be 16 years old;
- Read, speak, write, and understand English;
- Physically and mentally able to fly the UAV; and
- Pass a knowledge text.

The successful completion of those requirements under FAA's Small UAS Rule (Part 107) allows a person to be a Certified Remote Pilot. When performing bridge inspections, the pilot and inspector are *not* always the same person. However it is becoming more and more common for a bridge inspector to become a pilot since complying with the FAA pilot requirements are minimal (Campbell, 2018). Nevertheless, it is important to note that the FAA has not provided certifications or minimum requirements specifically applicable to pilots flying UAVs for inspection of bridge structures.

1.3.4 Qualification of an UAS

While federal agencies have provided some regulations regarding UAS, none of them addresses important issues specific to performing inspection of bridge structures. For example, there are no requirements on battery life, UAS flight capabilities, quality of the images obtained, camera requirements to obtain images, environmental conditions under which inspections must be able to occur, etc.

The Federal Highway Administration has provided comprehensive regulations for bridge inspection such as inspector qualifications, how to process data, and how to report the information collected that is subsequently stored in the National Bridge Inventory. Surprisingly, while UAS inspections are occurring across the U.S., there remains no competency or performance testing requirements of a given UAS.

In fact, the author has been unable to find holistic U.S. regulations, standards, or tests for UAS used in the inspection of structures, surveying, mapping, aerial photography, and other engineering applications. In fact, minimum requirements that an UAV has to comply before aiding in the assessment of a structure are not provided by any Federal Agency or National Standard.

Meanwhile, because the current industry in the U.S. is not regulated, when inspections are conducted using these technologies, the owners must rely solely on the claims of the vendors of UASs before deciding which technology suits their inspection goals. In other words, the reported capabilities of a given UAS are advertised without protocols or qualifications that prove their effectiveness, while they continue to populate the market.

1.4 Research Objectives

Due to the lack of performance-based evaluation criteria and standards for the use of UAS in bridge inspection, it is the objective of this research to develop validation criterion for inspection of civil engineering structures using UAS. As will be discussed, the objectives will include the development of a mix of objective, subjective, and standard tests an UAS must satisfy. While the overall research program is developing criteria related to camera requirements, pilot requirements, etc., this document focuses on the development of what is referred to as the evaluation chamber. The overarching objective of the evaluation chamber is to provide performance-based test for the qualification of UAS for use in bridge inspections.

Specifically, the research objectives for this project are as follows:

- Develop a repeatable test that a given UAS must complete to qualify before inspecting civil engineering structures. The test must resemble typical conditions of inspection and accommodate most of the commonly available UAVs used for inspection of bridges.
- During the test, the inspector must locate and document defects inside an environment that resembles conventional inspection conditions in civil engineering structures.
- Establish an environment for the test based on challenges and constraints that exist in bridge inspections. For example:
    - inspection in a GPS-denied environment,
    - control of wind, temperature, and lighting conditions,
    - line of sight when flying over, near, and under civil engineering structures.
- Develop a preflight checklist that a given UAS must fulfill before the start of the mentioned test and in-service, during a real inspection.
- Assess UAS inspection capabilities using a test based on the identification of steel and concrete defects in high-quality visual data information inside an environment resembling typical inspection conditions when flying close to structures.

In the next chapter, a comprehensive literature review is performed addressing the main challenges and considerations behind the development of a test using the evaluation chamber for UAS applied to inspection of structures.

2. LITERATURE REVIEW

2.1 Inspection of Structures Using UAVs

Rotor-type UAVs are being introduced more and more for the inspection of structures because of their ability to collect information from locations that are not easily accessible to inspectors. They may also provide a less expensive inspection tool compared to what is traditionally used to allow the inspector to be closer to the structure such as trucks, platforms or scaffolding, and they provide a "better hovering performance than other flying robots" (Yamada et al., 2017). UAVs are becoming a fundamental part of civil and military applications such as: surveillance, localization of threats, delivery of weapons, forensic monitoring in real-time, mobile mapping, and so on (Mashaly et al., 2016). Focusing on civil engineering structures, a myriad applications are presented in the literature: bridge and building inspections (Hallermann & Morgenthal, 2012, 2012; Salaan et al., 2018; Sanchez-Cuevas et al., 2017; Yamada et al., 2017), tower inspections (Hallermann & Morgenthal, 2013), power line inspections (Zhang et al., 2017), inspection of industrial facilities (Nikolic et al., 2013), and so on.

UAV technologies applied to bridges have been widely used in trail applications as documented in the literature. The majority of these studies agree that flights in which images are taken at a short distance from the object can generate high quality photographs (Bridge & Ifju, 2018; Dorafshan et al., 2017a, 2018, 2017b; Duque, 2017; D. T. Gillins et al., 2018; M. N. Gillins et al., 2016; Hallermann & Morgenthal, 2014; Otero, 2015; Pereira & Pereira, 2015; Ramon-Soria et al., 2019; Salaan et al., 2018; Seo, Wacker, et al., 2018; Tomiczek, 2018; Yamada et al., 2017; Zink & Lovelace, 2015).

Bridge & Ifju (2018) prepared a detailed report containing images and dimensions of defects found on bridge structures using UAS inspection, and they provided a rating and cost comparison with conventional bridge inspection. The authors concluded that in general, good results can be obtained through an UAV inspection. However, the authors also emphasized the limitations in their use specifically focusing on payload, lighting, flight control, GPS denied areas, local coordinate system, high data storage capacity, among others.

Sattar Dorafshan et al. (2017a, 2018, 2017b) prepared a feasibility report on UAVs applied to bridge structures, focusing on two main aspects: visual inspection and autonomous defect detection. For visual inspection, they conducted UAS inspections on a bridge in service, on a fracture critical bridge, and on a laboratory-made bridge, detecting defects on images obtained in normal and low lighting conditions. The authors also identified fatigue cracks in thermal images, with accurate detection results but they emphasized the constraint associated with this type of inspection is the need of a thermal source. For the autonomous defect detection part, the authors developed an image processing algorithm which identified more than 80 percent of the "real" cracks.

D. T. Gillins et al. (2018) prepared a detailed report with six bridges and three tower inspections using UAVs to propose recommendations on safety and operational procedures when conducting UAS inspections. The cost-benefit analysis obtained by the authors using UAS determined an average cost saving of $10,000 per bridge inspection and a benefit cost ratio of 9. M. N. Gillins et al. (2016) conducted a bridge inspection producing a catalog of high-quality images of connections, bearings, joints, banks, and structural members, demonstrating the capability of UAS to capture images in difficult-to-reach areas of bridge structures. Hallermann & Morgenthal (2014) detected in their bridge inspection relatively small displacements of ± 2mm in the horizontal and vertical direction, and ± 10mm in the in-and-out direction. They also provided an example of image geo-referencing. Otero et al. (2015), and Pereira & Pereira (2015), applied UAVs with digital image processing. In their findings, clear images were obtained for each structure inspected, and they were able to determine, with a high level of accuracy, the locations of defects based only on the images collected, and comparing the results to the already known defect information for each structure.

Ramon-Soria et al. (2019) developed an algorithm that determines the best location to capture an image of a target, and takes the UAV to that location by 'drawing' the best path to follow. Their system uses interest points established by the inspector and executes the tasks autonomously. The authors tested this system in a bridge structure, reporting an adequate trajectory drawn by the algorithm, and the UAS produced high quality images.

Salaan et al. (2018) and Yamada et al. (2017) proposed a passive rotating spherical shell, and a cylindrical cage, respectively, to be applied in UAVs used in inspection of bridge structures. Their proposed cages protected the UAV, allowing it to approach the structural elements from a closer distance without the fear of impact. Further, the cage reduced the concerns due to outside disturbances during the inspection, such as wind which can result in the UAV impacting nearby objects. High-quality images were obtained in both cases from the elements inspected.

Seo et al. (2018) conducted a research identifying structural damage in timber bridge structures and compared the experience with traditional inspections. The authors determined satisfactory results in UAV inspection in terms of image quality, and damage identification and quantification in the images taken by the system. Based on their experience, an inspection protocol was proposed. Tomiczek (2018) applied UAS inspection in six galvanized high mast light-poles and eight bridges. They used image quality, cost, and data storage as evaluation parameters to conclude the feasibility of UAS inspection in bridge structures. They also provided best practices to follow during UAS inspections.

Zink & Lovelace (2015) presented a detailed report on advantages and challenges of using UAS for bridge inspection, by inspecting four bridges and testing data collected: images, video, and images from infrared cameras. Their analysis determined an adequate inspection with a level of detail compared to a close-up traditional picture. The authors also found a cost-effective application of UAVs in inspection of bridge structures and recommended to consider UAS inspection when hands-on inspection is not required. At the end, they suggest the addition of best practices and safety guidelines of UAS inspection in bridge and structures inspection manuals.

Other authors have also suggested that more advanced and useful applications are yet to come. Hallermann & Morgenthal (2012) provided an example of a potential application in the inspection of structures using UAVs. Currently, many owners are flying close to structures, obtaining pictures of the elements of the structure, analyzing them, and determining further steps to follow. Later, those images are stored with no clear objective to use them again in the future. However, Hallermann & Morgenthal (2012) suggest geo-referencing the images taken by the UAV with Global Positioning Systems (GPS), and storing them in a database with a separate space dedicated

for each structure. In the future, the database can be used for reference in future inspections, but also for: reconstruction of the structure in a 3D model, and research analysis with academic purposes such as teaching, development of software to identify defects, and so on.

Morgenthal & Hallermann (2014) also explored the idea of finding defects by using automatic crack detection with computer vision methods. They suggest the creation of a system capable of giving a probability of detecting defects by combining engineering expertise and software applications, leading to a quantified and rationalized quality assessment.

In order to achieve the applications mentioned before, future applications, and in general, applications more complex than capturing images, the UAS is often equipped with sensors such as GPS and Inertial Measurement Units. Sensors allow the UAS to provide an accurate location in any environment, preplanned flights, obstacle avoidance technologies, balance towards wind effects, and so on.

But the addition of new or added sensors can also bring new issues to the rotorcraft and they must be addressed along with the UAS. Hallermann & Morgenthal (2012) compile the most important challenges that an UAS with additional devices must overcome:

- Due to the limitations on the payload, only small format and light digital compact cameras can be used for photo or video documentation. In fact, Hallermann & Morgenthal (2014) specify a maximum weight of the digital compact camera of 650g.
- The limited payload allows only small battery packs, which causes a short flight time.
- Due to the low weight, the flight system is very sensitive to changes in the weather conditions, especially in critical wind situations.
- Unexpected flight situations or failures in the GPS-signal cause a change from the automatic flight mode into a manual mode, which requires a well-trained pilot to handle those critical situations.
- Currently, UAVs do not have an effective collision avoidance system.
- There is a restriction for flights beyond line of sight.

Payload, battery life, and weather conditions are addressed in Chapter 3, GPS issues are addressed in section 2.2.1, sensors are covered in section 2.2.2, restrictions on line of sight are presented in section 2.3, and existing avoidance systems are covered in section 2.5.

2.2 GPS and IMU in UAVs

As noted by Metni & Hamel (2007), most UAVs will include an Inertial Navigation Systems (INS) and a Global Positioning System (GPS). The camera will often be included with the UAV, but in some cases, it can be replaced with a different imaging system if the inspector needs to achieve different quality, resolution, or capability.

Each of these additional devices are going to be explored in the next sections, to understand their functionality and their impact during an UAS inspection.

2.2.1 Global Positioning System (GPS) and GPS-denied Environment in UAVs

During the 1970s through 1980s, the U.S. Government developed a satellite system that provides localization services to a receiver on Earth. The system was referred as the Global Navigation Satellite System (GNSS) and part of it is the Global Positioning System (GPS), which is a cloud of 31 satellites at a height of 20,000 km around our planet (Pratap & Per, 2006). The unique signal provided by the satellites can be acquired by a receiver installed in cellphones, automobiles, UAVs, etc. Based on this information, the receiver can be used to determine the location of the object. Further, the calculations permit determination of the error of the estimated location, and infer other flight information (Gowda et al., 2016). Other nations use other satellite systems besides GPS such as BeiDou Navigation Satellite System (BDS) in China, Galileo in Europe, GLONASS in Russia, Indian Regional Navigation Satellite System (IRNSS) / Navigation Indian Constellation (NavIC) in India, and Quasi-Zenith Satellite System (QZSS) in Japan (National Coordination Office for Space-Based Positioning, Navigation, and Timing, 2020). In this document, the term GPS is used to refer to the GNSS most prevalent in the US.

When flying in an open environment, UAVs rely on GPS information to provide an accurate location. However, as noted by Cheng et al. (2012), GPS does not work in an indoor environment.

Even in cases where the flight is outdoors, GPS signals will be blocked when the UAV flies underneath a structure. The pilot will need to compensate for situations when GPS is lost and flight control becomes manual to ensure control of the UAV is maintained.

2.2.2 Inertial Measurement Unit (IMU) in UAVs

The Inertial Measurement Units, IMUs, are devices that help the UAV with orientation and balance from its takeoff to its landing with respect to gravity and movement. Simple tasks like hovering would become difficult to execute without these technologies. Examples of IMUs are accelerometers, gyroscopes, magnetometers, and the familiar compass (Gowda et al., 2016). A more complex technology is an Inertial Navigation System (INS), which contains IMUs in combination with a computer and a platform to keep track of measurements performed by the system (Christ & Wernli, 2014).

Two main issues with IMUs used in UASs have been reported by several authors: drift of gyroscopes (Rai et al., 2012; Shen et al., 2013; Zhou et al., 2014), and interferences to magnetic compasses (Manweiler et al., 2012; Mariakakis et al., 2014; Wang et al., 2012) in smartphone applications. These problems have been identified in UAVs as well, resulting in issues during flights (Gowda et al., 2016). Clearly it is important to evaluate the performance of the UAS without the use of these technologies, relying only on the skills of the pilot.

When the pilot must compensate the absence of GPS and some IMUs, vision technologies take a leader role in the inspection, in order to navigate through the structure and capture enough visual information to assess defects along the structure. The vision field of the pilot is discussed in the next section.

2.3 Line-of-sight

In most flights, the pilot is directing the UAV to fly to certain points by sight. This form of flight is referred to as line-of-sight flight. When line of sight is not present, the mission relies in autonomous navigation capabilities that compensate for the lack of vision (Andert et al., 2010), as well as real-time visual information, i.e. live video sent to the pilot.

When flying underneath or along some structures, line-of-sight (LOS) might not be available, a scenario called flying with no-line-of-sight (NLOS) or beyond visual line-of-sight (BVLOS). A successful flight under NLOS or BVLOS conditions can be achieved with a combination of a camera installed in the vehicle, a receptor of real-time video such as a tablet or smartphone, and the skills of the pilot.

In one way or another, the UAS must be able to obtain visual information from the environment to obtain its relative position to the objects nearby (Andert et al., 2010). When inspecting structures, the UAS will encounter a wide range of objects, i.e., structural elements, the more common ones presented in the following section.

2.4 Typical Structural Elements in Infrastructures

According to the U.S. Department of Transportation, there are hundreds of unique bridge elements in the current bridge infrastructure. When inspecting them, the inspector should expect to find at least one of the following: decks, slabs, railings, girders, stringers, trusses, arches, floor beams, bearings, columns, piers, abutments, piles, pier caps, footings, culverts, deck joints, wearing surfaces, protective coatings, and approach slabs (U.S. Department of Transportation, 2019).

The abundance of shapes in bridge elements imply that the inspector will find more than circular and planar surfaces in a bridge. In a conventional inspection compared to an UAS inspection, the inspector is looking for details in the complex shapes of the structure while looking for safe ways to protect themselves during the inspection and guarantee a complete assessment. On the other hand, in an UAS inspection the inspector is not in the vehicle and even the inspector may not necessarily be the pilot. In such a case, the inspector is looking for defects while the pilot avoids constant collision with the elements under inspection and provides the needed access based on the direction of the inspector.

2.5 Proximity Effects

When using UAVs for inspection, there are significant challenges associated with flying close to the object being inspected. When the UAV gets close to an object, the UAV will become more challenging to control due to local turbulence or disturbances. The result of that disturbance is known as proximity effect (Powers et al., 2013) and it is imperative to understand its effect on the UAV because even a low-speed collision with an object can cause crash of the UAV (Scherer et al., 2007).

Powers et al. (2013) argues that these effects are intensified when conditions around the object turn turbulent, i.e. high wind speed caused by changes of air flow generated by the rotors and colliding with nearby irregular objects, due to the change of dynamic flow surrounding the UAV, increasing the risk of collision with nearby objects (Yamada et al., 2017). To determine an exact zone where proximity effects start, Powers et al. (2013), and other authors conducted experiments flying an UAV close to objects. Powers et al. (2013) concluded that proximity effects are negligible at a distance less than 20 cm (7.87 inches) from the ground and 15 cm (5.91 inches) from the ceiling. Other authors reported similar results (these data are considered later in this research). The data determined by Powers et al. (2013) is presented here to illustrate the case that even when the UAV has been designed for research purposes, like Powers et al. (2013) and Yamada et al. (2017), they reported excess of maneuvering during landing operations to avoid collision.

Authors have argued that technologies exist and others are under development to help ensure that an UAV is capable of avoiding obstacles autonomously (Andert et al., 2010; Chakravarthy & Ghose, 1998; Cheng et al., 2012; Keshmiri et al., 2018; Mashaly et al., 2016; Mon, 2013; Scherer et al., 2007; Watanabe et al., 2007). However, most of these technologies rely on GPS, cameras, and IMUs to navigate underneath objects, and these systems lose autonomy when the more complex the objects inspected are, still requiring a pilot to maneuver and make decisions. In fact, most of the time the pilot will have to deactivate such technologies to adequately conduct the inspection, becoming an important matter to explore proximity effects while flying near elements.

In the literature covered in previous paragraphs, authors have mentioned the effect of wind, gust wind, and changes of wind speed in inspection with UAVs (Powers et al., 2013; Yamada et al.,

2017). However, wind effects are not addressed in proximity effects because they act independently to the actions of the UAV. For future considerations, a separate test must be designed to isolate the performance of the UAV under wind changes.

When flying close to objects, two effects are widely recognized in the literature: ground effect and ceiling effect. A third was identified in this research and has been introduced as: surrounding effect. In the following sections, these three proximity effects are discussed in the context of why they are important to consider when flying close to structures.

2.5.1 Ground Effect

Ground effect is present in two cases: when hovering over a surface and in low speed flights (Cheeseman & Bennett, 1955; Hayden, 1976; Tanner et al., 2015). This can be easily perceived when landing the rotorcraft. Obviously, the pilot has to consider the presence of ground effects when flying over elements at low speed or while hovering.

Ground effect is dangerous to the vehicle and the pilot because it pushes the UAV away from the ground. As noted by Hooi et al. (2015), ground effect is a challenge for the pilot controlling the vehicle, even when landing at low speed or hovering above the ground where one would assume is easy to fly an UAV. These conditions presented by Hooi et al. (2015) are also seeing when the UAS is inspecting structures: the case when the UAV flies above structural elements resembles what happens when the UAV is hovering above the ground, but in this case the structural elements are irregular and several feet from the ground. Several authors studied ground effect to determine a zone where an UAV can safely fly close to structures (Hooi et al., 2015; W. Johnson, 2009; Powers et al., 2013; Tanner et al., 2015).

Hooi et al. (2015) modeled the flow-field of an UAV, normalizing the size of the ground effect zone in terms of the radius of the rotor of the UAV. They found that the pushing effect from the ground is relevant in distances closer to h=0.5R, where h is the rotor height relative to the ground and R is the rotor radius. The authors only explored the case where the UAV has one rotor and they also mentioned h=2R as the distance where ground effects will begin to have an influence on flight stability. The model applied by Hooi et al. (2015) differs from models by previous authors

mainly because Hooi et al. (2015) considered turbulence and potential flow theory, increasing the reliability in their work. This is an important consideration in the modeling of air flow because the model recognizes the presence of turbulence when flying UAVs, i.e. chaotic movement of air flow, and the application of potential flow theory that better captures the behavior of external flow around an object, according to the authors (Hooi et al., 2015).

Compiled by Johnson (2009), and later by Tanner et al. (2015), 19 experiments and models were developed to determine ground effect dimensions. They determined a value of 2.0 z/R will be the start of ground effect zone until 0.5 z/R where the effect will be strongly perceived. z is defined by the authors as the rotor hub height relative to the ground, the equivalent to h defined before, and R is the rotor radius, as previously defined. They also disagreed with prior investigations with different rotor diameters that used UAVs not applicable in bridge inspection, from small ones (1 foot to 5 feet) to large ones (37.5 feet to 46 feet), because they did not parameterize all the components that play into account when hovering. Further, they stated that the effect of the fuselage in a small UAV used in engineering applications, not only for inspection, is also an important parameter to consider in the definition of ground effect. In their research they addressed this issue, normalizing the model with respect to the height of the vehicle and the diameter of the rotor, showing the ground effect zone will start to present changes of velocity of the wind surrounding the UAV at 0.3 h/R, where h is the measurement vertical location when the location of the UAV in the vertical direction has been fixed (Tanner et al., 2015). The model that produced the value of 0.3 h/R takes into account the fuselage of the UAV, differing from 2.0 z/R to 0.5 z/R previously stated by Johnson (2009).

Powers et al. (2013) did not normalize their experiments. However, they detailed that the rotorcraft used had four fixed-pitch propellers with a diameter of 8 cm (3.15 inches), a distance between tips of the propellers of 21 cm (8.27 inches), and a weight of 76 grams. They observed that ground effect was present up to about 15 cm - 20 cm (5.91 inches - 7.87 inches). A table comparing the values provided by the authors mentioned in this section is presented in Chapter 3, and a quick analysis to these expressions provides an understanding that the addition of extra rotors increases the distance where ground effect starts to be perceived by the UAV.

2.5.2 Ceiling Effect

A less-known effect, ceiling effect, pulls the UAV towards the roof. Ceiling effect appears when the vehicle, and propellers, are close to a surface above an UAV. The result is the generation of an upward suction effect and increase of revolutions per minute (rpm) on the propellers (Sanchez-Cuevas et al., 2017). If the rotors hit the ceiling, the vehicle could lose balance, and crash. Similar to ground effect, several authors developed their own experiments to determine the influence zone of ceiling effect (Powers et al., 2013; Sanchez-Cuevas et al., 2017).

Powers et al. (2013) performed similar experiments for ground effect and ceiling effect using a research focused UAV with a propeller-tip-to-propeller-tip distance of 21 cm (8.27 inches) and 76 grams of weight. They concluded that ceiling effect has less influence on the vehicle compared to ground effect, determining a value of the approaching zone of about 15 cm (5.91 inches) measured from the ceiling to the rotors.

Sanchez-Cuevas et al. (2017) analyzed ceiling effect the same way other authors analyzed ground effect, with the goal to determine where this zone starts in terms of the diameter of the rotor (R). Their findings establish that this zone starts to show some signs of effect in the vehicle around 1.5-2 z/R and it fully affects the flight of the UAV around 0.5 z/R. In this case, z is the distance of the rotor to the surface, i.e., ceiling. In terms of increase of rpm, this zone seems to start from 1.5 z/R and show significant effect on the UAV at 0.5 z/R. The previous were obtained in an UAV with 1 rotor. They also performed the same analysis with a complete quadrotor (four rotors), concluding that “the increment in thrust due to the ceiling effect is larger for the complete multirotor, and it becomes more significant at a larger distance to the surface than for a single rotor” (Sanchez-Cuevas et al., 2017). In their findings, the zone starts at 2.5 z/R for multi-rotor UAV but the most significant effects are present between 1 z/R and 0.5 z/R.

2.5.3 Surrounding Effect

When flying, ceiling and ground effects are not the only concern. Field experiments have reported disturbance in the UAV when it flies close to objects although there is no elements above or below the UAV (Scherer et al., 2007). In the literature, surrounding effect is not explicitly recognized as

a proximity effect but it has been indirectly identified (Chakravarthy & Ghose, 1998; Lei et al., 2018).

Chakravarthy & Ghose (1998) recognizes two scenarios while flying close to objects: one where the environment is not known for the pilot and/or inspector, i.e. the pilot or inspector are not familiar with the area, the elements, or potential challenges; and another one where the environment is partially known for them, with incomplete or unknown information about the elements and its surroundings. In their research, they introduced the concept of collision cone to develop an obstacle avoidance automated system, providing a first idea of a delimiting zone around an UAV when flying close to structures.

Lei at al. (2018) reported high quality results from their crack detection methods applied for bridge inspection flying as close to elements as 40 cm (15.78 inches). In their research, it is not clear if they tested how close the UAV can approach the element but the distance provided is a starting point towards identifying a surround effect zone in which reasonable data can be collected in spite of being close to the object.

To address the lack of information in the literature, several experiments were performed and they are described in the methods section of this research work.

2.6 Bridge Element Inspection and the Use of UAVs

This section presents a review of current and past regulations, specifications and standards related to UAS inspections, specifically addressing what needs to be done in the field. The discussion will focus on how this research project addresses some of the gaps of UAS qualifications when applied to civil engineering inspections.

2.6.1 UAVs in the Inspection of Structures

The market of UAVs used for inspection is growing, in part due to decrease in costs of the UAV but also the increasing development of additional features in the UAVs, such as thermal scanners.

Further the potential benefit of UAS providing expensive inspection techniques is also attractive to owners (Mohan & Poobal, 2018).

Even though several authors have reported "successful" results with UAS inspection, some of which were discussed in section 2.1 of this thesis, Salaan et al. (2018) argues that a general procedure and minimum requirements have not been provided from a national perspective. Salaan argues such requirements are needed to ensure that an UAS inspection is at the same level as the traditional inspections of bridge structures. The next section details the existing standards and manuals available and applicable for UAS inspection and what is missing on them.

2.6.2 Standards and Manuals Available

A literature review was performed to determine the extent of tests, standards, manuals or minimum requirements that an UAS has to comply when inspecting structures.

From international references, Salaan et al. (2018) presented in their research the Next Generation Robots for Social Infrastructure (NGRSI) requirements implemented by the Japanese government for close visual bridge inspection robots. These include mandatory requirements such as:

- use of robots instead of human bridge inspectors,
- acquisition of data to evaluate the degree of damage,
- elimination of scaffolding for access, and
- provide safe and secure operation of UAS.

As optional, UAVs may (Salaan et al., 2018):

- access/inspect complex parts of the bridge,
- eliminate the use of ladder/inspection truck,
- demonstrate less sensitivity to external illumination,
- facilitate inspection of critical parts of the bridge, and in indoor works to document degree of damage,
- provide complete information to summarize inspection results,
- improve the efficiency or accuracy in characterization of damage,
- ease of transport and deployment,

- allow general use for a wide range of bridge types,
- include manufacturer information of clear and objective specifications of the system performance.

Some of the requirements are obvious and already considered in this research work, but the optional requirement of less sensitivity to external illumination is not considered applicable for inspection of bridges, due to the amount of exposure and sun light that the UAV might receive during inspection and the existence of camera technologies that already take into account the change of illumination. In addition, the scope of this research is to qualify the final result of the inspection and not the camera feature of adapting to external illumination.

In other countries, such as Netherlands, research has been conducted to write a manual considering "requirements and boundary conditions to fully explore the possibilities and create policy" (Jongerius, 2018) for the use of UAS in inspection of structures, but nothing specific has been provided in that area yet. However, in December 2020 the Dutch aviation authority ILT published the first predefined risk analysis (PDRA) providing requirements for implementation of self-flying drones and drone boxes for monitoring and inspection over controlled ground areas within a populated environment (Inspectie Leefomgeving en Transport (ILT), 2020).

No further guidance was found during the literature review that is directly applicable to UAS. Further, no testing requirements have been identified in which UAS performance is evaluated. But there are publications aiming to provide some guidance for Unmanned Aerial Vehicles when inspecting structures. The most relevant to this work are described in the next paragraphs.

Starting with 'Introduction to UAV Systems', where the authors present a complete review (*though nearly ten years old today*) from history of the vehicles, parts, performance, stability and recovery parameters, payloads, and planning of missions (Fahlstrom & Gleason, 2012). The Department of Transportation and the Federal Aviation Administration present a literature review covering technologies used in UAVs such as: detection, sense, and avoidance (Hottman et al., 2009). Albaker & Rahim (2010) presented a literature review of different approaches to implement collision avoidance in UAVs, addressing maneuvering techniques and design factors. In 'On

integrating unmanned aircraft systems into the national airspace system: issues, challenges, operational restrictions, certification, and recommendations', the authors address topics starting from the pilot to the vehicle of an UAS. In their book, certifications around the world are presented, parts of the vehicle, safety issues and regulations (Dalamagkidis et al., 2011). In some ways, these are also somewhat dated considering the developments in UAVs in the past decade.

However, the literature lacks of resources that provide parameters that an UAV has to comply in order to fly close to structural elements. There are references where obstacle-avoidance technologies are evaluated, but they usually refer to environments not common in civil engineering structures, as detailed in the next paragraphs.

Sebastian Scherer et al. (2007) conducted their experiments in a site arranged with boxes placed in random places with object dimensions greater than 5 m (16.40 feet). Andert et al. (2010) tested their obstacle avoidance technology in a series of gates with 6 m (19.68 feet) of width and height. One of the most common settings to test UAVs close to obstacles is the one used by Mashaly et al. (2016). Specifically, flying next to a building in an open environment where the main obstacles are vegetation nearby. While none of these studies focused on the shape of the obstacles, they all emphasize the need for some form of test that any UAS has to comply in order to be qualified when used near structures. Further, none of the studies explicitly focus on bridge structures to the best of the author knowledge.

Related to official guidance in the U.S., The American Society for Testing and Materials (ASTM) used to have available the 'Standard Specification for Design and Performance of an Airborne Sense-and-Avoid System' (F38 Committee, 2007), formerly under the jurisdiction of Committee F38, that used to cover requirements to support detection of airborne objects and its safe separation from elements surrounding them and other UAVs. However, it was withdrawn in 2014 because it was considered no longer relevant to the industry (ASTM International, n.d.). In addition, Committee F38 has created 25 active ASTM standards for topics related to UAS: assembly parameters of UAV, design parameters of UAVs, identification of operational hazards, among others, but none of them cover: beyond visual line-of-sight operations, performance of UAS, training, and most importantly: protocols and minimum requirements for UAS inspections.

ASTM Committee E54 has created 18 active standards for topics related to homeland security applications for protecting responders and the public in preparation or response to natural disasters, chemical, biological, radiological, nuclear, explosive detection and response, among others. These standards refer to emergency response robots and some of them include robots with flying capabilities and no human in the vehicle, i.e., UAS. Even though some of the standards developed by Committee E54 cover topics related to visual line-of-sight (E54 Committee, 2021a, 2021b) and visual acuity (E54 Committee, 2017), none of them address directly UAS or UAS inspections.

In regards to aviation side of the UAS, the Federal Aviation Administration (FAA) has not provided clear guidance to regulate UASs yet, however FAA stated that these systems have to comply with "see-and-avoid" provisions 91.113 (b) of Title 14 of the Code of Federal Regulations (CFR) (1989), and amended in 2004:

> "When weather conditions permit, regardless of whether an operation is conducted under instrument flight rules or visual flight rules, vigilance shall be maintained by each person operating an aircraft so as to see and avoid other aircraft. When a rule of this section gives another aircraft the right-of-way, the pilot shall give way to that aircraft and may not pass over, under, or ahead of it unless well clear."

In the 2017 version of the CFR, the provision remains as amended in 2004.

This provision is outdated, as noted by the U.S. Department of Transportation (2013), because "the absence of an onboard pilot means that the "see-and-avoid" provisions of 14 CFR part 91, § 91.113, cannot be satisfied". They go further, suggesting the need of an alternative method of compliance of this regulation. As a response to that comment, on June 21, 2016, the FAA added Part 107 to Title 14 of the Code of Federal Regulations (CFR) with 3 steps to follow for owners of small UAVs (less than 55 pounds) detailed below (Federal Aviation Administration, 2020c):

- read Part 107 rules with general guidance on how to fly an UAV,
- get certification to be a drone pilot following four steps provided in the regulation, and
- register the vehicle with the FAA.

But no direct solution was provided to the "see-and-avoid" provision cited before. In other words, even though Part 107 clears the path to use small UAVs following the 3 steps detailed above, part 91.113 (b) still requires the pilot to see the vehicle at all times. A FAA order of July 2020, clarifies

that any operation beyond visual line of sight, i.e., when neither the pilot nor the inspector can see or maintain sight of the UAS, requires a waiver submitted via email to FAA Headquarters. (Federal Aviation Administration, 2020a). Since the implementation of Part 107 in 2016 until the end of 2020 only 59 waivers were issued (Zoldi, 2020).

Much is still unclear under these regulations. No appropriate standard regarding bridge inspection using UAS have been provided by federal agencies or standards organizations. Topics such as how to handle GPS-denied environments, beyond line-of-sight operations that do not require a waiver, obstacle avoidance, proximity effects and lighting conditions have not been covered in the existing provisions.

3. METHODS

In this chapter, the development of the performance test for UAS is presented. The test was developed with the objective that it could be easily replicated thereby facilitating use by various agencies independently. In other words, a universal and standardized test. The discussion pertaining the selection of the shapes, dimensions, and minimum requirements for the proposed evaluation chamber is presented. The basic geometry required to size the obstacles and general test space is presented in section 3.1. In section 3.2, the structural elements considered for the design of the shapes of the obstacles are presented, as well as general procedure to follow during the test.

3.1 Design Parameters for the Test

For the design of the evaluation chamber, two important constrains were identified when an UAV is flying close to elements. First, the horizontal dimension or overall size of the vehicle and second, the relative distance from the UAV to nearby objects. While the overall size may be an obvious factor that must be considered, the proximity to an object may not be. As the proximity between the UAV and the object decreases, the resulting turbulence that will be generated can become highly influential on the quality of the data collected. Both of these become critical in the process of establishing the overall dimension of the test area as well as the size of the UAVs that can be included in the evaluations.

In section 3.1.1, an overall size of UAV is identified based on common UAVs used in inspection of bridges. In section 3.1.2 and 3.1.3 maximum distances are determined that an UAV can safely fly in relation to objects, leading to a final design parameter in section 3.1.4.

3.1.1 Dimension of Copters in Commonly Used UAVs

Several UAVs have been used throughout the literature for inspection of bridges and other structures. After a review of UAVs commonly identified in the literature review, various configurations of the most common models were summarized as shown Table 1.

Table 1 Dimensions of UAVs utilized in the literature

Model	Greatest dimension	Length	Found to be used in bridge inspection	Reference
DJI Inspire 1	Diagonal length	581 mm (1.91 ft)	Yes	(Seo, Wacker, et al., 2018)
Voyager 3	Diagonal length	346 mm (1.14 ft)	Yes	
DJI Matrice 100	Wingspan	650 mm (2.13 ft)	Yes	
DJI Phantom 3 Pro	Diagonal length	350 mm (1.15 ft)	Yes	
DJI Phantom 4	Diagonal length	350 mm (1.15 ft)	Yes	
Yuneec Typhon H	Size	520 mm (1.71 ft)	Yes	
DJI S900 airframe	Frame Arm Length	358 mm (1.17 ft)	Yes	
Yuneec Typhon 4K	Dimension	420 mm (1.38 ft)	Yes	
Blade Chroma	Width	325 mm (1.07 ft)	Yes	
Autel Robotics X-Star Premium	Diagonal length	352 mm (1.15 ft)	Yes	
SenseFly eBee	Wingspan	960 mm (3.15 ft)	No	
SenseFly albris	Wingspan	800 mm (2.62 ft)	Yes	
Topcon Sirius Pro	Wingspan	1630 mm (5.35 ft)	No	
Personalized model	Diameter of the spherical shell	0.95 m (3.12 ft)	Yes	(Salaan et al., 2018)
Personalized model	Diagonal length	660 mm (2.17 ft)	Yes	(Hallermann & Morgenthal, 2014)
DJI Matrice 100	Wingspan	650 mm (2.13 ft)	Yes	(Seo, Duque, et al., 2018)
DJI S900 airframe	Frame Arm Length	358 mm (1.17 ft)	Yes	
DJI Phantom 3 Pro	Diagonal length	350 mm (1.15 ft)	Yes	
DJI Phantom 4	Diagonal length	350 mm (1.15 ft)	Yes	
DJI M600 Pro	Diagonal length	1133mm (3.72 ft)	No	(Lin et al., 2019)

Table 1 continued

Personalized model	Whole width	400 mm (1.31 ft)	Yes	(Yamada et al., 2017)
DJI 2312	Diameter	18.8 in (1.57 ft)	Yes	(Sanchez-Cuevas et al., 2017)
DJI 2312	Diameter	18.8 in (1.57 ft)	Yes	(Hooi et al., 2015)
DJI Matrice 100	Wingspan	650 mm (2.13 ft)	Yes	
DJI Phantom 4	Diagonal length	350 mm (1.15 ft)	Yes	

In Figure 1, the horizontal dimensions of UAVs have been grouped in increments of 0.5 feet obtained from column 3 of Table 1, to illustrate the number of UAVs used in civil engineering applications, such as bridges, towers, and buildings. The goal of Figure 1 is to show the reader that the majority of UAVs in civil engineering applications, in particular as used in bridge inspection, are less than 2.5 feet in diameter, as illustrated by the dotted green box surrounding the first 4 columns of the same figure.

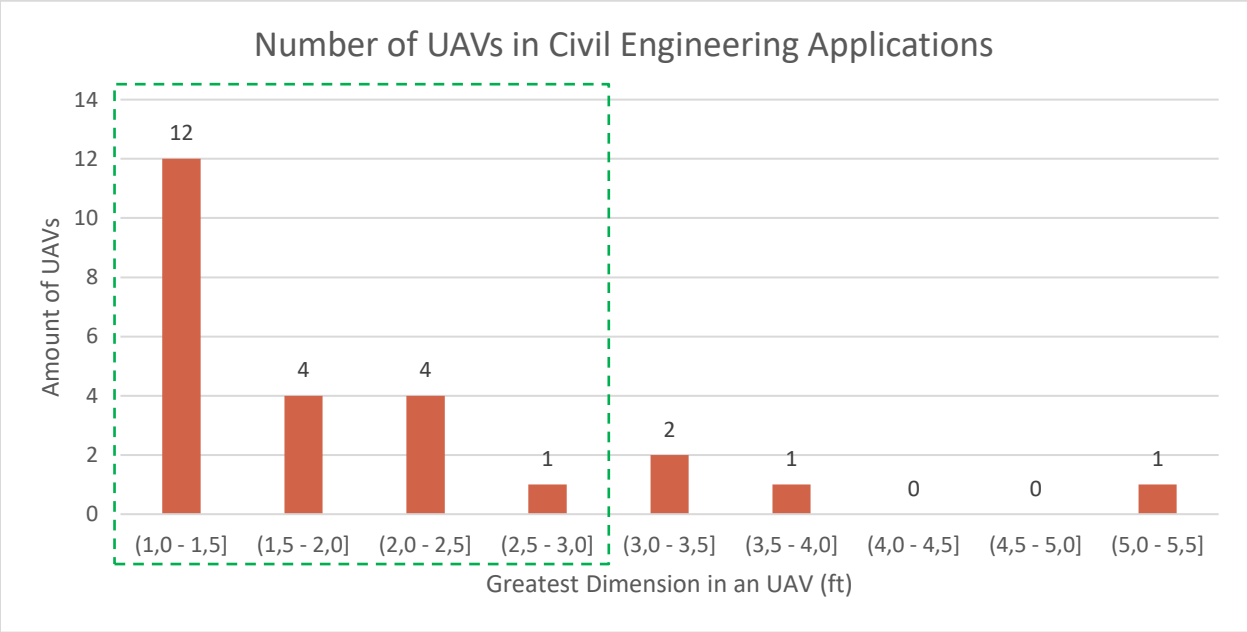

Figure 1 Representation of number of UAVs used in Civil Engineering Applications

As can be seen, there is considerable variation in the range of sizes of UAVs that have been used in civil engineering applications presented in the literature review. The larger models such as SenseFly eBee, SenseFly albris, Topcon Sirius Pro, and DJI M600 Pro are mainly used on large areas with low risk of collision with structures (Seo, Wacker, et al., 2018). In fact, of the larger UAV models, only the SenseFly albris have been reported to be used in bridge inspection, as presented in column 4 of Table 1. Based on the data presented, it can be seen that a majority (about 80%) of the systems used in bridge inspection are less than 3.0 feet out-to-out (see green dashed box). In fact, only one of the UAVs, the SenseFly albris is between 2.5 and 3.0 feet at 2.62 feet. If the larger UAVs are eliminated, it can be seen that selecting 2.5 feet as the representative size captures nearly all of the platforms used in bridge inspection today. Therefore, a value of **2.5 feet** is selected as the maximum typical dimension of an UAV to be used in the design of the evaluation chamber, forming a sphere around the UAV with the selected diameter. As shown, this value covers 20 models presented in Table 1 and a great range of UAVs used in inspection of bridge structures.

3.1.2 Surrounding Effect: Proximity Effects with Lateral Displacements

As mentioned in the literature review, while flying close to objects two effects have been widely recognized as influencing the overall performance of the inspection. The first actually includes two similar proximity effects. Specifically, what is commonly referred to as the "ground effects" and "ceiling effects". These are primarily related to the interaction of the wash or suction from the rotating propellers to horizontal planar *surfaces* above or below the UAV.

The second effect is related to the interaction between the wash from the rotating propellers and any nearby object that influences the effective thrust. While pilots are well aware of this effect, the influence and the importance of evaluating this proximity effect, or rather its influence on data quality have not been discussed in the literature as far as the author can find. The proximity effect will be referred to as the "surrounding effect" herein.

Surrounding effect, and the associated influence on inspection, was readily identified while trying to determine a safe distance around the aircraft between the farthest point of the UAV and a nearby object. In flights conducted in open environments, authors such as Erdos et. al (2013) have reported

no significant effect on the UAV when flying at speeds between 20 mph to 40 mph. However, when the author of the research project attempted to hover or fly at low speeds (<10 mph) within 18 inches of an object, local turbulence due to the surrounding effects and the irregularities of the objects was present resulting in erratic movement of the vehicle. Since the objects being inspected are highly variable in shape, the turbulence is also highly variable resulting in a very difficult and at times, unstable flight.

Clearly, if the area or overall geometry of the space where the test is conducted is such that proximity effects make it impossible to obtain quality data, the test is effectively invalid. Thus, the test space needed to be sized to accommodate the established physical size of the UAV (up to 2.5 feet) without also compromising the objectives and validity of the test due to proximity effects.

Unfortunately, manufactures do not report the dimension within which proximity effects will become excessive. In order to estimate the zone where surrounding effects are relevant and possibly excessive; tests were conducted to gain insight into when proximity may become a concern or influential parameter. Specifically, the approach below was followed:

1. Several flights were performed at different distances between planar and circular structures (doors, walls, steel plates with rivets and bolts) and the UAV;
2. The distance where the UAV position began to be influenced by the object without any action of the pilot or became difficult to control was recorded;
3. Based on 1 and 2, a minimum “safe” distance could be determined based on: the diameter of the UAV, and the proximity effects reported.

The process is discussed in further detail in the following sections.

3.1.3 Delimitation of Zones Around an UAV

As stated, there are objects that could alter the flight performance of an UAV such as the elements being inspected or a ceiling over the path of flight. One must also recognize that the skills of the pilot will influence the degree to which the effects produced by the action of flying close to elements affects the inspection. In other words, some pilots may need to be further from an obstruction to ensure a stable flight while others may be able to fly closer. It would be

advantageous to differentiate between the two scenarios and identify where the skills of the pilot end and the effect of the outside elements in the UAV begin when sizing the test space. However, since it is the UAS that is tested/qualified (i.e., pilot and platform), isolation of the two is not critical. While it was not possible to fully isolate these two parameters within the scope of this project, a comparison was made using a single pilot flying two UAVs to gain insight into the proper size of the test space, and a different pilot with another UAV to additionally flight along bridge structures.

In total, there were three UAVs used to identify safe zones (as defined above). Two UAVs commonly utilized in bridge inspection: DJI Phantom 3 Professional and a DJI Mavic 2 Pro using the same pilot, and a third model (ANAFI Thermal) using a different pilot. A summary of the UAV specifications is presented in Table 2, with additional information that will be referenced in future sections such as maximum flight time, operating temperature, and camera specifications.

Table 2 Specifications of UAVs used in this research.

Parameter	**DJI Phantom 3 Pro**	**DJI Mavic 2 Pro**	**ANAFI Thermal**
Reference	(DJI, 2015)	(DJI, 2018)	(Parrot, 2019)
Aircraft			
Takeoff weight	1280 g (2.82 lb.)	907 g (2.00 lb.)	315 g (0.69 lb.)
Diagonal distance*	350 mm (1 ft 1.78 in)	354 mm (1 ft 1.94 in)	360 mm (1 ft 2.17 in)
Max. flight time	~23 min	~31 min	~26 min
Operating temperature	0°C to 40°C (32°F to 104°F)	-10°C to 40°C (14°F to 104°F)	-10°C to 40°C (14°F to 104°F)
Camera			
Effective pixels	12.4 M	20 M	21 M (thermal camera 160x120)
Image size	4000x3000	4000x3000	5344x4016
Video recording mode	UHD, FHD, HD	4K, 2.7K, FHD	4K Cinema, 4K UHD, FHD, HD
Sensors			
GNSS	GPS + GLONASS	GPS + GLONASS	GPS + GLONASS
Other	Gimbal, IMU, compass	Gimbal, IMU, compass	Barometer and magnetometer, vertical camera, ultra-sound sensor, IMU, accelerometer, gyroscope

* Diagonal distance concept is later introduced and explained.

Based on observations in more than 30 flights performed for this research, three zones were determined and delimited around a common UAV. They are illustrated in Figure 2 and described below.

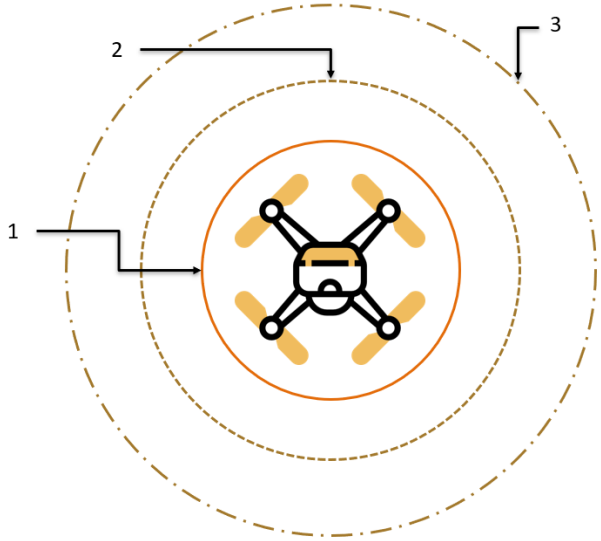

Figure 2 Zones delimited around an UAV.

Zone 1

Zone 1 is delimited by a circumference formed by either the tips of the propellers, the rotor, the spherical shell or the element in the UAV that is located at the farthest from the center of the vehicle in the horizontal plane. The center of the circumference of Zone 1 effectively matches the center of the UAV. In most cases this measurement can be easily found by pointing two opposite propellers towards each other and drawing a circumference with center in the center of the UAV, as presented in Figure 3. For some UAVs, this could vary based on extra features added to the vehicle, such as a protection cage or propeller guards. In the absence of a protective cage around the UAV, Zone 1 is the zone in which collision with the UAV will result in the pilot almost certainly losing control of the vehicle since the rotor blades will inevitably be damaged or destroyed. This obviously represents a risk to the pilot or other elements in the nearby environment. This value is given for all the UAVs described in Table 2 as diagonal distance.

Figure 3 Process to measure Zone 1 around an UAV.

The space beyond Zone 1 has been divided in two parts: Zone 2, and Zone 3 as shown in Figure 2.

Zone 2

Zone 2 describes the area where proximity effects will first begin to influence the stability and balance of the UAV. This means that the pilot must take extra precautions in order to avoid collision with nearby objects and/or ensure a stable flight. The effects that the UAV experiences inside Zone 2 cannot be compensated by the training or experience of the pilot because they are dominated by proximity effects, and the pilot must avoid interacting with objects entering Zone 2. In other words, the UAV cannot be fully controlled to ensure a safe/stable flight. Hence, there may be impacts to the quality of the data collected.

Zone 3

Zone 3 is where proximity effects are first observed as the UAV approaches an object, but they can be overcome by a trained pilot and should not affect a flight or quality of data collection. Zone 3 begins where the proximity effects of Zone 2 ends. The exact boundary between Zone 2 and Zone 3 will vary from UAS to UAS as it is due to a combination of pilot skills and the UAV itself.

To summarize, a trained pilot will be able to maneuver safely without any issues when an object is within Zone 3, but the UAV will present stability or balancing issues when the same element is

within Zone 2, regardless of the skills of the pilot. Zone 2 becomes the more important between the two to consider because proximity effects will affect the UAV entering this zone. In the next section, the process followed to estimate the location of Zone 2 is presented, and for future reference the diameter of Zone 2 will be referred to as "clearance distance".

3.1.4 Clearance Distance

Clearance distance is delimited within the zone where proximity effects cannot be compensated by the skills of the pilot and affect the performance of the vehicle. This is defined as Zone 2 in section 3.1.3. It is the diameter of a circumference drawn with center matching the center of the UAV, and diameter drawn around Zone 2, as presented in Figure 2.

The clearance distance will be determined with an analysis of proximity effects and the dimensions of the UAV. It was determined in section 3.1.1 that a reasonable diameter of the rotorcraft 'D' can be assumed to be 2.5 feet (radius R = 1.25 feet). In this document, 'z' is defined as the height of the UAV. *(It is noted that in some other references 'z' is sometimes defined as 'h'*). Generally in bridge inspection and for the design of the proposed test, the height of the UAV does not govern the delimitation of the zones where proximity effects are relevant and can be neglected because manufacturers design small and medium UAVs with a height ('z' or 'h') less than the radius ('R') due to dynamic constraints: i.e., less payload, air flow distribution, and pressure distribution that allows a smooth operation of the UAV (Abdullah, 2020; Dempsey & Rasmussen, 2010). In the case that the UAV has a surrounding protective cage, the radius and the height will most likely be the same because most cages are spherical. As a consequence, to estimate general dimensions of UAVs, the height ('z' or 'h') and the radius ('R') of the UAV are assumed to be equal (z = h = R).

The diameter around the UAV where proximity effects are relevant to its performance are summarized in Table 3 based on findings from the literature review presented in Chapter 2 and adapted for values of D, R, and z = h = R from this research presented in the paragraph above. Column 1 of Table 3 describes the parameter obtained by the authors cited in Column 3, described in detail in Chapter 2. In their experiments, they determined a distance where proximity effects started to become relevant to the performance of the UAV, presented here because those parameters are important to determine a clearance distance around an UAV. Some authors

determined a fixed value for all UAVs (such as 6 inches) while others normalized their findings in a single expression in terms of the dimensions of any UAV (such as 0.3 h/R). Column 2 of Table 3 is the result of the normalized expression in Column 1 (when provided) for the dimensions of D, R, and z of this research. The answer corresponds to the distance where proximity effects are relevant to the performance of the given UAV according to each author. If an expression was not provided in Column 1 by the authors in the references cited, Column 2 includes a fixed value provided by those authors. A detailed analysis of how the parameters presented in Table 3 were obtained was described in Chapter 2. In the same chapter, a discussion is presented on different ways that authors take values of z and h, with the reasoning behind the conservative assumption of taking both parameters as equal for this research project.

Table 3 Proximity effects in an UAV

Parameter	Dimension	Reference
Ground effect		
Distance to the object	15 cm (6 inches)	(Powers et al., 2013)
h=0.5R	0.625 feet (7.5 inches)	(Hooi et al., 2015)
0.5 z/R	0.5 feet (6 inches)	(W. Johnson, 2009)
0.3 h/R	0.3 feet (3.6 inches)	(Tanner et al., 2015)
Running motion on floor	0.15 m (6 inches)	(Yamada et al., 2017)
Ceiling effect		
Distance to the object	15 cm (5.91 inches)	(Powers et al., 2013)
0.5 z/R	0.5 feet (6 inches)	(Sanchez-Cuevas et al., 2017)

Since the objective of this research is to develop a *standard* test, the largest distance where ground effects can be expected is required to ensure the test will not be biased toward UAVs where less distances are acceptable. Based on Table 3, an estimated distance of 7.5 inches is thus taken as the distance where ground effect will start to affect the UAV. Similarly, an estimated distance of 6 inches is taken as the distance where an UAV will start to be affected by ceiling effect, the greatest from Table 3 (ceiling effect) considered an upper bound.

To estimate the distance of the surrounding effects (which are not related to ceiling or ground effects), a series of tests were performed by running flight tests with the UAV close to planar and circular elements, as presented in Figure 4. In the three images, the UAV flew from bottom to top of the elements, varying the distance to those elements for each flight.

Figure 4 Testing surrounding effects.

The first flights were conducted in open environments where surrounding effects are not relevant due to the absence of objects close to the UAV but this situation was important to consider as a comparison point for future flights. The UAVs used in the flights described were DJI Phantom 3 Pro and a DJI Mavic 2 Pro. An example of these situations is presented in Figure 25.

The next flights were performed in open environments but with objects on one side: outside face of a warehouse, side face of a house, and side face of bridges from S-BRITE at Purdue University. The flights were repeated from distances at 10 feet and 5 feet. In neither of them surrounding effects were relevant to the performance of the UAV. An example of these situations is presented in Figure 17 and Figure 26.

For the next step, a series of flights were performed inside a shed at S-BRITE Center and inside a cargo container, specifically close to their internal face at distances of 1 foot and 2 feet. The flights were started at the desired distance, hover over the place where the UAV took off, and then flew from the bottom to the top of the face. Again, no relevant effect was observed in the UAV. The

flights were repeated in the same locations to a distance closer to the side faces of the shed and the container: 6 inches and 8 inches, and no significant event was observed in the UAV.

Finally, the same flights were performed to distances less than 6 inches. At this distance, the performance of the UAV began to be affected. Specifically, the UAV experienced "pull-out" and "pull-in" effects towards (or away) the side walls of the shed and the container. As expected, the effect was increased when the UAV took off or when flying closer to the roof. In order to isolate those effects from surrounding effect, several distances were evaluated only at the medium height of the walls. The distances recorded from the flights to test proximity effects were between 3 inches to 5 inches: 5 inches the distance where the effects started to affect the UAV, as presented in Figure 5; and 3 inches as the maximum approaching distance without compromising the integrity of the UAV, as presented in Figure 6.

Figure 5 Distance where UAV performance will start to be affected by surrounding effect: 5 inches.

Figure 6 Delimitation of the end of Zone 2 around UAVs performed inside a shed and a cargo container at S-BRITE.

As a result, the clearance distance obtained in the three directions is added to the diameter of 2.5 feet (2 feet 6 inches or 30 inches) of the sphere around the assumed UAV in section 3.1.1 to account for proximity effects, obtaining the following possibilities of increase in Zone 1, giving as a result Zone 2:

- In the horizontal direction, the UAV diameter of the sphere around the assumed UAV increases 5 inches (the greatest for surrounding effects) in each direction, giving a safe diameter of 3 feet 4 inches (30 inches + 5 inches + 5 inches = 40 inches).
- Ground effects below the UAV begin at 7.5 inches (the greatest for ground effect in Table 3) from the lowest point on the UAV. Considering the key scenario where the UAV has a Zone 1 with equal diameter on all sides of the sphere, the 7.5 inches will already be included on the diameter of 2.5 feet (30 inches) because the sphere around the UAV has a value under 1.25 feet (15 inches) in radius (7.5 inches < 15 inches). Evidence of this assertion was observed every time the UAV landed, maintaining balance and stability at all times.
- Ceiling effects will begin 6 inches from the highest point. Similar to the case mentioned before, 6 inches will already be included in the diameter of 2.5 feet and radius of 1.25 feet (7.5 inches < 15 inches). However, authors (Sanchez-Cuevas et al., 2017; Tanner et al., 2015) agree that ceiling effect cannot be underestimated because the propellers are located at the top of the UAV where they are in direct contact with roof surface and there is a greater possibility of fatal contact with ceilings rather than ground. Thus, in contrast to

ground effect, ceiling effect will be conservatively considered to increase the diameter of 2 feet 6 inches, to 3 feet 6 inches (2 feet 6 inches + 6 inches + 6 inches) conservatively in both directions (top and bottom) and to maintain the regularity of the assumed sphere of Zone 2 surrounding the UAV.

Based on the above and to be conservative in the design, to cover additional UAVs, and to account for the importance of proximity effects during inspection, the overall safe clearance diameter is considered as 3 feet 6 inches (3.5 feet or 42 inches), and a minimum diameter of 3 feet 4 inches (40 inches) around the UAV. Both diameters must be considered when testing UAVs for inspection of structures, to protect the UAV from proximity effects while qualifying the skills of the UAS to aid in inspection.

3.2 Evaluation Chamber

After identifying a common dimension of UAV that encompasses most of the vehicles used in bridge inspection in section 3.1.1, and having assumed a clearance distance considering proximity effects in section 3.1.4, the author introduces the idea of a series of obstacles and elements inside an enclosed space. The objective is to develop standardized obstacles (or objects) that resemble components of bridge structures to be inspected using UAVs that allow for repeatable testing. The elements and environment for this test will be referred in future sections collectively as the evaluation chamber.

In section 3.2.1, the environmental conditions of the evaluation chamber are discussed. In section 3.2.2 general flying parameters are visited. In section 3.2.3, general considerations for evaluating the imaging and battery of the UAV are presented. Finally, in section 3.2.4 the dimensions and shapes of the elements inside the container are determined, and in section 3.2.5 the parameters to evaluate a successful completion of the evaluation chamber are discussed.

3.2.1 Environment Conditions to Perform the Test

As identified in Chapter 1 and 2, bridge inspection using UAS faces challenges imposed by the environment, in addition to temperature effects. For example, changes in wind speed or gusts

unbalancing the UAV, variation of lighting conditions impacting the quality of the images obtained, loss of GPS signal in zones of the structure, among others. However, the main goal of the research is to provide a repeatable and standard test able to perform in any place of the U.S. regardless of the time of the day, presence or absence of sun light, ambient temperature or location. To achieve the main goal of this research and covered by the scope of this project, the author proposes to control these parameters as much as possible during this test and they are addressed separately in the following sections: lighting, weather conditions, and GPS signal. Weather conditions are addressed in three parts: wind, precipitation, and temperature.

Lighting

To consider that the space will be located in any place in the U.S. where sunlight times vary during the year and to allow the proctor to perform the test in cloudy or partially cloudy days, the space will contain supplementary lights provided in key locations where natural light does not provide enough visibility inside the evaluation chamber. The purpose of these lights is to guarantee that all elements are correctly illuminated to achieve collection of high-quality images but also to resemble typical conditions in bridge inspection where natural or artificial light is not always available.

Wind

To ensure repeatability, the test results must not be influenced by ambient wind. Evaluating different UAS under different wind conditions would obviously bias the outcomes of each test. Therefore, the test must be configured such that ambient wind effects are eliminated. Further, to evaluate proximity effects referenced in Chapter 2, ambient wind must also be eliminated as this will also bias the observed interference. This allows objective evaluation of the ability of the UAS to navigate adjacent to and around the obstacles.

Precipitation

The literature review and discussion with pilots suggests UAS inspections are not performed during active precipitation (snow, rain, sleet, or hail). Therefore, precipitation will not be explicitly included in the testing program.

Temperature

The scope of this project does not cover testing under a fixed temperature but the author acknowledges the effect of testing UAS under temperatures outside the range of recommended temperatures by the manufacturer of the UAV (examples of recommended temperature ranges are presented in Table 2). For that reason, effects of temperature are compensated by allowing change of battery during the test as detailed in section 3.2.3. In addition, an enclosed space (one with a roof, ceiling, and walls) surrounding the evaluation chamber and the UAV will be enough to protect them from sudden changes in temperature.

GPS Signal

The location selected must provide a barrier that inhibits GPS signal to allow testing of navigation skills of the pilot without the aid of GPS, resembling typical inspection underneath bridge structures or under structural elements. The location must also allow to fly in any place where the test will be performed without FAA restrictions in no-fly zones (NFZ), such as close to airports.

Repeatability of the Test

Finally, the "test facility" cannot be so complex and unique such that all testing in the United States must be conducted at a single facility. Thus, while specific criteria, obstacles and simulated details must be included, it is advantageous if several such testing facilities could be strategically located around the country without compromising repeatability of results.

Considering the mentioned requirements, a few things become apparent. First, the overall weather conditions must be relatively controlled and repeatable. Second, there must be complete control over the lighting conditions during the test. Third, the test must take place within a GPS denied environment. Fourth, the overall test must not be complex in materials that it is prohibitively expensive to construct or overly complex that is very difficult to replicate.

After exploring several alternatives, a cost-effective solution was identified as the base setting for the test. Specifically, it is proposed to develop the evaluation chamber test such that it can be housed within the familiar 40 feet standard steel cargo container. The typical container provides

sufficient space to host the proposed evaluation chamber while blocking GPS signal, blocking changes of wind speed, protecting the elements from forms of precipitation. Further, cargo containers are readily available throughout the U.S. As an additional advantage, an "outfitted" container can be easily loaded on a truck and be located where testing is needed.

The dimensions of the container were selected to provide enough space for the test to take place, while ensuring at all times the clearance distances for the UAV determined in section 3.1.4. The external dimensions of the container are detailed below and Figure 7 presents the container used in this research.

- 40 feet of length,
- 8 feet of width,
- and 8 feet 6 inches of height.

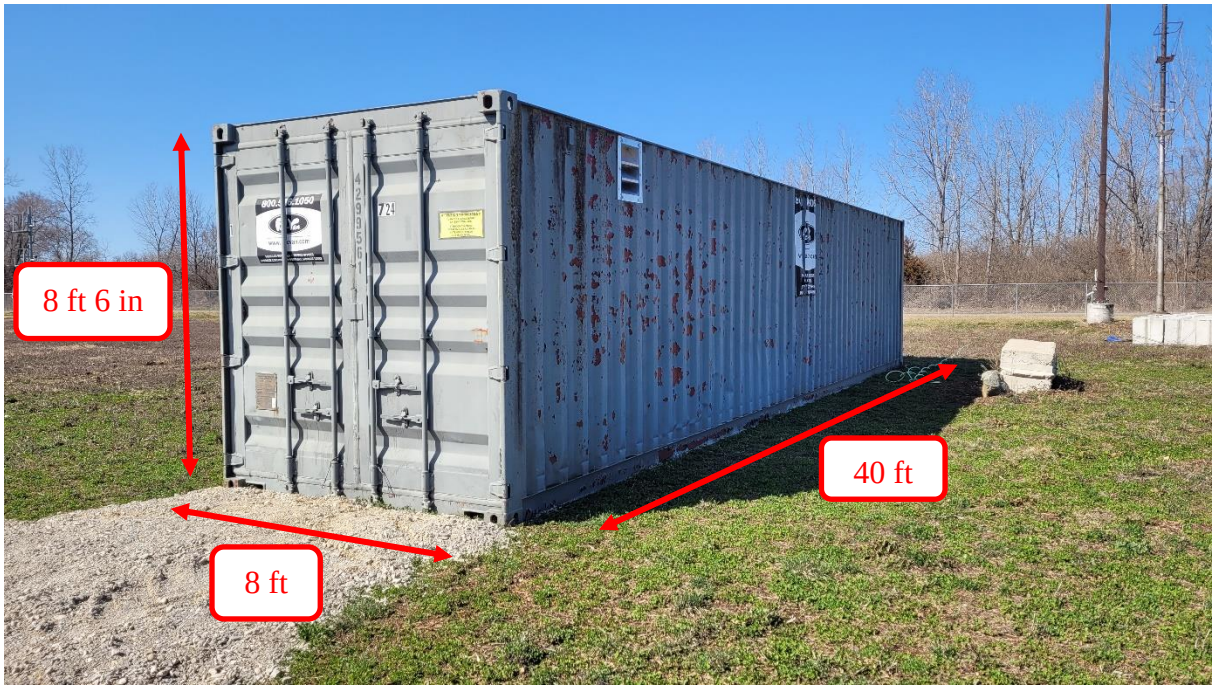

Figure 7 Container where the proposed evaluation chamber test takes place.

3.2.2 Takeoff, Flying, and Landing

After determining the place where the test will be located, flying parameters are visited. No minimum or maximum speeds are required during the test and the pilot will decide appropriate

speeds to navigate through the obstacles, stop when necessary, and collect high-quality visual information.

After the inspector has determined that all required information has been collected to provide a complete UAS inspection of the evaluation chamber, the UAV must return to the starting point. The pilot is not allowed to land the UAV in any place inside the container, resembling real-life scenarios of a bridge inspection. The only instance where the UAS is allowed to pause the test, come back to the place where it took off, land, takeoff again, and return to the pausing point is in the case of a battery change, detailed in the next section.

3.2.3 Battery and Camera Considerations to Perform the Test

Battery Considerations

Battery life varies widely with respect to model, use of UAV, condition of the UAV (new or old), battery capacity, and weather conditions at the time of test. In fact, as presented in Table 2, manufacturers provide an estimated flight time for a specified temperature range. For example: from Table 2, the battery of a DJI Phantom 3 Pro is expected to last around 23 min operating from 32 °F to 104 °F. Below or above those temperatures, the UAV is able to operate but battery life is reduced, thus having shorter flight times.

The author tested flights outside the manufacturer recommended range on 02-05-21 at 26 °F, 02-12-21 at 25 °F, and at the lower limit provided by the manufacturer of 32 °F on 12-17-20. From these 3 experiences, the average flight time to complete the evaluation chamber decreased by a half compared to a typical flight in temperature ranges between 40 °F and 66 °F. The average flight time to complete the evaluation chamber under temperatures below the lower limit provided by the manufacturer also decreased by a half comparing to the expected flying time provided by the manufacturer. As a consequence, two fully charged batteries were required to finish the inspection inside the proposed evaluation chamber. The author recognizes that the pilot on the mentioned tests and his skills are biased due to his knowledge of details of the proposed evaluation chamber and the several repetitions of the test that gives him privileged knowledge on the inspection performed. The author also recognizes the batteries were not new and they might affect UAV

performance on winter weather. To consider battery variations between models, status of the battery, temperature ranges in different states of the U.S., and the possible bias of the total flight time of the visual data collected by the pilot on this research, any UAS to be tested inside the evaluation chamber must comply with the following battery requirements before the start of the test:

1. At least two fully charged batteries must be available: one will be used by the UAV to take off and perform the test, and a second fully charged replacement battery must be available to facilitate efficiency of the test should the first battery die. Extra batteries are encouraged but not required to start the test, thus it is the responsibility of the pilot to bring an appropriate number of batteries for their UAV to complete an inspection (two or more).
2. Verification that the controller is fully charged.

During the test, the UAS is allowed changes of batteries when the minimum battery limit specified by the manufacturer has been reached, (i.e., for Mavic 2 Pro is 30%), or if the pilot considers necessary to avoid uninterrupted data collection, whichever happens first. When a change of battery is required, the pilot must land the UAV in the same area where the UAV took off and immediately proceed to change the battery. After the change of battery has been executed, the UAV takes off in the same position where it landed and resumes the test. The goal of this procedure is to reasonably resemble a real-life UAS inspection of bridges by minimizing contact of the pilot with the elements to be inspected and allowing a reasonable change of batteries during inspection tasks.

Camera Considerations

During the test, the inspector is allowed to record video or take the images necessary to provide a complete assessment of the evaluation chamber. The purpose of the images and videos collected during the test is to provide visual information to the inspector and help in their assessment. They work as an aid in the inspection task and are not tested or qualified in any way by the proctor of the test. The instrument to collect visual data, i.e., the camera, can vary of model, brand, lens, resolution, and any variation of those elements can provide high-quality images of the structure. The camera and video resolution of the UAV are not relevant for this test because the test qualifies

the final inspection results and not specific video or image quality. For that reason, no minimum requirements for the camera are required to complete the test.

To provide a brief guidance, the author includes two references that can provide a general idea of camera resolutions, but are not requirements or suggestions to pass the test. Mohan & Poobal (2018) recommend a 10 megapixels camera for practical defect detection and in a 2018 Federal Highway Administration publication by Joe Campbell from the Minnesota Division recommended a camera of 12 megapixels and a 4K video resolution. These values are references and do not imply a better performance will be achieved if the inspector uses one of them or a different one.

3.2.4 Obstacle Dimensions and Shapes

In achieving an appropriate configuration and sizing of the obstacles inside the selected container, the research objectives were followed to cover the goals of this research work.

For the general design of the evaluation chamber, to cover the repeatability part of the test in Objective 1, and to provide a configuration that can be repeated in any part of the U.S., the material selected to fabricate the obstacles was a combination of sheets of plywood purchased in 4 feet by 8 feet dimensions and 2 inch by 4 inch lumber. For round elements, Sonotube with a diameter of 24 inches was used. In the same Objective 1 and tied to Objective 5 which refers to the assessment of steel and concrete defects in high-quality visual data information, the obstacles were designed with clear faces to place images of concrete and steel defects presented in Appendix A, including corrosion, cracks, spalling, delamination, leaking signs in concrete, defects in welds.

In order to cover Objective 2 related to the environment resembling conventional conditions/situations in bridge inspection, two approaches were taken. First, the obstacles were painted in three colors found on typical bridges: green, blue, and brown, to resemble a bridge environment. Second, the scaled dimensions of the obstacles, meaning the size of the obstacles arranged to fit the container, were developed considering a range variety of bridge structures as well as by using the bridge inventory available at Steel Bridge Research, Inspection, Training, and Engineering Center (S-BRITE) and Center for Aging Infrastructure (CAI) at Purdue University (Purdue University, 2021). For other structures considered in this research, the largest database of

pictures and general bridges online was used: Bridge Hunter, founded by James Baughn in 2002 and now maintained by the Historic Bridge Foundation since 2020 (Historic Bridge Foundation, 2021). For other elements, the Manual for Bridge Element Inspection was used to identify other defects not found in the references mentioned before (American Association of State Highway and Transportation Officials, 2019).

With those considerations for the design, the inventory of situations and images is utilized to satisfy Objective 2 related to location and documentation of defects in an environment resembling inspection conditions. The most relevant conditions are detailed in the following paragraphs and illustrated in the following pages. The situations and images described for each obstacle were selected with the goal to capture a pattern that repeats in most of the bridges in the U.S. In the description of each obstacle a reference to a Figure and a color is presented in parenthesis that represents the color of an arrow or line pointing the referenced object on that Figure. Final dimensions, renders, and location of the obstacles inside the evaluation chamber are presented in detail in Chapter 4.

Obstacle 1

The first situation to portray is the UAV approaching elements from above to test ground effects, as presented in Figure 16 (red). The second situation is captured in Figure 17 (orange) for an inspection of the deck and substructure of a truss bridge and similar elements on other bridges. The third situation is an inspection of elements in side faces of a bridge, as portrayed in Figure 18 (red). Similarly, a fourth situation is considered when inspecting decks as presented in Figure 23 (orange). A fifth situation is captured for inspection of small spaces between pier and deck as presented in Figure 30 (red and orange). The result of these considerations provides an object with two main rectangular faces (front and back), small to test ground effect, and easy to accommodate in any place inside the container, giving the design of *Obstacle 1* as presented in Figure 8. A rectangular base has been added to the bottom of the obstacle to provide stability.

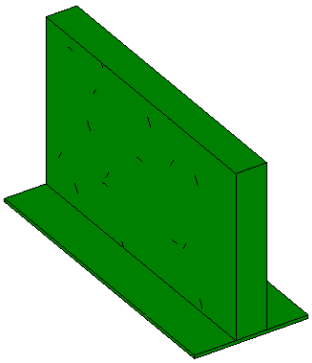

Figure 8 3D Illustration of Obstacle 1.

Obstacle 2

The same process was followed for the next obstacles. Tall and slender faces in bridge elements such as piers or piles were considered as presented in Figure 16 (orange). Tall bridges and girders with high depth were considered as presented in Figure 18 (orange) and Figure 23 (yellow). Planar structures in open environments, similar to elements found on long-span bridges were considered as presented in Figure 26 (red). The height of a tall cover was considered from Figure 28 (red). Tall and slender connectors in concrete bridges were considered as presented in Figure 29 (orange). The height of bridges over roadways and pier elements were also considered as presented in Figure 30 (red). For that reason, the new obstacle must be high enough to test both ground and ceiling effect, and also provide two faces where defects will be located. The result of the situations and images mentioned above provide the design of *Obstacle 2* in Figure 9. A rectangular base has been added to the bottom of the obstacle to provide stability.

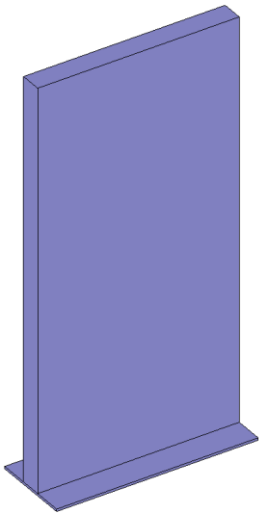

Figure 9 3D Illustration of Obstacle 2.

Obstacle 3

The shape, slenderness, and height of piers found on Figure 27 (red) were considered. The piers of Figure 29 (orange) and Figure 30 (red) were also considered. The new obstacle must provide round surfaces where the shape will force the UAV to take different images of the same area to provide a complete assessment of the element in the horizontal and vertical direction. The obstacle must not be accessible from all sides (not a 360° assessment), instead the obstacle must be placed against a wall achieving that some areas will be hidden and difficult to reach by the UAS. The results of these situations provide *Obstacle 3* in Figure 10.

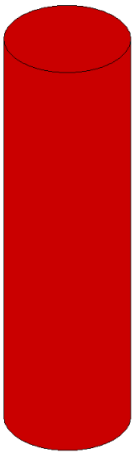

Figure 10 3D Illustration of Obstacle 3.

Obstacle 4

With the use of a cargo container as the place where the evaluation chamber is going to be located, Objective 4 bullet point 1 referring to GPS-denied environment has been satisfied. To provide another layer that guarantees the inhibition of any remaining GPS signal (if any remains after the roof of the container has blocked it), the next obstacle must have a roof in its design. The addition of a roof in the new obstacle provides an area where the UAS must inspect looking from ground level. In addition, the situation presented in Figure 17 (blue) was considered to portray a passage inside a bridge structure. The challenge to flight inside a steel bridge as presented in Figure 19 (blue) is considered. At this point, the new obstacle has a roof and faces, but these faces are adapted to portray the situation in Figure 21 (red) for side faces of bridge structures. The safe passage while flying over tall structures is considered based on the situation presented in Figure 23 (blue). The complete situation that an UAS would have to overcome while flying underneath a bridge as presented in Figure 27 (blue), Figure 29 (blue), and Figure 30 (blue) is portrayed in the new obstacle. These situations provide the design of *Obstacle 4* in Figure 11.

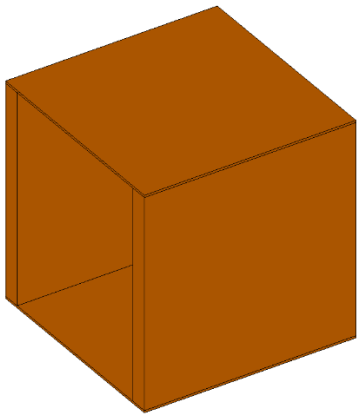

Figure 11 3D Illustration of Obstacle 4.

Obstacle 5

Several considerations on the faces of bridge structures were presented in the previous obstacles, but the complex shapes in some bridges must be addressed. In the next obstacle, situations from Figure 19 (red) in a bridge structure with cross components were considered. The same obstacle must include plane surfaces as presented in Figure 21 (red) and a space to fly inside the elements to inspect, as presented in Figure 23 (blue) and Figure 29 (blue). The skill to fly across and inside

thin and long elements will be tested in this obstacle, as presented in the cables of Figure 31 (orange). K frames will be located at the beginning and end of the obstacle, similar to the ones presented in Figure 32. These situations provide the design of *Obstacle 5* in Figure 12.

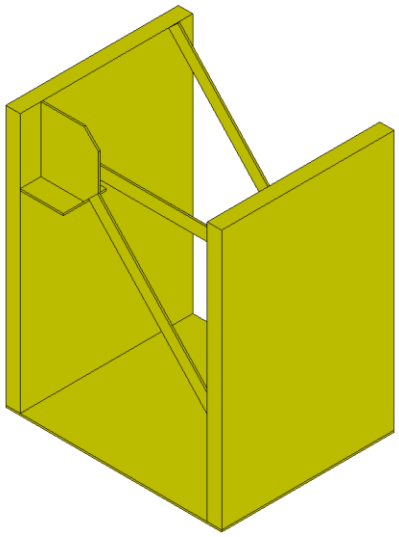

Figure 12 3D Illustration of Obstacle 5.

Obstacle 6

The next obstacle must consider box structures as presented in Figure 19 (orange) and Figure 21 (red), tight spaces as presented in Figure 22 (orange) with a combination of tall and slender structures as presented in Figure 23 (yellow) and Figure 26 (red), and underneath bridge structures with side faces as presented in Figure 28 (orange). Objective 2 bullet point 1 referring to GPS signal is emphasized again with a roof at the top of the obstacle. The roof also provides another opportunity to inspect defects from ground level, but with a higher view in contrast to what was presented in Obstacle 4. These situations provide the design of *Obstacle 6* in Figure 13.

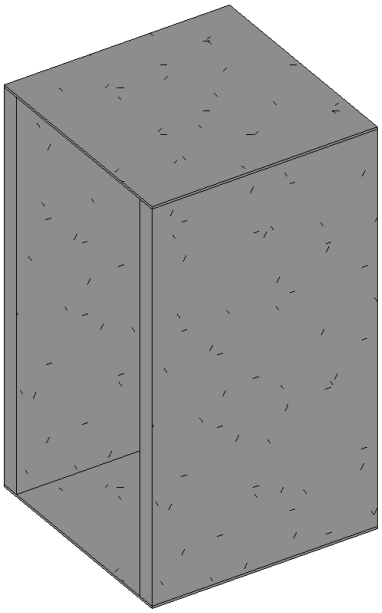

Figure 13 3D Illustration of Obstacle 6.

Obstacle 7

Finally, Objective 2 bullet point 3 is emphasized in the last obstacle, when considering the complete loss of line of sight. Up to this point, line of sight has been progressively lost, but the last obstacle must guarantee that any remaining visual sight of the pilot or the inspector is denied as in the scenario illustrated in Figure 19 (blue and orange) where neither the pilot nor the inspector would be able to access the structure. Additionally, situations where the pilot has no visual line of sight from the ground are captured, as presented in Figure 22 (orange and red). Inspection in tight spaces is considered from the bridge of Figure 29 (red) and will be achieved with the addition of round surfaces as presented in Figure 28 (red) that would make difficult the navigation inside the obstacle. Additional enclosed and tight spaces in abutments (yellow), piers (red), and decks (orange) are considered from Figure 30. The last set of situations and goals are considered in the design of *Obstacle 7* in Figure 14.

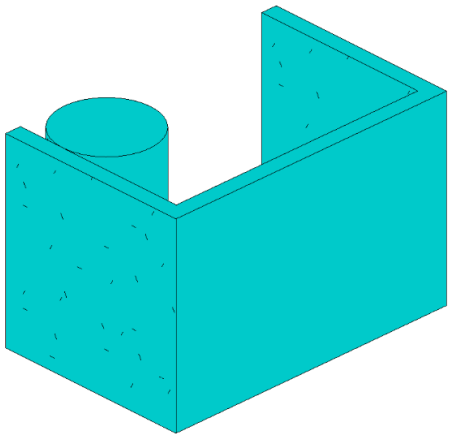

Figure 14 3D Illustration of Obstacle 7.

The obstacles are scaled to fit in the container selected in previous sections but also to consider at all times the minimum distances provided by the dimensions where proximity effects would affect the UAS. The final distribution of the obstacles inside the evaluation chamber is presented in Figure 15. The previous numbering of the obstacles follows the numbers presented in Figure 35. Plan views and dimensions are detailed in Chapter 4.

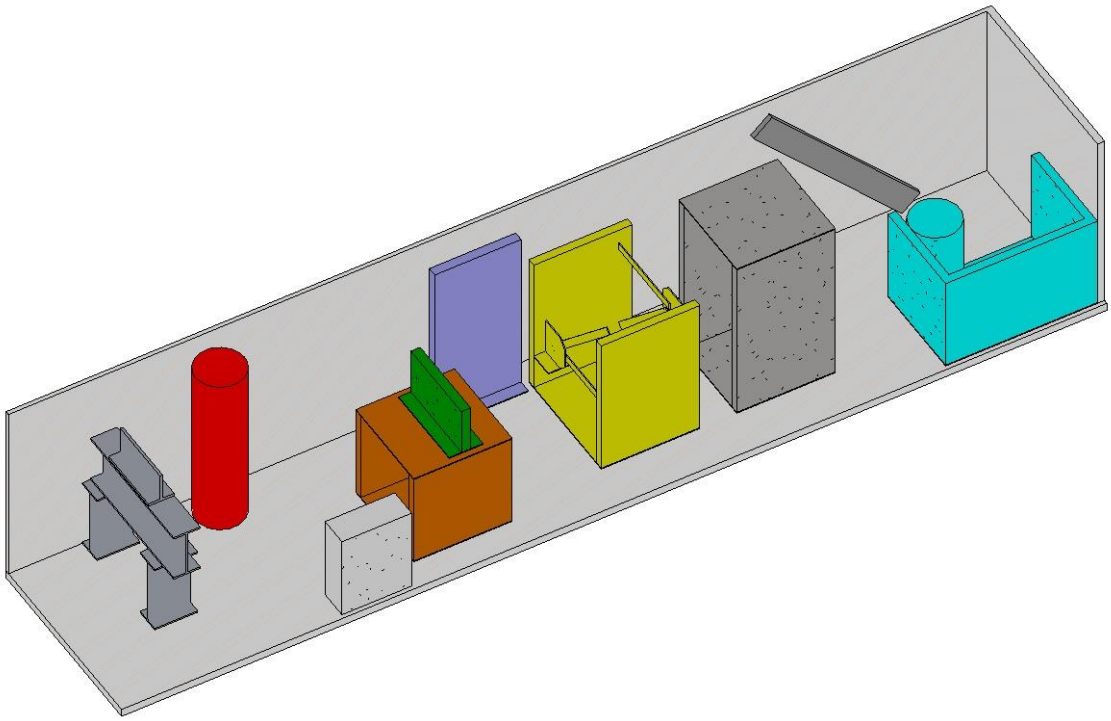

Figure 15 3D Illustration of elements inside evaluation chamber.

Situations and Summary of Bridges Considered in the Design

In the next pages, the situations and images from typical bridges used in the design of the obstacles inside the evaluation chamber are explored in detail, with an illustration of the areas considered in the design. For the following figures, the numbering of the obstacles follows the order presented in Figure 35. The color in arrows, lines, and circles show the considerations depicted in the obstacles referenced when the image was introduced in the design of each obstacle.

Figure 16 presents a typical flight to gather information of performance of UAV while gathering data for proximity effects inside a shed in S-BRITE facility at Purdue University. Such situations were considered in the design of obstacles representing tall and slender horizontal faces (orange and red).

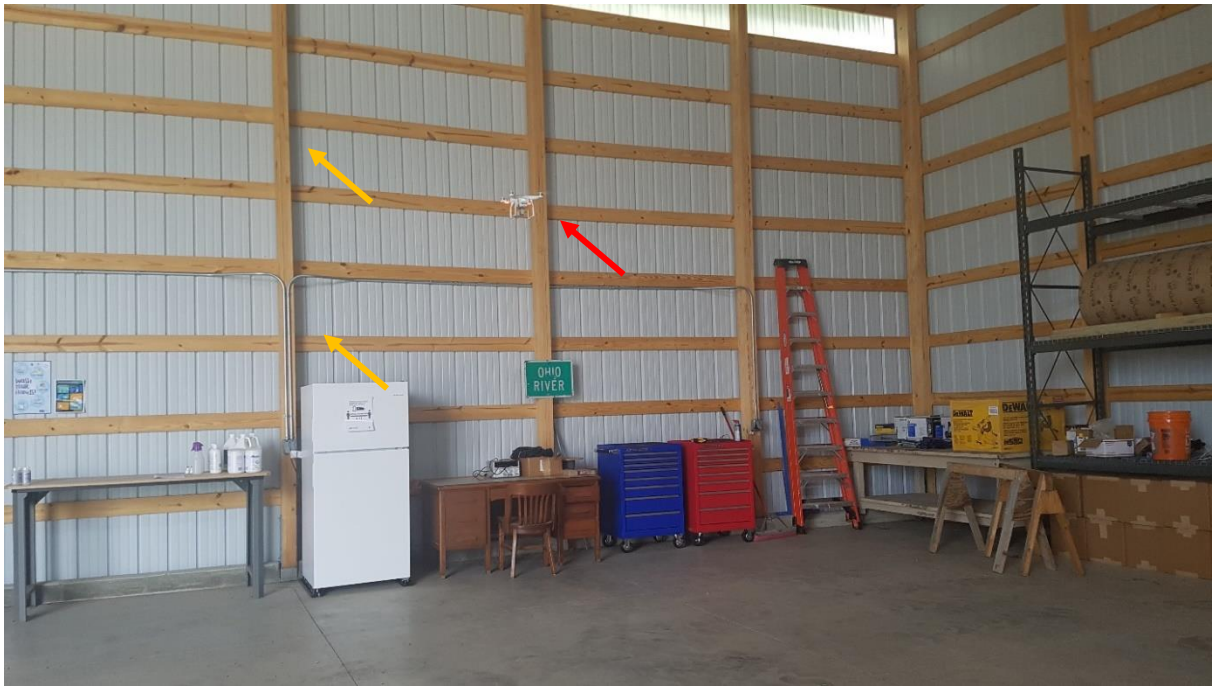

Figure 16 Flight inside a shed at S-BRITE to study proximity effects.

Figure 17 presents a flight in a truss structure to gather information regarding challenges and important features to consider in the design of the evaluation chamber (red and blue). The behavior of the UAV with this structure was portrayed as a segment of a truss in Obstacle 6. The deck and substructure elements (orange) are represented by Obstacle 1 and Obstacle 4.

Figure 17 Inspection of truss bridge at S-BRITE.

Figure 18 presents a flight along steel plate girders (orange). This situation is portrayed in Obstacle 1, the height of this type of inspection is reflected in Obstacle 2 and the side faces of the structure in the Figure (red) in Obstacle 5. In addition, the blue arrows represent the situation considered to portray a passage along steel members to reach inside a bridge structure, from the side face and below.

Figure 18 Inspection of welded bridge at S-BRITE.

Figure 19 presents a flight test inside a bridge structure (blue) with cross components (red). This situation was portrayed in the truss elements of Obstacle 5, and the closed space on Obstacle 7.

Figure 19 Flight test inside a bridge welded structure at S-BRITE.

Figure 20 presents inspection in concrete structures (red), portrayed in the floor and faces of Obstacle 4 and Obstacle 6. In addition, the concrete element inside the evaluation chamber presents concrete with exposed rebar.

Figure 20 Inspection in concrete elements at S-BRITE.

Figure 21 presents inspection in riveted bridge structures (red). This situation is represented by the side faces of Obstacle 4, Obstacle 5, and Obstacle 6.

Figure 21 Inspection of riveted bridge structure at S-BRITE.

Figure 22 presents inspection in bolted structures and zones in-between steel elements (red and orange). This situation is represented in Obstacle 6, and the tight space of Obstacle 7. Additionally, the steel elements located at the entrance of the evaluation chamber portray girder, steel beams, and rivets.

Figure 22 Inspection of bolted and spaces between steel structures at S-BRITE.

Figure 23 presents inspection in tall structures (yellow) and decks (orange) over bridges. This situation is portrayed in Obstacle 1, Obstacle 2, Obstacle 4, and Obstacle 6. Additionally, girders (red) similar to the ones presented in Figure 23 are located at the entrance of the evaluation chamber for inspection.

Figure 23 Inspection of tall bridges, deck, and other steel elements.

Figure 24 presents inspection on rivetted elements (red) from sections of the I-35W Bridge. Those elements are represented in the steel structures located at the entrance of the evaluation chamber.

Figure 24 Inspection of I-35W Bridge elements at S-BRITE.

Figure 25 presents UAV inspection in open environments surrounded by vegetation. This situation allowed the author to obtain information from flying in an environment with no structures nearby and provide a comparison when flying close to structures.

Figure 25 UAS flight in an open environment surrounded by tall vegetation.

Figure 26 presents a flight performed next to a planar structure (red) in an open environment, depicted in the faces of Obstacle 2, and Obstacle 6.

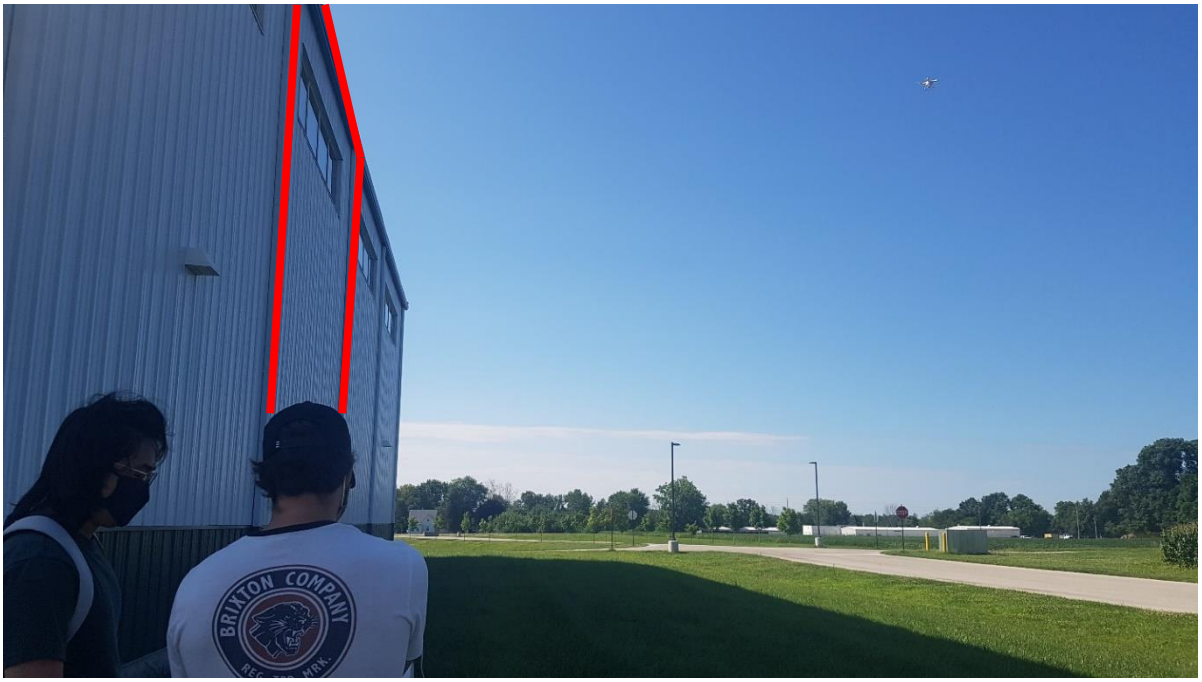

Figure 26 Flight Test performed next to a planar structure surrounded by vegetation.

Figure 27 represents one of the bridge structures used to conceive Obstacle 2 and Obstacle 3, covering tall and slender elements in concrete (red).

Figure 27 Trendley Avenue Underpass in St. Clair County, Illinois (Historic Bridge Foundation, 2021).

Figure 28 is represented in the roof (red) of Obstacle 6 and the round surfaces of Obstacle 2 and 7.

Figure 28 Orchard Road Bridge in St. Francois County, Missouri (Historic Bridge Foundation, 2021).

The shapes in Figure 29 (orange) are represented in Obstacle 2, Obstacle 3, Obstacle 5 and the tight spaces (red and blue) in Obstacle 7.

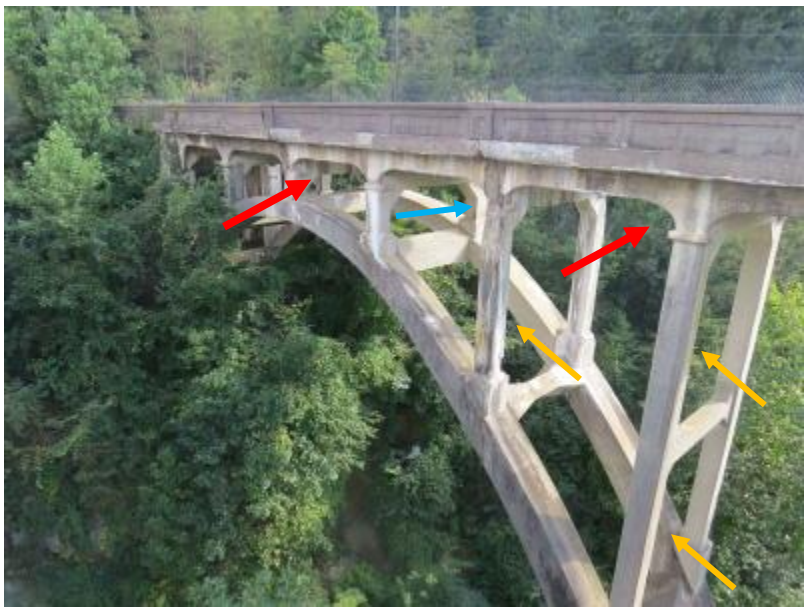

Figure 29 High Bridge in Henderson County, North Carolina (Historic Bridge Foundation, 2021)

The deck of Figure 30 (orange) is represented in Obstacle 1 and Obstacle 4, the height of the piers (red) in Obstacle 2, and the round shapes (red) and small spaces (yellow) in Obstacle 7. The situation of flying underneath structures (blue) is presented in Obstacle 4 and Obstacle 6.

Figure 30 UP - IA 5 Overpass in Warren County, Iowa (Historic Bridge Foundation, 2021).

Figure 31 is represented in Obstacle 5, Obstacle 6, and in steel elements placed along the container (red).

Figure 31 Deer Isle-Sedgwick Bridge in Hancock County, Maine (Historic Bridge Foundation, 2021).

Figure 32 shows a truss bridge, with K bracing (orange) represented in the elements of Obstacle 5.

Figure 32 I-895 Curtis Bay Steel Bridge in Baltimore, Maryland (Historic Bridge Foundation, 2021).

After the analysis of similar pictures and comparison with other bridge elements, the first draft of the evaluation chamber is presented in Figure 33. Notice the numbering of the elements is not in order, because it follows final numbering of the evaluation chamber.

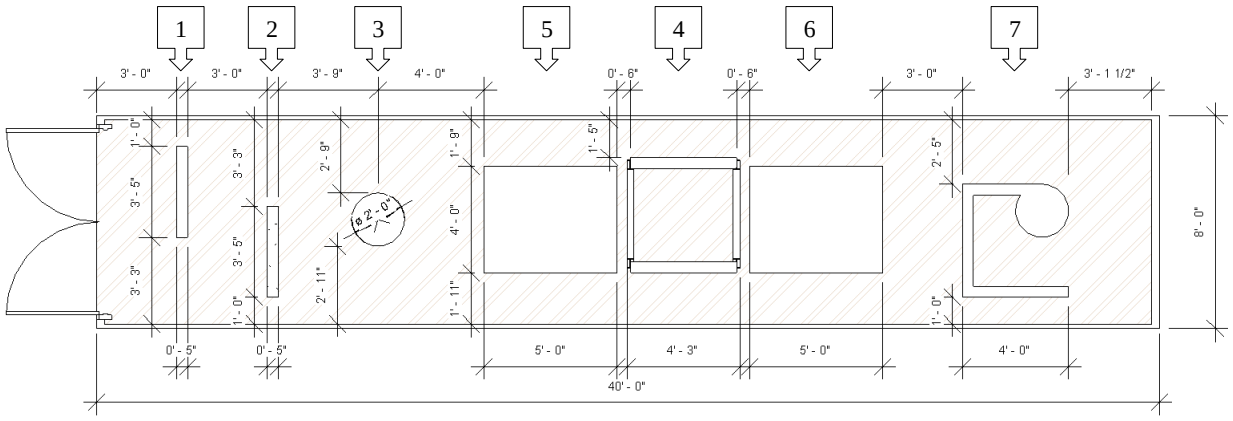

Figure 33 Plan View of first draft of evaluation chamber.

Issues with the design were encountered while performing trial runs in a mockup of the first draft of the evaluation chamber. The main issue was encountered when a check was performed to guarantee that the UAV has the recommended clearance distance between obstacles and elements. The problems were solved by changing the shape and order of three obstacles (4, 5, and 6), rotating one obstacle (7), and adapting the clearance distance for the first three obstacles.

The dimensions of the evaluation chamber follow the constraints provided by proximity effects and clearance distance, but also the shapes and situations presented before from bridge structures across the U.S.

The fabrication of the evaluation chamber was made following the final dimensions presented in the next chapter. Images of high-quality defects found in steel and concrete structures were located in the faces of each obstacle. Those images include elements with delamination, spalling, cracks in different places, corrosion, loss of material. A complete gallery of the defects used is presented in Appendix A.

The images presented in Appendix A were taken with a Camera Sony ILCE7RM4 from steel and concrete elements in S-BRITE and Bowen Laboratory at Purdue University. The images were compared to the real elements to find noticeable differences between the elements and the image. For all the images, a high level of accuracy and matching was encountered, determined by visual inspection and analytical tools such as S-CIELAB and CIEDE2000 (G. M. Johnson & Fairchild, 2003).

The images presented in Appendix A or any image of a defect to be used inside the container must follow the guidelines:

- Be printed in a white non-glossy paper. Papers heavier than normal paper are recommended.
- Be scaled to the actual size of the element. For that purpose, the image must contain an element with known size to scale using computer technologies. For the majority of images in Appendix A, a measuring tape was included next to the steel or concrete element, to later determine the appropriate scale of the image. For others, a small thin object with known length and height was included next to the steel or concrete element, for scale purposes.

In addition, to provide further quality assessment with real structures, several steel elements and a concrete element with known defects were introduced to the evaluation chamber, and placed along with the obstacles complying with the clearance provided in past sections.

The evaluation chamber intends to cover the majority of shapes of elements in structures. Following the recommendation of determining Commonly Recognized Elements by AASHTO, “it is important for element definitions to accommodate foreseeable technological change, and to remain acceptable and usable to each new generation” (Thompson & Shepard, 2000). That is the reason why the obstacles shapes are general and were adapted to the clearance distance determined in this research.

3.2.5 Parameters for Evaluation of the Test

As mentioned before, images from Appendix A and elements made of concrete and steel are located in different places along the evaluation chamber. The goal of the inspector is to find defects inside the evaluation chamber.

Takeoff will be performed at the entrance of the container. The pilot must have two batteries available at the beginning of the test: one used by the UAV, and an additional fully charged battery. The controller is verified to be fully charged. The pilot shall disable obstacle avoidance technologies and, in some cases, they must seek permission from the manufacturer to deactivate avoidance technologies before the start of the test. GPS must be disabled if possible, and the controller of the UAV must show no GPS signal detected inside the container.

The inspector receives a general sketch of the placement of the test, providing locations of the obstacles inside the evaluation chamber. Not all the obstacles present defects. A list of targets to follow is presented following the sketch of Figure 34:

a) Inspect steel elements located inside the evaluation chamber.
b) Inspect concrete elements located inside the evaluation chamber.
c) Inspect front and back face of Obstacle 1.
d) Inspect visible face of Obstacle 2. Defects are placed at the bottom, middle, and top.
e) Inspect visible area of Obstacle 3. Defects are place at the bottom, middle, and top following the visible circumference of the element.
f) Inspect left, right, and top face inside Obstacle 4.
g) Inspect left and right face inside Obstacle 5. Defect are located at the bottom, middle, and top of the faces.
h) Inspect two sides of the cross elements and gusset plates located inside Obstacle 5.
i) Inspect left, right, and top faces inside Obstacle 6.
j) Inspect left, front, and right faces inside Obstacle 7.
k) Inspect circular element inside Obstacle 7.

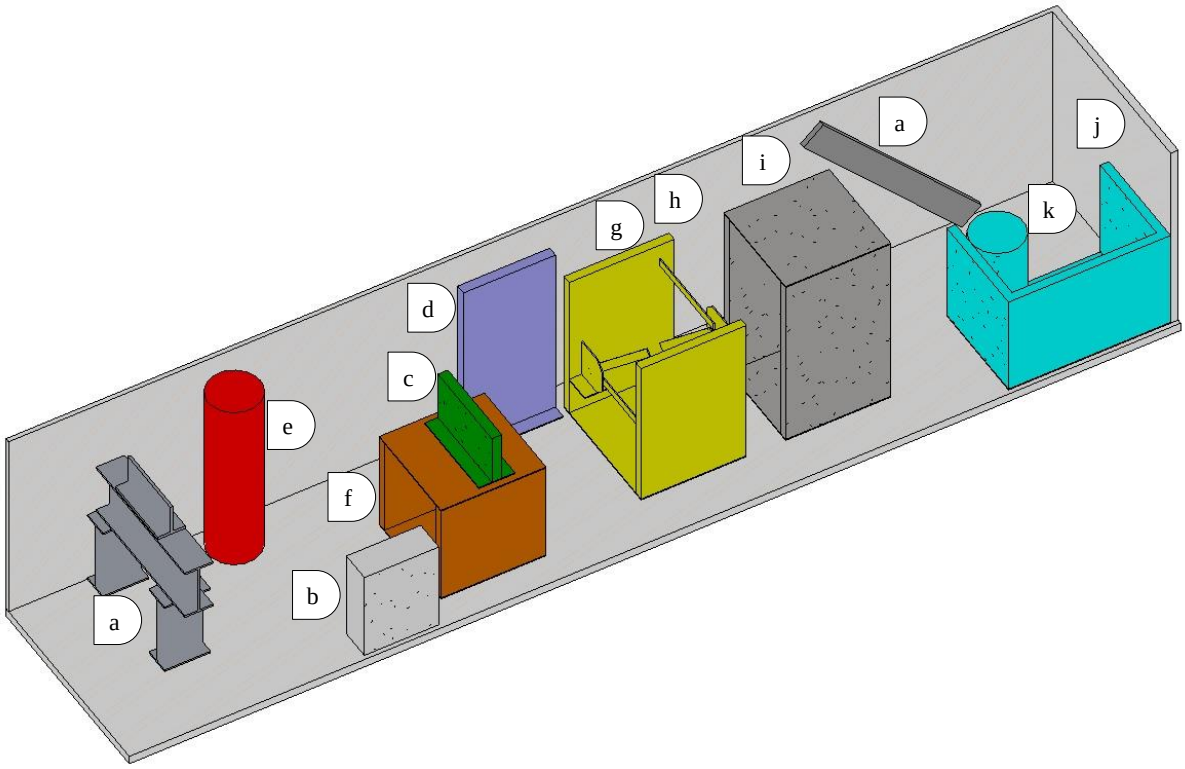

Figure 34 Inspection interest points.

The test ends when the inspector considers the UAS has captured all possible defects inside the evaluation chamber and they can be assessed either in real-time flight or in post-processing work. Evaluation criteria based on the UAS performance during the test is not included in the scope of this research; however, some considerations and suggestions for future work are presented in the next chapters.

4. RESULTS

4.1 Evaluation Chamber

The main goals of the evaluation chamber are:

- Assess UAS capabilities flying through the evaluation chamber that represents the general shapes of common elements found in bridge structures.
- Assess UAS capabilities to navigate without using GPS signal and in limited line-of-sight and limited lighting conditions using real-time observations of the environment through visual media.
- Obtain images of elements that include representative and common defects found in steel and concrete bridge structures.

The final design of the evaluation chamber is presented in Figure 35 and a detailed explanation of all components follows. Dimensions and clear distances are detailed next to each element in Figure 36, Figure 37, and Figure 38. Components include both “real” steel and concrete specimens as well as those intended to simulate various geometric configurations on which other features are mounted (Obstacle 1 through 7).

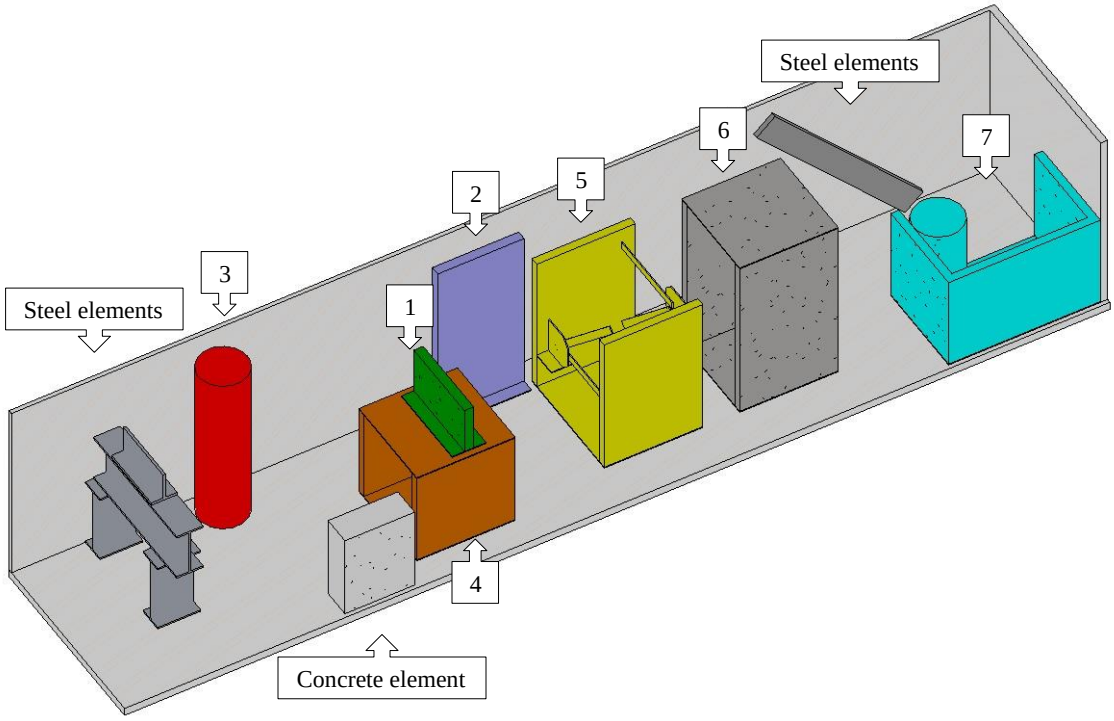

Figure 35 3D representation of elements inside evaluation chamber.

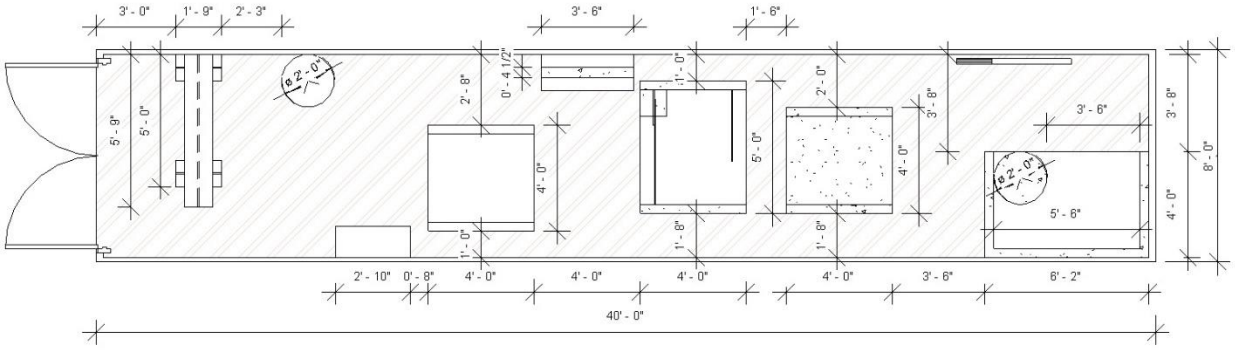

Figure 36 Plan view of the evaluation chamber – first level (4 feet).

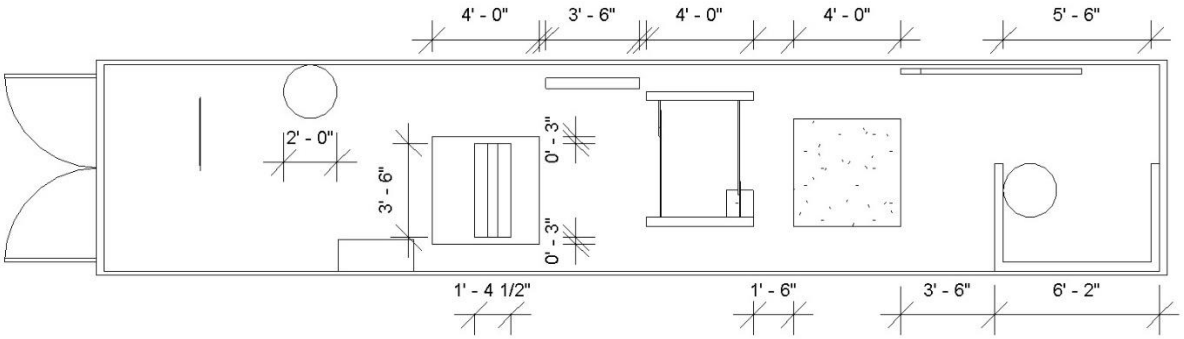

Figure 37 Plan view of the evaluation chamber – general view.

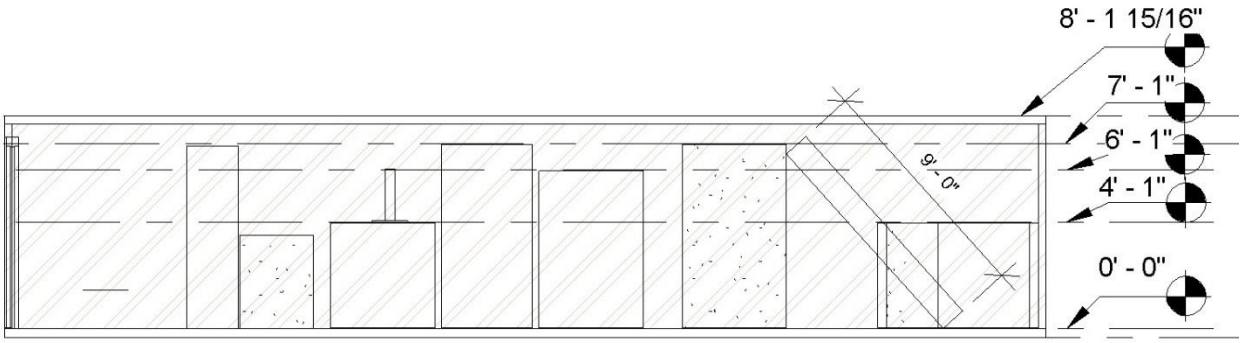

Figure 38 Elevation view of the evaluation chamber.

Steel and concrete elements

Several steel and concrete structural elements taken from S-BRITE components from bridge structures and from donation of other research projects at Bowen Laboratory at Purdue University are placed inside the evaluation chamber. These elements cover steel girders, steel beams, small steel columns, shear studs, and reinforced concrete components.

Obstacle 1

A wall element with the following dimensions, presented in Figure 39:

- Width: 3 feet 6 inches.
- Height: 2 feet.
- Depth: 4.5 inches.

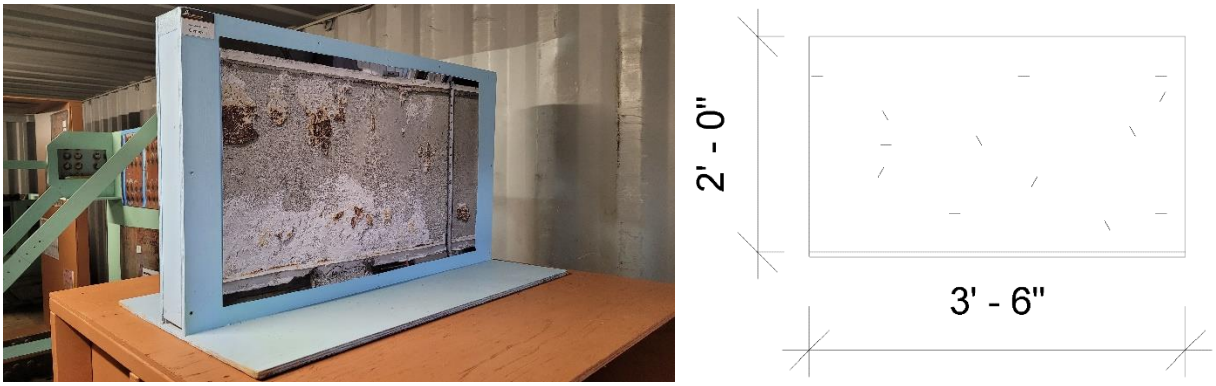

Figure 39 3D Illustration and front view of Obstacle 1.

Its rectangular face contains images of defects. The main focus of this obstacle is spalling in concrete, delamination, and cracks. Its faces and size represent an inspection in small areas of structures.

Obstacle 2

A tall element with the following dimensions presented in Figure 40:

- Width: 3 feet 6 inches.
- Height: 7 feet.
- Depth: 4.5 inches.

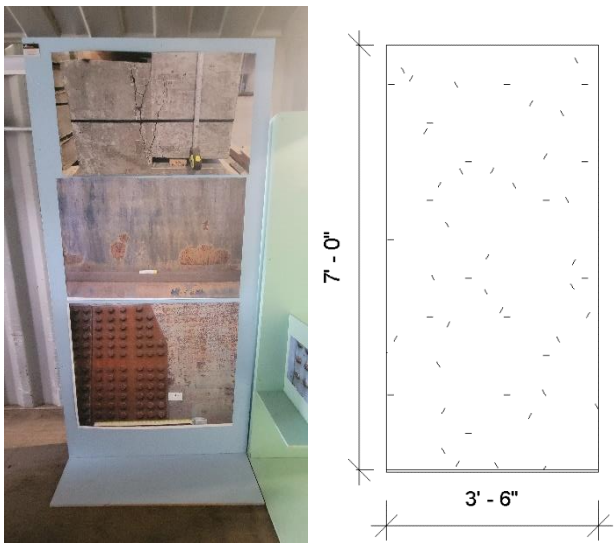

Figure 40 3D Illustration and front view of Obstacle 2.

Obstacle 2 has rectangular faces, and its main focus is on cracks, delamination, and spalling in concrete using images from Appendix A. This obstacle represents the most common type of geometries found in tall and slender structural elements. The inspection focuses in the ability of the UAS to overcome ceiling and ground effect.

Obstacle 3

A circular element with the following dimensions presented in Figure 41:

- Diameter: 2 feet.
- Height: 7 feet.

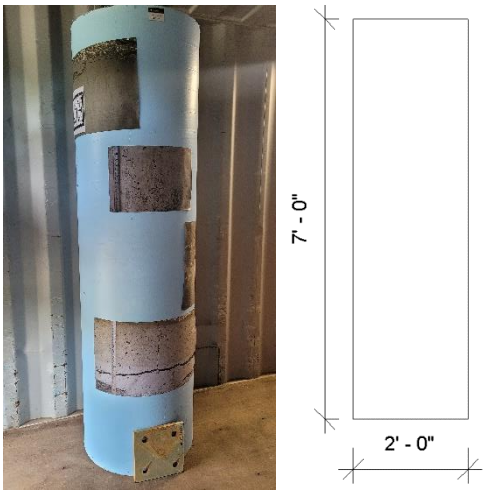

Figure 41 3D Illustration and front view of Obstacle 3.

A tube shape representing circular slender and tall structures, such as towers, signal and luminaire structures. Obstacle 3 also represents the shape of circular columns, piers, and circular foundations. For that purpose, several pictures from Appendix A have been selected and placed along the face of the obstacle depicting concrete defects and located at different levels following the path of the round surface.

Obstacle 4

A box element with the following dimensions presented in Figure 42:

- Internal width: 3 feet 4 inches.
- External width: 4 feet.
- Height: 4 feet.
- Depth: 4 feet.

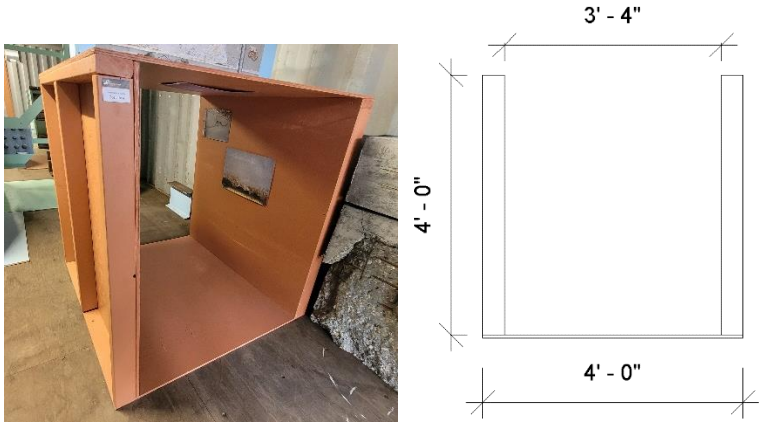

Figure 42 3D Illustration and front view of Obstacle 4.

The internal and external dimensions have been carefully determined to guarantee the minimum clearance distance presented in Chapter 3. For this research, the internal dimension is 3 feet 4 inches, the minimum permitted by surrounding effects.

Obstacle 4 represents a flight underneath structures short spans (less than 140 feet) and long spans (more than 140 feet). The main focus of the inspection on these elements is on defects on top and side faces where images from Appendix A have been located. The UAV will not have GPS signal inside the container but this obstacle adds another barrier to block any remaining signal.

Obstacle 5

A tall half-boxed element with the following dimensions presented in Figure 43:

- Internal width: 4 feet 4 inches.
- External width: 5 feet.
- Height: 6 feet.
- Depth: 4 feet.
- Gusset plate bottom base: 12 inches by 12 inches.
- Gusset plate top and bottom length: 12 inches.
- Gusset plate middle length: 16 inches.
- Gusset plate height: 18 inches.

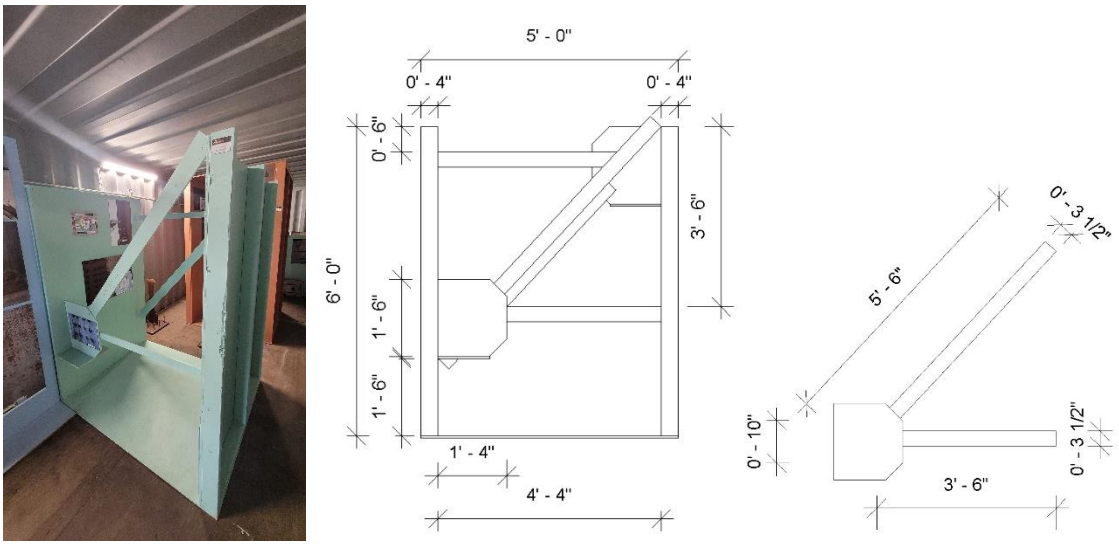

Figure 43 3D Illustration and front view of Obstacle 5

The external dimensions might vary depending on the material used but the internal dimensions are fixed due to clearance distance constraints.

Obstacle 5 represents truss bridges and any steel element located in the side faces of its structure. Inspection shall focus on defects in common areas and faces. The capability of the UAS to navigate and access various locations of the elements will be evaluated.

Obstacle 6:

A tall boxed element with the following dimensions presented in Figure 44:

- Internal width: 3 feet 4 inches.
- External width: 4 feet.
- Height: 7 feet.
- Depth: 4 feet.

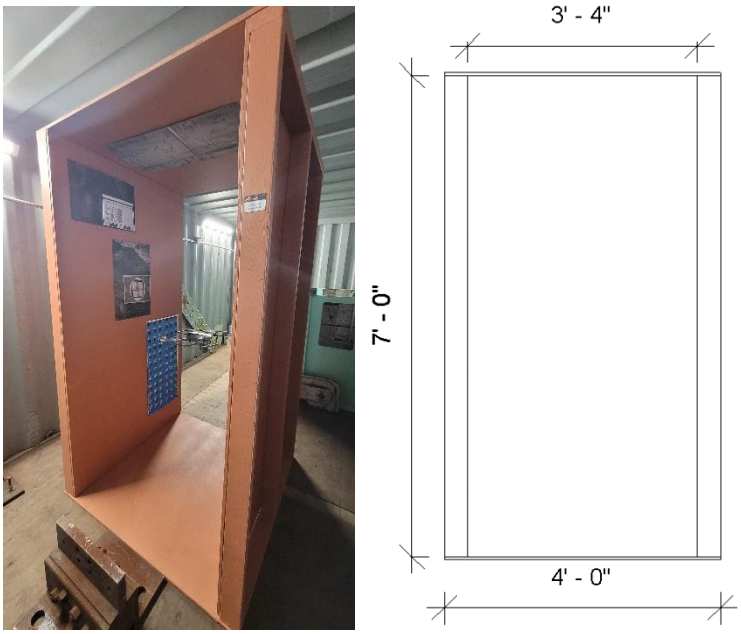

Figure 44 3D Illustration and front view of Obstacle 6

Obstacle 6 focuses on bridge elements in tall and box structures. The focus of the inspection in this obstacle is to test the skills of the pilot to fly between walls while gathering visual information of the printed images located on top and side faces. The internal and external dimensions have been carefully determined to guarantee the minimum clearance distance presented in Chapter 3.

Obstacle 7:

A half-closed element with the following dimensions presented in Figure 45:

- Internal width: 5 feet 6 inches.
- External width: 6 feet 2 inches.
- Height: 4 feet.
- Depth: 5 feet 6 inches.
- Diameter of the circular element: 2 feet.
- Height of the circular element: 4 feet (it will vary depending on the base, but the goal is to reach the same level of the overall obstacle).

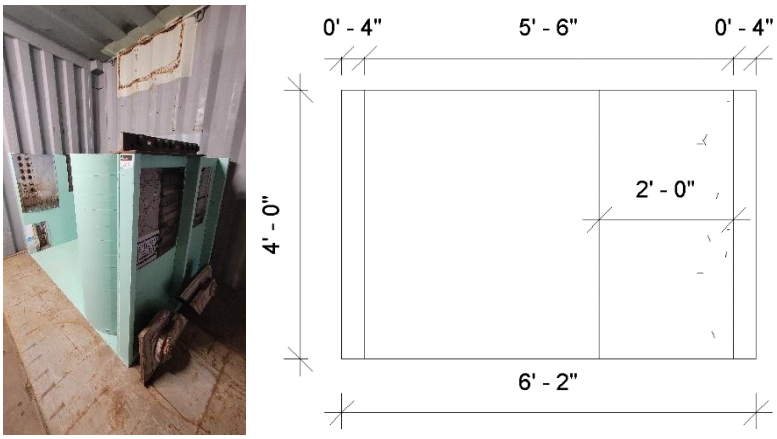

Figure 45 3D Illustration and front view of Obstacle 7

Obstacle 7 represents locations in structures where the pilot will not be able easily view the UAV, and in order to navigate in locations where line of sight is limited, the pilot needs to rely on real-time video, and their skills to maneuver the UAV. Pictures from Appendix A depicting damages of steel and concrete elements have been placed in the internal faces of the obstacle aiming to be difficult to reach in the horizontal direction if the camera keeps its original position (0° angle looking up measured from an imaginary lined formed by looking directly to an image located in front of the UAS and the direction where the camera is pointing), forcing the UAS to either maneuver closer to the faces of the obstacle or to change the angle of the camera.

4.2 Results and Comparison with Objectives of this Research Project

More than 20 flights have been performed inside the final configuration of the evaluation chamber using DJI Phantom 3 Pro and DJI Mavic 2 Pro as described in Table 2. Further, 10 additional flights (more than 30 adding to the ones mentioned before) including individual flights with obstacles of the course were performed to determine features, characteristics, dimensions, and locations of the designed obstacles. Those flights included a third UAV: ANAFI Thermal.

During the inspection flights performed inside the evaluation chamber, high-quality images were obtained from the obstacles and elements, allowing the inspector to determine with accuracy location and quantities of defects inside the container. Figures in section 4.2.5 present images of the elements analyzed.

In the flights performed along the final distribution of the evaluation chamber, the UAV finished the test providing high-quality images locating defects along the course. When the flights were performed inside the temperature range recommended by the manufacturer, no replacement of the battery was needed at the middle of the test. However, a battery change was required when the test was conducted outside the recommended temperature range of operation of the UAV, i.e., when the temperature dropped within 10°F below the 32°F lower limit recommended by the manufacturer. In all the flights executed, the clearance distance provided allowed adequate navigation across the obstacles.

GPS signal was not detected by any of the three UAVs used in this research project during any of the flights performed inside the container. Obstacle avoidance was deactivated for models Mavic and ANAFI, to allow close approach to the faces of the obstacles. Additional results according to objectives of this research work are explored in the next sections.

4.2.1 Evaluation Chamber Test

The evaluation chamber test was developed with dimensions presented in Figure 35, Figure 36, Figure 37, and Figure 38. A summary of the final obstacles is presented below. In the next pages, images of each obstacle and elements in the evaluation chamber are presented.

As detailed in the previous chapter, the dimensions of the obstacles are based on the concept of clearance distance of UAVs, proximity effects, and common shapes and features found on bridge structures presented in Chapter 3. Figure 46 to Figure 54 demonstrate the compliance with the first objective of the research project, which refers to the development of a repeatable test resembling inspection conditions.

Obstacle 1 is presented in Figure 46.

Figure 46 Obstacle 1 built.

Obstacle 2 is presented in Figure 47.

Figure 47 Obstacle 2 built.

Obstacle 3 is presented in Figure 48.

Figure 48 Obstacle 3 inside the container.

Obstacle 4 is presented in Figure 49.

Figure 49 Obstacle 4 built.

Obstacle 5 is presented in Figure 50.

Figure 50 Obstacle 5 inside the container.

Obstacle 6 is presented in Figure 51.

Figure 51 Obstacle 6 built.

Obstacle 7 is presented in Figure 52.

Figure 52 Obstacle 7 built.

The steel and concrete elements are located inside the evaluation chamber and presented in Figure 53.

Figure 53 Steel elements inside the evaluation chamber.

The final arrangement of the evaluation chamber from an outside view is presented in Figure 54.

Figure 54 Final arrangement of the evaluation chamber inside the container from outside view.

4.2.2 Location of Defects Inside the Evaluation Chamber

Defects have been placed along the faces of the evaluation chamber, from concrete to steel defects, and based on the gallery of images included in Appendix A. In the flight tests performed inside the evaluation chamber, images were obtained of the images printed following the requirements described in Chapter 3.

Some images are explored in section 4.2.5 to evaluate their quality in comparison with the original images, but others will be presented in the next sections to illustrate compliance with other objectives of this research project.

4.2.3 Addressing Challenges and Constraints Identified in this Project about UAS Inspection

GPS-denied Environment

None of the flights performed inside the evaluation chamber registered GPS signal. The absence of GPS signal was checked on the screen of the controller, as presented in Figure 55, located with a red circle where a sign of GPS signal would appear if it is detected.

Figure 55 Absence of GPS signal confirmed in the screen of the controller of the UAV.

A second way to confirm the absence of GPS signal is described in the next paragraph.

The container and the evaluation chamber are located inside S-BRITE at Purdue University. The research facility is positioned inside a no-flight zone (NFZ) for being within a 5-mile radius to Purdue Airport, and labeled as "Class D airspace" by FAA. To flight inside an NFZ, the pilot must request permission to FAA or the nearest tower available. The zone around the research facility is presented in Figure 56, where S-BRITE is marked with a yellow star and color lines show the proximity of the surrounding areas around Purdue Airport, where the color red shows the 5-mile radius around the airport, and colors yellow and green are outside of this radius.

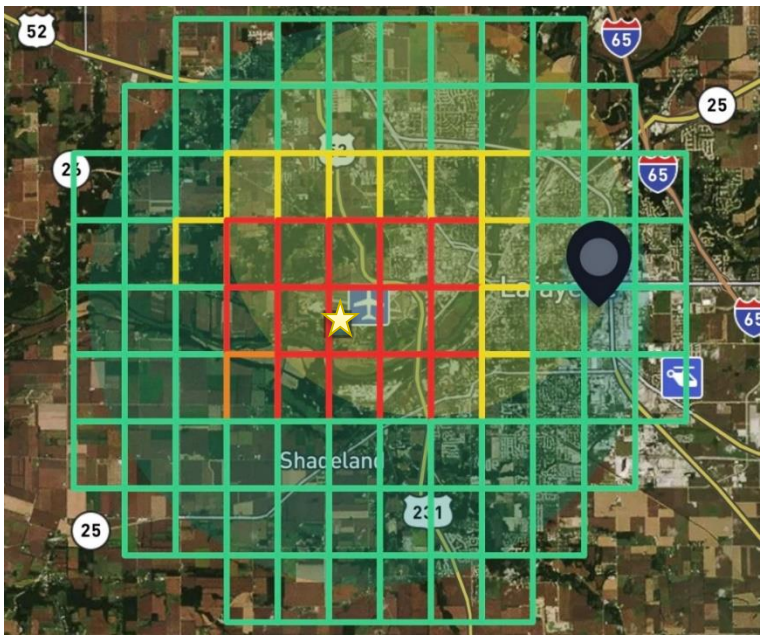

Figure 56 No-flight zone around Purdue Airport, showing West Lafayette and Lafayette cities, and S-BRITE is presented with a star shape.

When an UAV takes off, immediately receives GPS information and the system compares the location to the no-flight zones provided by FAA, like the one presented in Figure 56. If the UAV takes off inside a no-flight zone and permission has not been granted for the UAV to fly within

that zone, the UAV stops the flight and lands itself. But if the UAV takes off in a place where GPS information is not accessible, even if the location is within NFZ, the UAV is able to fly as long as the location continues to block GPS signal. This reasoning was used as a clear indication to check if GPS is blocked inside the evaluation chamber. As a result, since none of the flights performed inside the evaluation chamber forced the UAV to land itself, the author concludes that the evaluation chamber provides an adequate block for GPS signal.

Wind and Lighting-Controlled Conditions

To present a comparison of the results in terms of environmental conditions, local climatological data was obtained from the National Oceanic & Atmospheric Administration (NOAA) and National Centers for Environmental Information (NCEI). The station used to obtain climatological information was 'Lafayette Purdue University Airport' due to its closeness to S-BRITE, less than 1 mile (3900 feet), where the evaluation chamber is located. The exact location of the station is 40.41222°, -86.93694°; with station ID: WBAN:14835, and presented in Figure 57, where the location of the evaluation chamber is located in a red circle, and the weather station is presented in a blue circle.

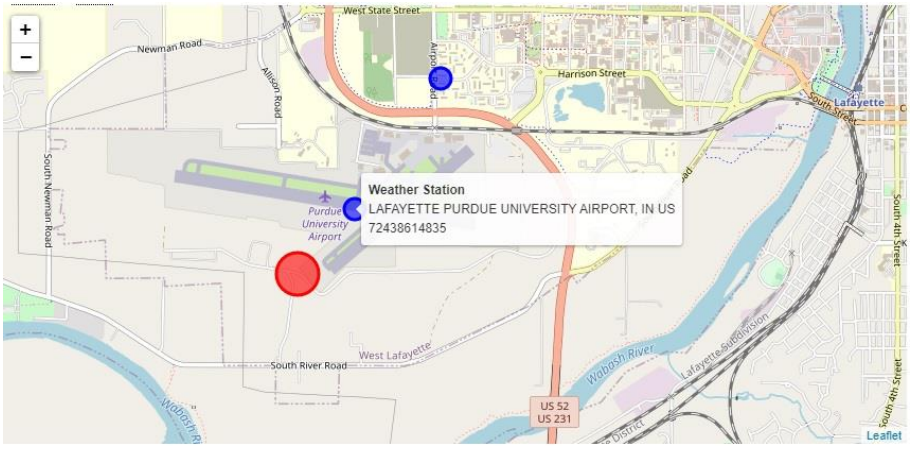

Figure 57 Location of weather station at Purdue Airport with respect to S-BRITE.

Several flights were performed inside the evaluation chamber, and the relevant ones in terms of climatological data are summarized in Table 4 to show the variation of environmental conditions in different months and their effect in the evaluation chamber. From Table 4, Column 1 and 2

present the date and start time of the flight. Column 3 to 6 were obtained from the records of the station described. Column 3 is the time when the information was recorded. Column 4 is the sky condition at the time in Column 3. Column 5 is the wind speed in mph recorded in the station. Column 6 is the ambient temperature, recorded as dry bulb temperature (NOAA/NCEI, 2021).

Table 4 Local Climatological Data from station located at Purdue Airport from NOAA/NCEI database for selected flights on this research.

Date of flight	Start time of flight	Registered time	Sky conditions	Wind speed (mph)	Dry Bulb Temperature (F)
11-30-20	14:24	14:54	Overcast	20	34
12-04-20	10:03	09:54	Clear sky	7	38
12-17-20	10:14	09:54	Broken clouds	3	32
01-20-21	14:35	14:54	Clear sky	14	33
02-05-21	13:06	13:03	Scattered clouds	20	26
02-12-21	12:40	12:54	Few clouds	10	25
03-01-21	16:25	16:54	Scattered clouds	11	40
03-24-21	12:48	12:54	Broken clouds	16	66
04-02-21	12:16	12:54	Clear sky	5	48

From the table, sky conditions varied from clear sky to overcast, presenting different lighting conditions to the area. To guarantee the replicability of the results, LED lights were installed along the elements and they are turned on during the experiment. When flying along the evaluation chamber, two scenarios were explored: when the doors of the container were opened and when they were closed. Figure 58 presents an image from flight on 04-02-21 (clear sky) with the doors closed. Figure 59 presents an image from flight on 03-01-21 (scattered clouds) with the doors opened. Both images reflect the same visual results with the defect visible and with no loss of quality, pointed with a red arrow in both images. Similar results were observed with other flights in both conditions: container door opened and closed, showing that none of the sky conditions affected the images obtained inside the evaluation chamber.

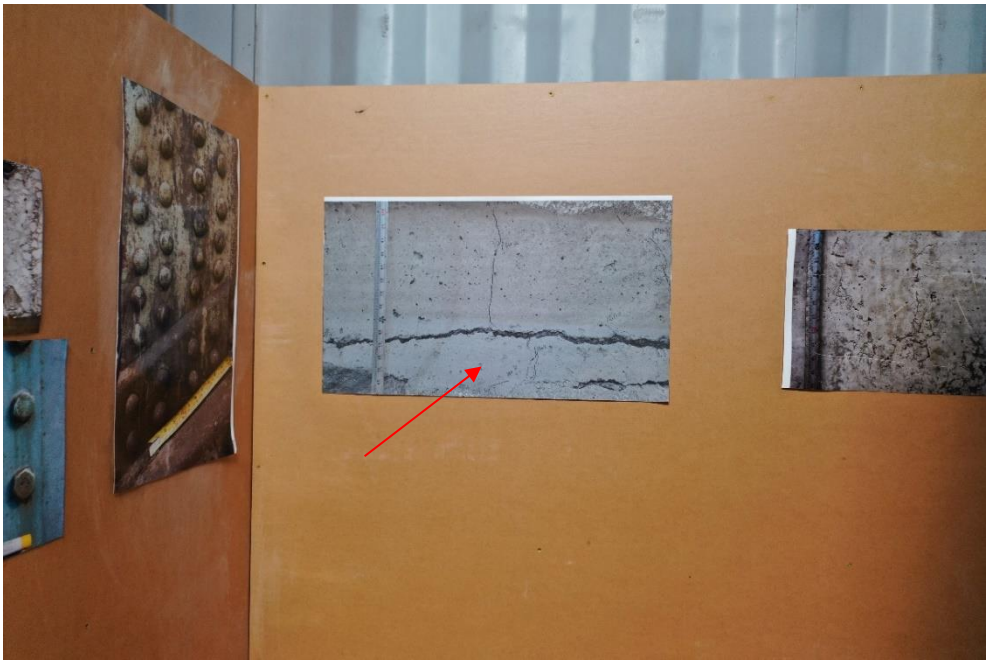

Figure 58 Image from flight on 04-02-21 (clear sky) with the doors closed from Obstacle 7.

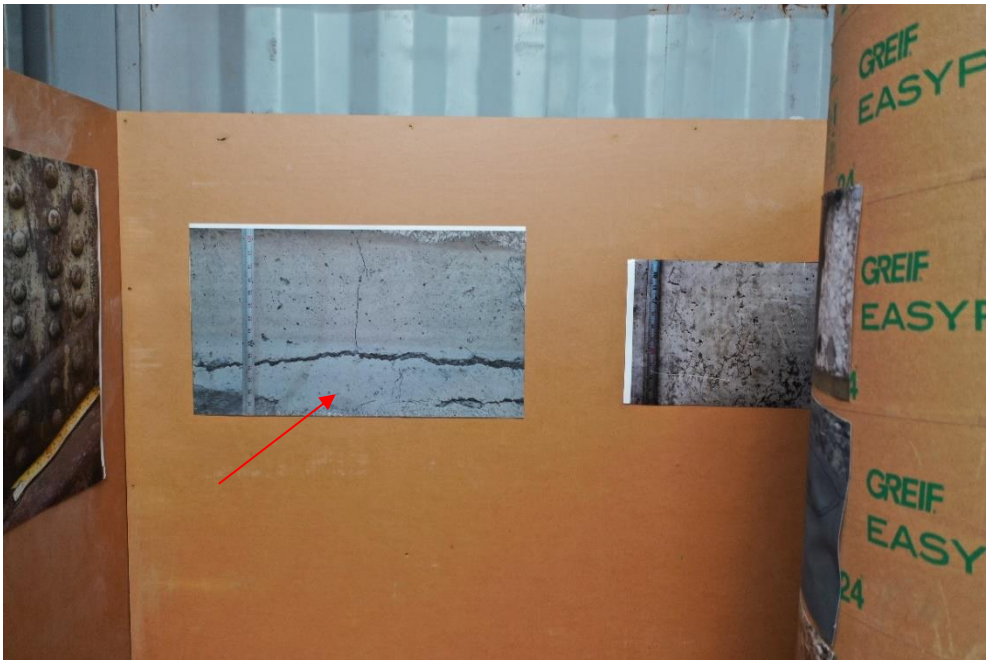

Figure 59 Image from flight on 03-01-21 (scattered clouds) with the doors open from Obstacle 7.

Wind speed in Table 4 varied from 3 mph to 20 mph. But none of the flights reported an effect of outside wind in the stability of the UAV while flying or hovering inside the evaluation chamber. The faces of the container protected the UAV and the obstacles from gust and wind, avoiding disturbances to UAV performance during the tests.

Finally, ambient temperature affected the duration of the battery of both the controller and the UAV. Shorter times of flight (around 15 min) were recorded on low temperatures, such as 25 °F from Table 4, compared to the average duration of a flight (around 25 min) when flying close to 38 – 48 °F temperatures. In that case, the methodology presented in Chapter 3 for battery requirements was applied, guaranteeing a successful completion of the flight.

Line of Sight

Line of sight is directly available to the pilot in the elements at the start of the evaluation chamber and Obstacle 2, and 3 as observed in Figure 61. With the progress of the test, Obstacles and elements limit the visual range of the pilot, as in a typical bridge inspection. The availability of line of sight is depicted in Figure 60, where the evaluation chamber has been divided by a scale of three colors: green, where the pilot can see the obstacles directly (with their eyes and no need to use any visual information from the controller); yellow, where the pilot can partially see the elements in the evaluation chamber; and red, where the elements are positioned in limited line-of-sight environment, meaning that the pilot will have to rely on the images and video provided in the controller to navigate and perform the inspection of that obstacle. A scale of line-of-sight availability inside the evaluation chamber has been provided at the bottom of Figure 60. This figure was obtained by performing observations at the entrance of the container, by dividing the container in 5 sections and determining an approximate percentage of objects and areas a visual observer is able to see from each section. Later, the percentage in each area was represented by a color obtaining Figure 60.

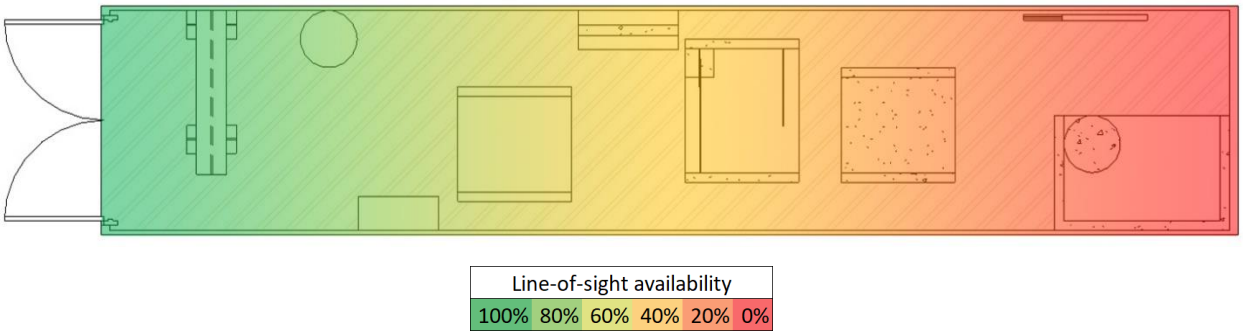

Figure 60 Line of sight availability inside the evaluation chamber with color scale.

Figure 61, Figure 62, and Figure 63 provide arrows with three colors: green, yellow, and red, following the same color scale presented in Figure 60. Line of sight is partially available in Obstacle 1, 4, 5 and 6, as presented in Figure 61 and Figure 62. Finally, the goal and location of Obstacle 7 is to fully block line of sight, as presented in Figure 63. The scale on line-of-sight availability provided in Figure 60 and the absence in view of Obstacle 7 in Figure 61 proves that the goal was achieved.

High-quality images and successful completed flights were obtained inside the current arrangement of the evaluation chamber, complying with an objective of this research: adequate design that tests no-line-of-sight environment while being able to obtain high-quality visual data information.

Figure 61 Distribution of Line-of-Sight environment at the entrance of the evaluation chamber

Figure 62 Distribution of Line-of-Sight environment inside the evaluation chamber

Figure 63 Location of Obstacle 7 blocking line of sight.

4.2.4 Minimum Requirements and Guidelines Fulfilled Before the Start of the Test

A set of minimum guidelines and requirements was developed for the evaluation chamber, presented in Chapter 3, and summarized as follows: verification of two fully-charged batteries, verification of a fully charged controller, absence of GPS signal, 12-megapixel camera.

From the situations and information collected of the flights performed inside the evaluation chamber, and details mentioned in past sections, the requirements were followed and allowed to have a complete and uninterrupted flight inside the evaluation chamber.

4.2.5 High-quality Visual Data Information

In the next pages, some figures have been selected to portray the high-quality images that have been obtained inside the evaluation chamber. First, images were obtained from steel and concrete elements in S-BRITE and Bowen Laboratory at Purdue University with defects on their faces. Second, the images were printed following the methodology detailed in Chapter 3. Printed images were distributed in the faces of the obstacles in locations detailed in the last section of Chapter 3. Finally, UAV inspection was performed along the evaluation chamber to capture defects on images. A comparison is presented in the next pages. The original is presented first followed by

an image of the image obtained by the UAV. The resolution charts found in some of the figures will be addressed in the final section this chapter. The names of the Exhibit in each figure follow the numbering in Appendix A. Arrows and circles have been placed to show the appearance of the defect in each image.

Figure 64 presents the original image inside the evaluation chamber and Figure 65 presents the image obtained during UAS inspection.

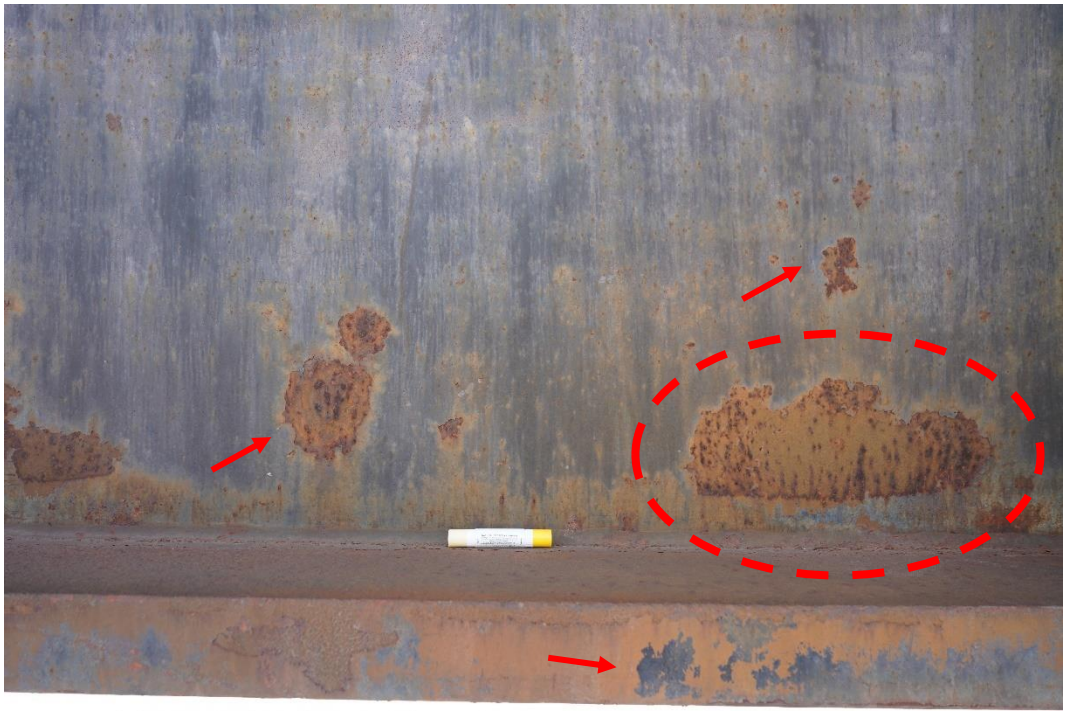

Figure 64 Exhibit 5757 of steel element.

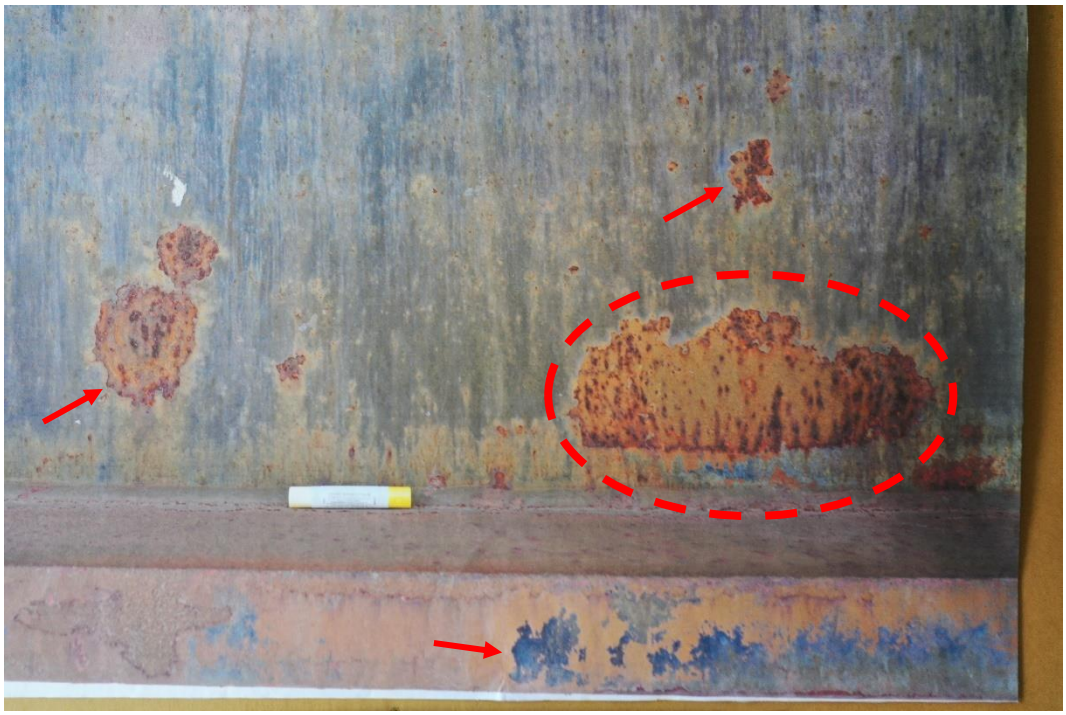

Figure 65 UAS inspection of Exhibit 5757.

Figure 66 presents the original image inside the evaluation chamber and Figure 67 presents the image obtained during UAS inspection.

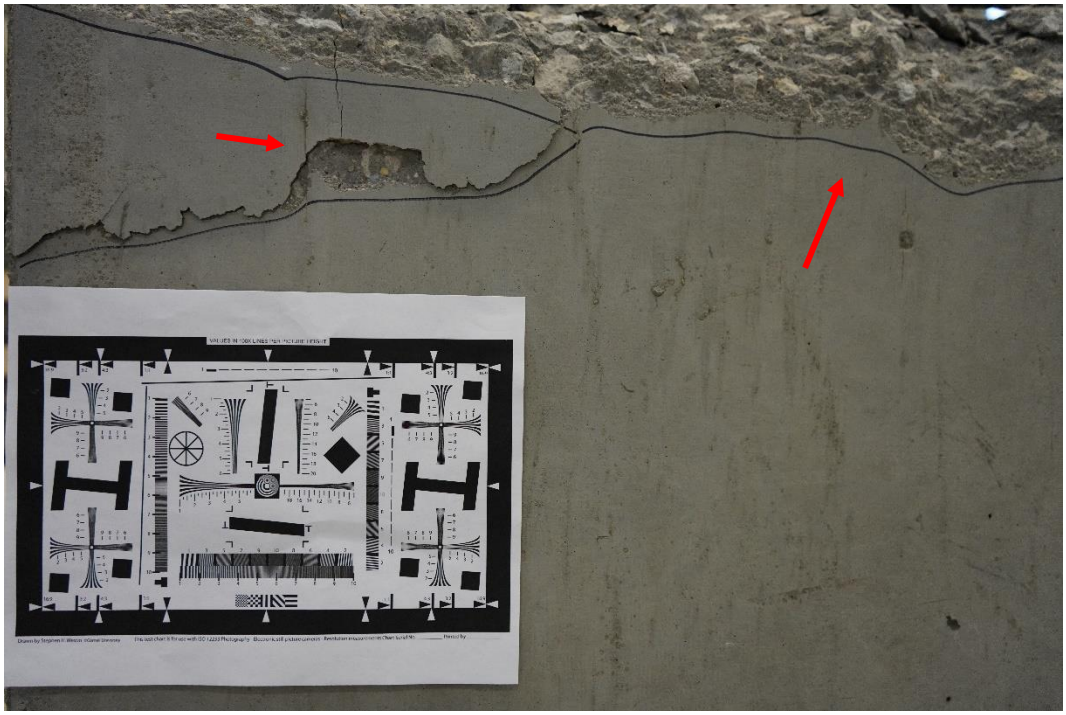

Figure 66 Exhibit 5501 of concrete element.

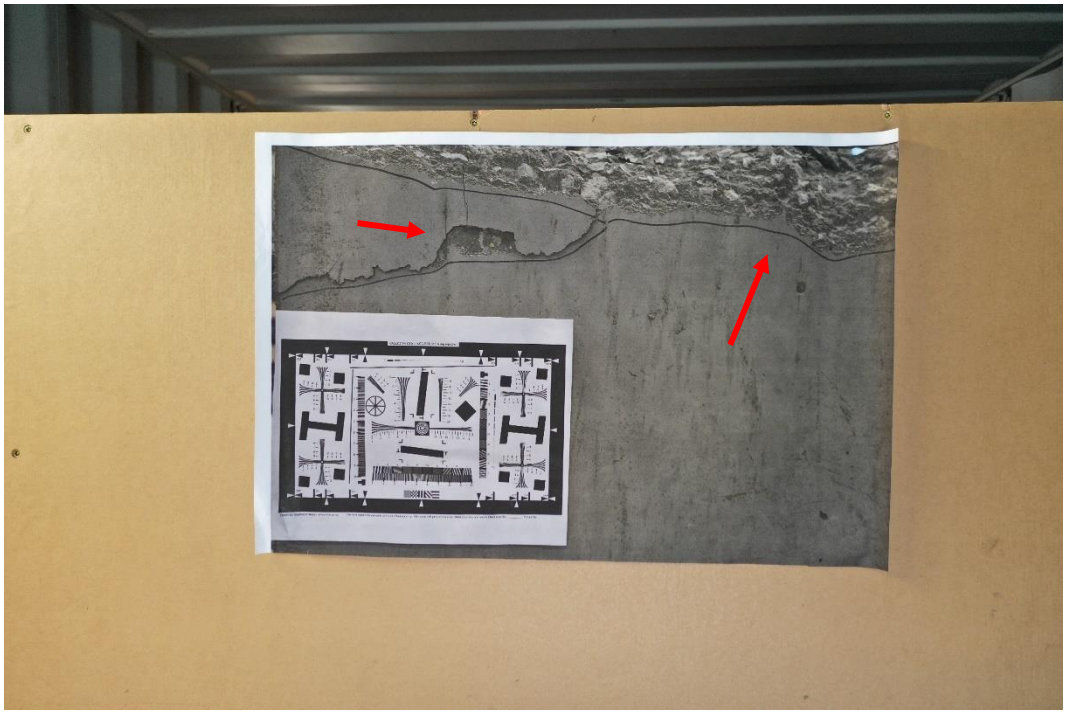

Figure 67 UAS inspection of Exhibit 5501.

Figure 68 presents the original image inside the evaluation chamber and Figure 69 presents the image obtained during UAS inspection.

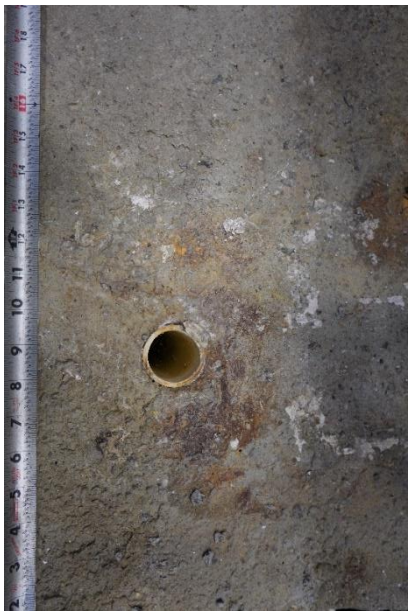

Figure 68 Exhibit 5538 of concrete element.

Figure 69 UAS inspection of Exhibit 5538.

Figure 70 presents the original image inside the evaluation chamber and Figure 71 presents the image obtained during UAS inspection.

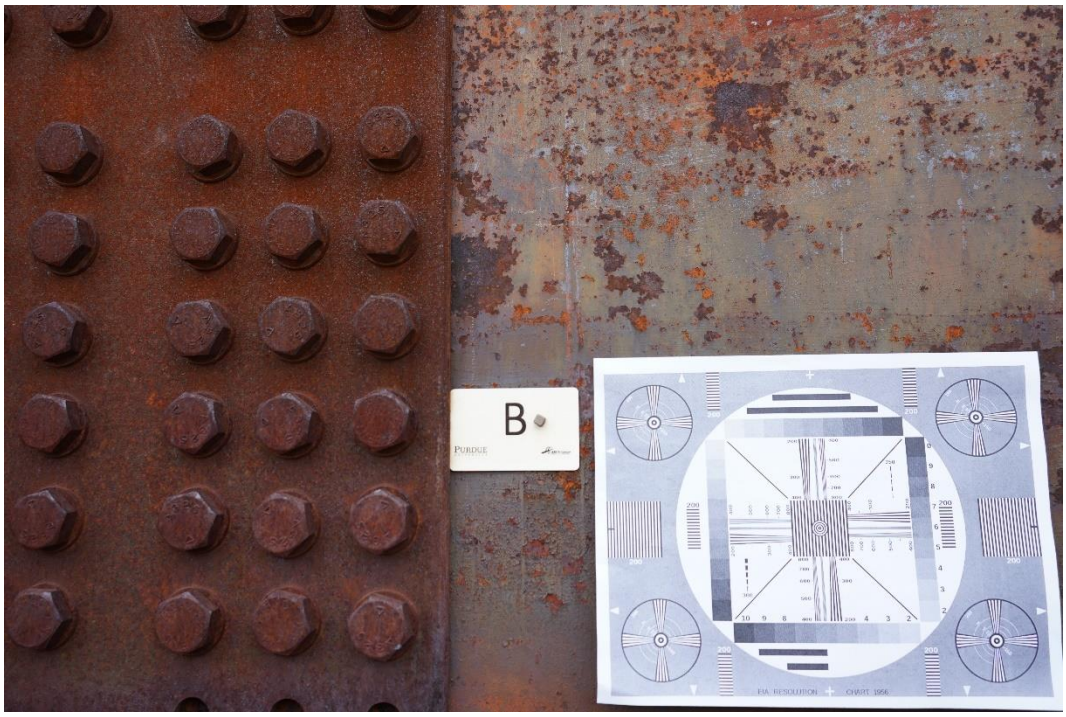

Figure 70 Exhibit 5605 of steel element.

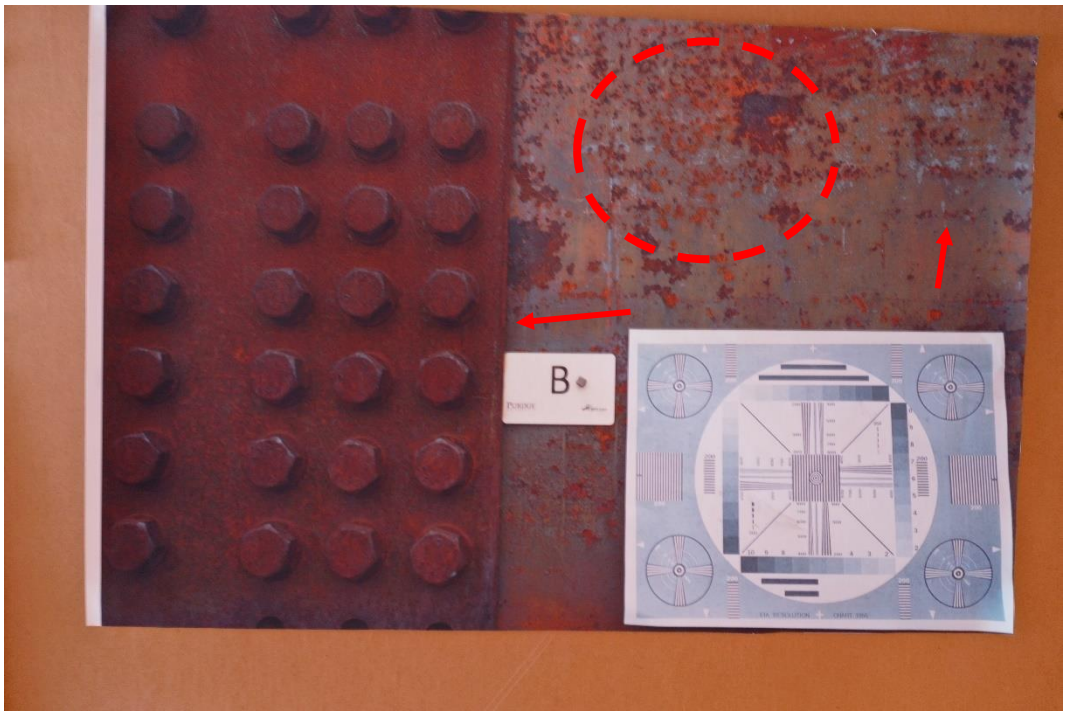

Figure 71 UAS inspection of Exhibit 5605.

Figure 72 presents the original image inside the evaluation chamber and Figure 73 presents the image obtained during UAS inspection.

Figure 72 Exhibit 5803 of steel element.

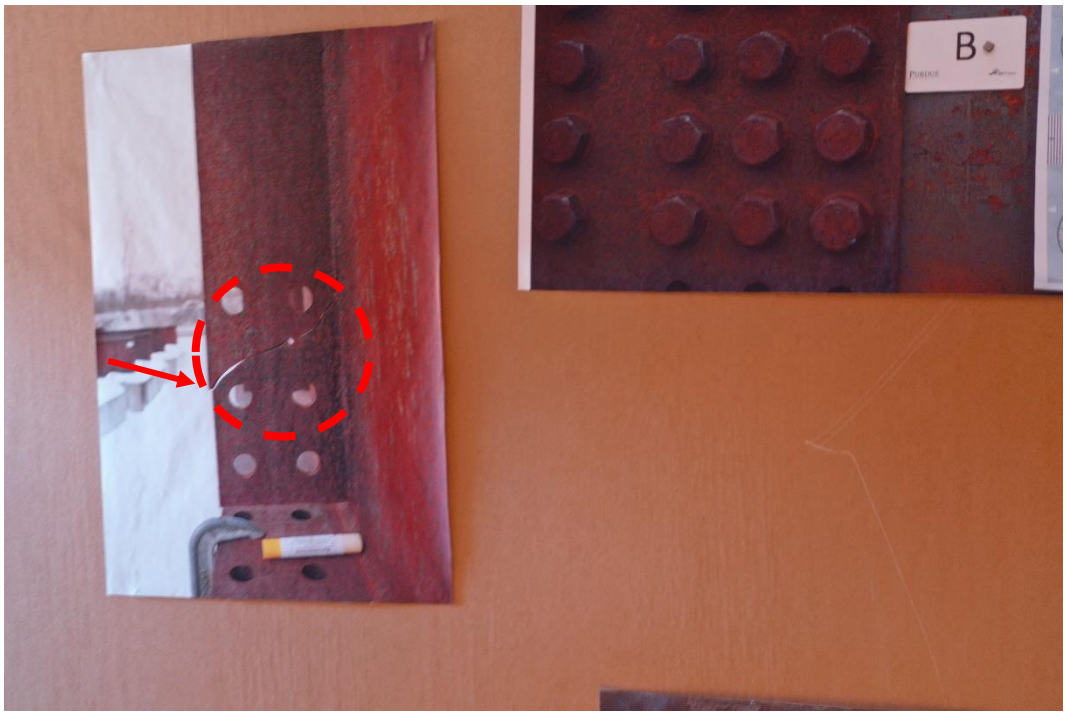

Figure 73 UAS inspection of Exhibit 5803.

Figure 74 presents the original image inside the evaluation chamber and Figure 75 presents the image obtained during UAS inspection.

Figure 74 Exhibit 1516 of concrete element.

Figure 75 UAS inspection of Exhibit 1516.

Figure 76 presents the original image inside the evaluation chamber and Figure 77 presents the image obtained during UAS inspection.

Figure 76 Exhibit 5603 of steel element.

Figure 77 UAS inspection of Exhibit 5603.

Figure 78 presents the original image inside the evaluation chamber and Figure 79 presents the image obtained during UAS inspection.

Figure 78 Exhibit 5635 of steel element.

Figure 79 UAS inspection of Exhibit 5635.

Figure 80 presents the original images inside the evaluation chamber and Figure 81 presents the image obtained during UAS inspection.

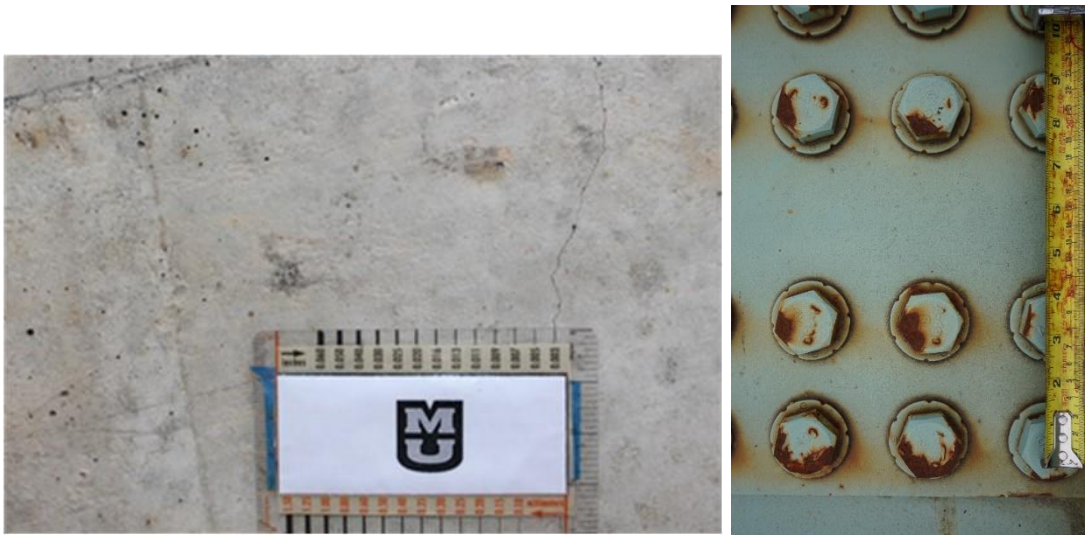

Figure 80 Exhibit 0101 (left) of concrete element (American Association of State Highway and Transportation Officials, 2019) and Exhibit 5678 (right) of steel element.

Figure 81 UAS inspection of Exhibit 0101 and 5678.

Figure 82 presents the original image inside the evaluation chamber and Figure 83 presents the image obtained during UAS inspection.

Figure 82 Exhibit 1518 of concrete element.

Figure 83 UAS inspection of Exhibit 1518.

Figure 84 presents the original images inside the evaluation chamber and Figure 85 presents the image obtained during UAS inspection.

Figure 84 Exhibit 5550 (left) of concrete element and Exhibit 5786 (right) of steel element.

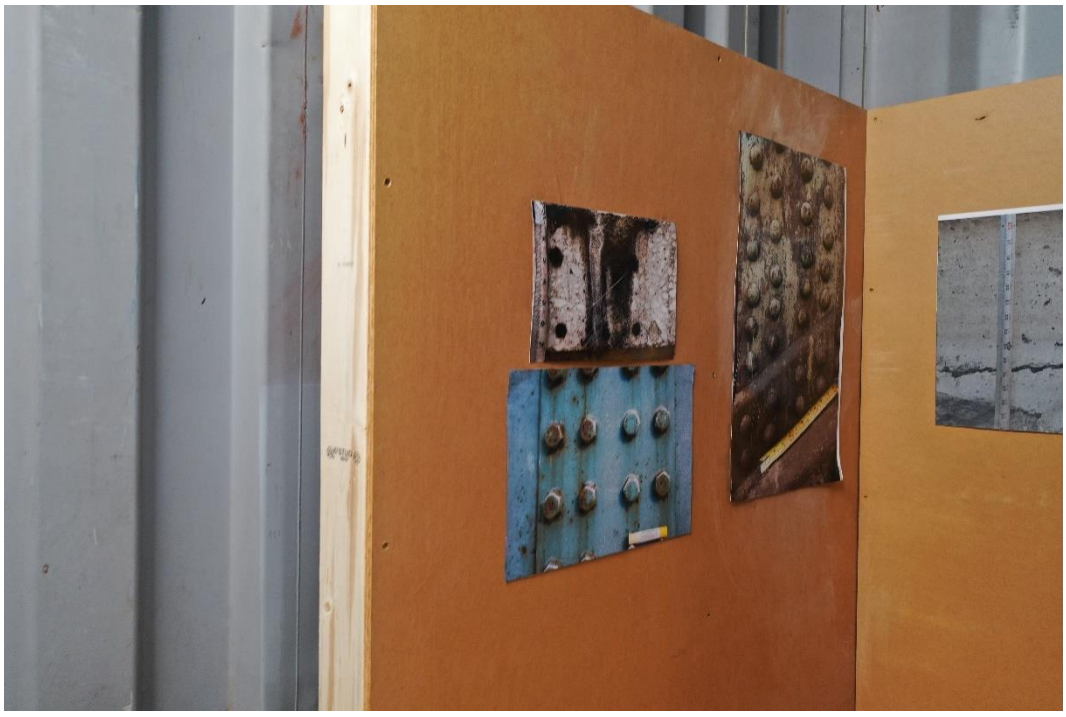

Figure 85 UAS inspection of Exhibit 5550 and 5786.

Figure 86 and Figure 87 present the original images inside the evaluation chamber and Figure 88 presents the image obtained during UAS inspection.

Figure 86 Exhibit 5564 of concrete element.

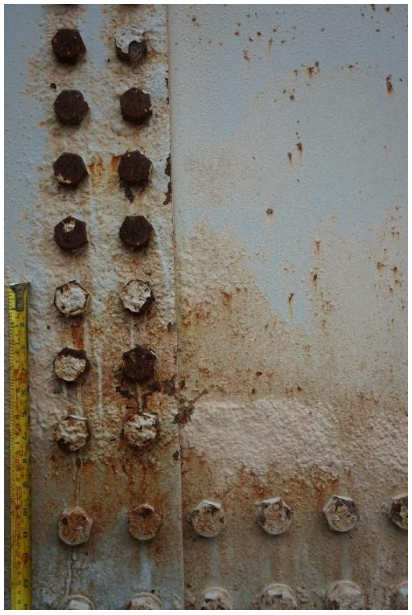

Figure 87 Exhibit 5656 of steel element.

Figure 88 UAS inspection of Exhibit 5564 and 5656.

Figure 89 presents the original image inside the evaluation chamber and Figure 90 presents the image obtained during UAS inspection.

Figure 89 Exhibit 5619 of steel element.

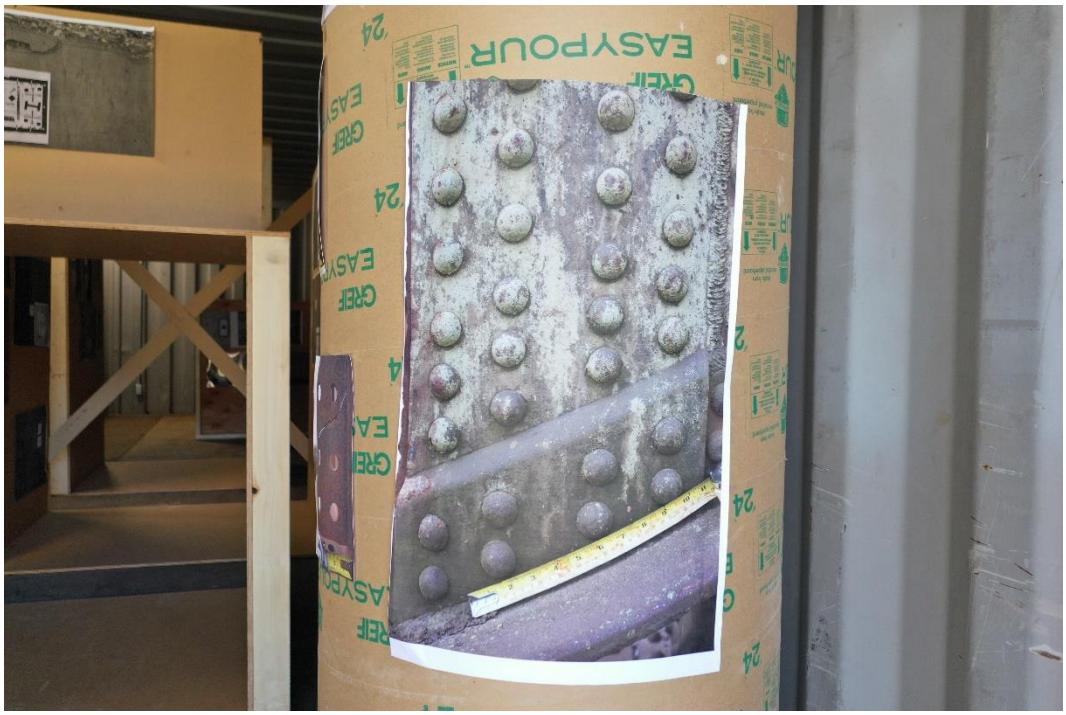

Figure 90 UAS inspection of Exhibit 5619.

Figure 91 presents the original image inside the evaluation chamber and Figure 92 presents the image obtained during UAS inspection.

Figure 91 Exhibit 1527 of concrete element.

Figure 92 UAS inspection of Exhibit 1527.

Figure 93 presents the original image inside the evaluation chamber and Figure 94 presents the image obtained during UAS inspection.

Figure 93 Exhibit 5675 of steel element.

Figure 94 UAS inspection of Exhibit 5675.

In the next pages, high-quality images are presented for steel elements located inside the container. In Figure 95 and Figure 96, defects are easily located from the images obtained, and the most relevant ones are presented with red arrows.

Figure 95 UAS inspection of steel elements.

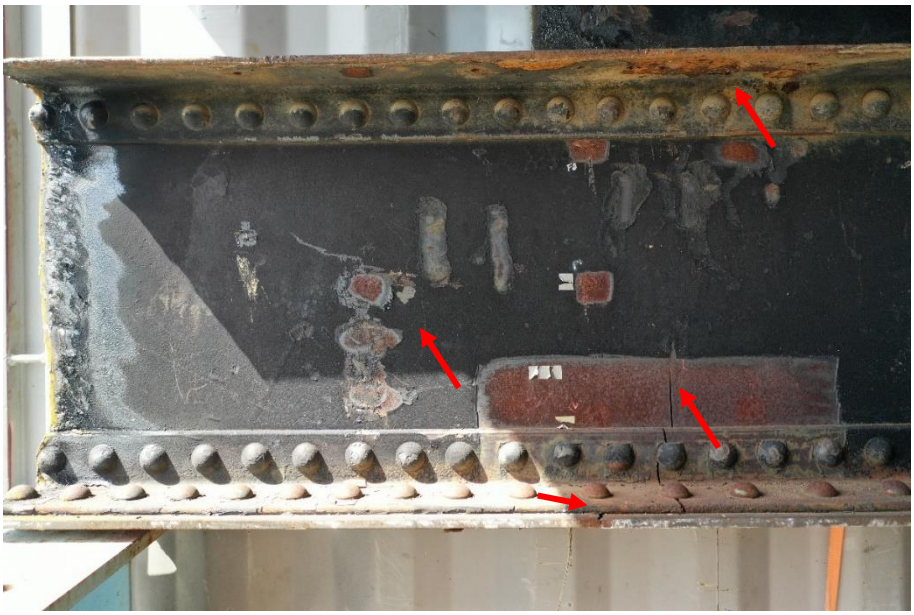

Figure 96 UAS inspection of steel elements.

Figure 97 has been overexposed due to the change of lighting from the left side to the right side of the girder. However, information is not lost. With the use of an image editor, contrast has been adjusted to -100, exposure to 100, and shadows to 100, obtaining Figure 98, where a significant defect in terms of size missed in Figure 97 is now visible and presented in red arrows.

Figure 97 UAS inspection of steel elements.

Figure 98 UAS inspection of steel elements, enhancing to see defects hidden by shadows.

A crack was identified with the images obtained during inspection in the steel element from Figure 99 and Figure 100, presented with a red arrow in both images.

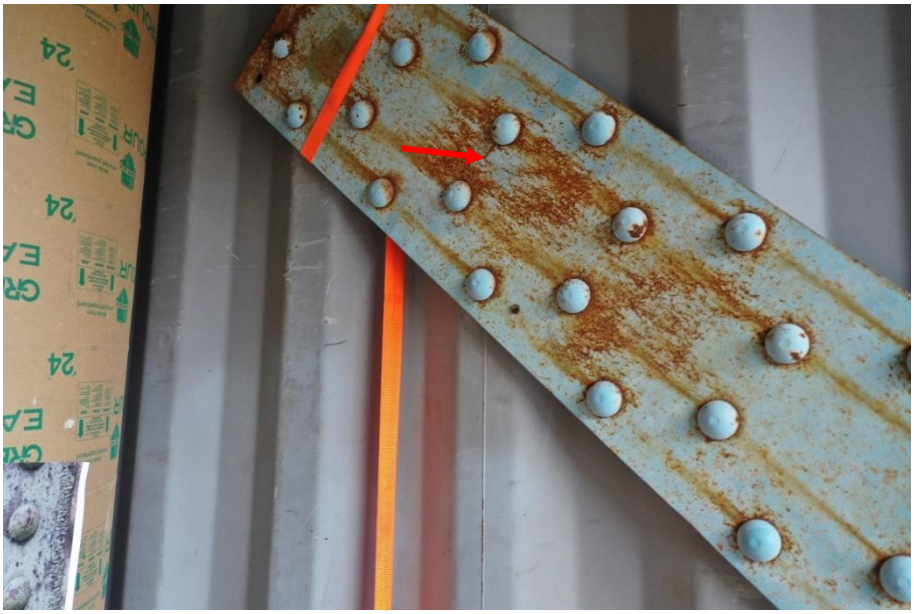

Figure 99 UAS inspection of steel elements.

Figure 100 UAS inspection of steel elements.

Finally, an objective and quantitative method to analyze quality of images was introduced in three obstacles in the form of resolution charts, presented in the last section of this chapter.

4.2.6 Resolution Charts

As a final verification of the quality of the images obtained inside the evaluation chamber, three resolution charts were located in the original images and as a result appeared in the images printed and placed inside the evaluation chamber. Each goal of the resolution charts is described below. Notice that only relevant analysis for this research was conducted with the resolution charts as described in each section.

2008 Bob Arkings Resolution Chart

2008 Bob Arkings is a lens testing chart to verify optimal characteristics of the lens from the camera used in the UAV to obtain the images during the UAS inspection. For Mavic 2 Pro, the sensor of the camera is 35 mm wide and contains 5472 pixels across the width (DJI, 2018).

Following the procedure detailed by the author of the test (Atkins, 2017): first, the magnification factor of the images is determined, calculating the distance of the bottom line of the chart in pixels. For Figure 101, distance of bottom line is 1403 pixels. Applying the following expression using lens dimensions: (1403 / 5472) * 35 mm = 8.974 mm; and dividing 100 by that value, the magnification factor is obtained as: 100 / 8.974 = 11.14 x.

Second, an analysis of the left side of the chart is performed to determine the finest set of line patterns which are resolved, i.e., lines that are clearly defined. Up to 2.8 (2.8 lp/mm, or line pairs per mm) is very well resolved, as presented with the red arrow on Figure 101. The resolution is obtained by multiplying the finest set of line pattern resolved by the magnification factor: 2.8 x 11.14 = 31.19 lp / mm.

The camera is 20M of resolution, as presented in Chapter 3. The quality of the lens is considered appropriate if the resolution obtained is greater than the resolution of the camera. Since 31.19 > 20, the lens applied is appropriate for taking pictures inside the evaluation chamber and the images obtained are adequate.

A visual assessment is performed at the bottom of the chart. At the design magnification factor of 11.14 x, the text ‘A Block of Text’ is visible, as presented with the blue arrow on Figure 101, confirming the quality of the lens and lighting conditions.

The last analysis is performed in the ‘Siemens star pattern’ shown by the green arrow on Figure 101, a pattern of alternating black and white segments in star shape. As a general rule: the higher the resolution of the lens generating the pattern in the image, the closer to the center of the star they will appear to merge. In Figure 101, the lines are clearly defined and visible until the black circle. By visual assessment, the images obtained present a high resolution with an adequate lens.

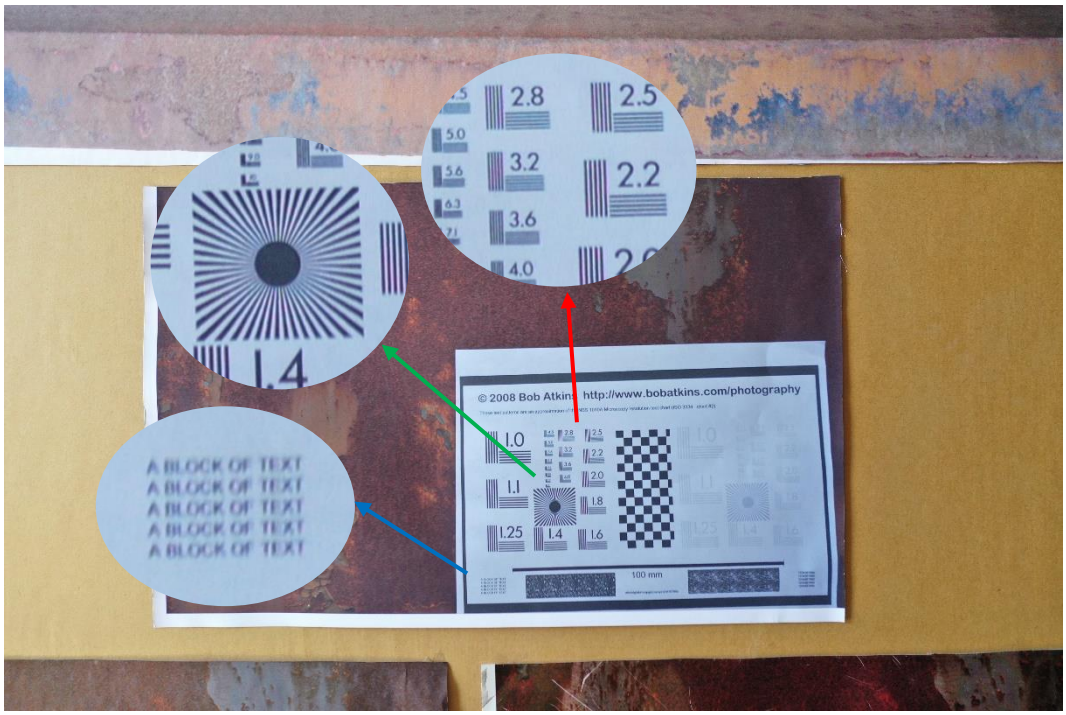

Figure 101 Exhibit 9999 with 2008 Bob Atkins resolution chart inside evaluation chamber.

ISO 12233 Resolution Chart

General visual assessments were performed for the resolution chart presented in Figure 103, to analyze sharpness, chromatic aberration and distortion (Carnathan, n.d.). First, to analyze for sharpness, the red arrow in Figure 103 shows one of the elements prepared to detect ‘stair’ stepping, i.e., line with straight edge. The less the stepping, the better the sharpness of the lens of the camera. 6 steps are visible in the image, which denote a medium quality of the image. For sharpness in

curved details, the pattern presented by a blue arrow in Figure 103 is used. The lines are revolved up to level 3 and start to merge at 4, providing again a medium quality of image.

For chromatic aberration, the image was printed in black and white and as a result, no other color should appear on the image. No other color than black and white have been detected in the resolution chart of Figure 103 by simple observation. This was confirmed by using a software that generates image histograms as presented in Figure 102 for the resolution chart from Figure 103. An image histogram shows how pixels are distributed within an image, where the far left represents blacks or shadows and the far right represents whites or highlights. The histogram shows a clear accumulation on both the left side and the right side of the plot, portraying the strong presence of both colors. The wider area of the bars on the right side compared to the ones on the left side shows the number of white/highlights pixels is greater than black/shadows pixels.

The percentages of color from the original resolution chart were: black 32%, white 57%, and others or not detected 11%. The percentages of color from the image taken by the UAS of the resolution chart of Figure 102 were: black 28%, white 56%, and others or not detected 16%. Minimum variation in percentages of black and white means that no other colors have been significantly introduced by the UAS camera, so no aberration is detected.

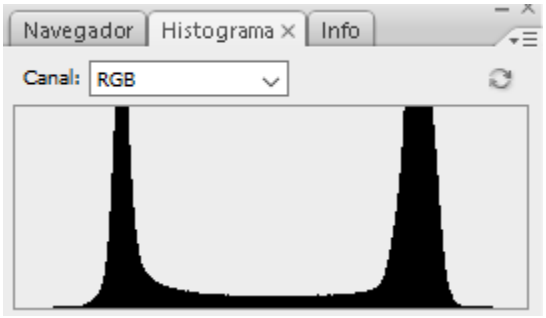

Figure 102 Image histogram for the resolution chart from Figure 103.

Finally, for distortion, the elements presented with the green arrow in Figure 103 are analyzed. The lines are resolved in up to level 6, showing a medium level of distortion of fine details. This led to the conclusion that the quality of the image is medium, appropriate to general applications

in image inspection. Other details of the resolution chart have not been analyzed because they are not relevant to this research work.

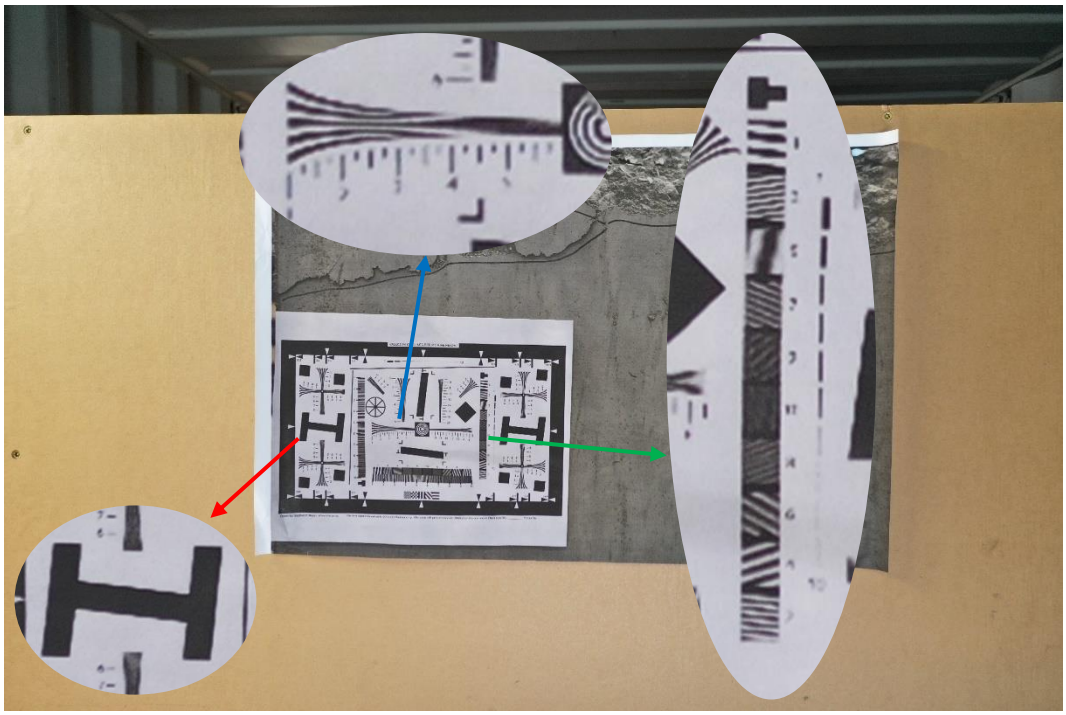

Figure 103 Exhibit 0009 with ISO 12233 resolution chart inside evaluation chamber.

EIA Resolution Chart 1956

Finally, a simpler resolution analysis is obtained with EIA chart (Beale, 2011). The regularity of the four circles at the corners of the chart presented with a red arrow in Figure 104 shows the appropriate point of view that the image was taken, meaning that there is no major variation on dimensions in the picture and dimensions can be safely inferred using a reference element in the same picture such as a measuring tape.

The lines on the sides of the chart are resolved, showing that the image has at least 200 lines of resolution (200 dpi: dot per inch), as presented with the blue arrow in Figure 104. However, the lines continue to be resolved up to 400 dpi, as presented with the green arrow in Figure 104. At 500, they start to merge, so the general resolution is assumed as 400 dpi. For a standard high-quality image, 300 or more is desired, which in comparison with 400 dpi obtained in this picture, it can be concluded that the quality complies with the minimum requirements.

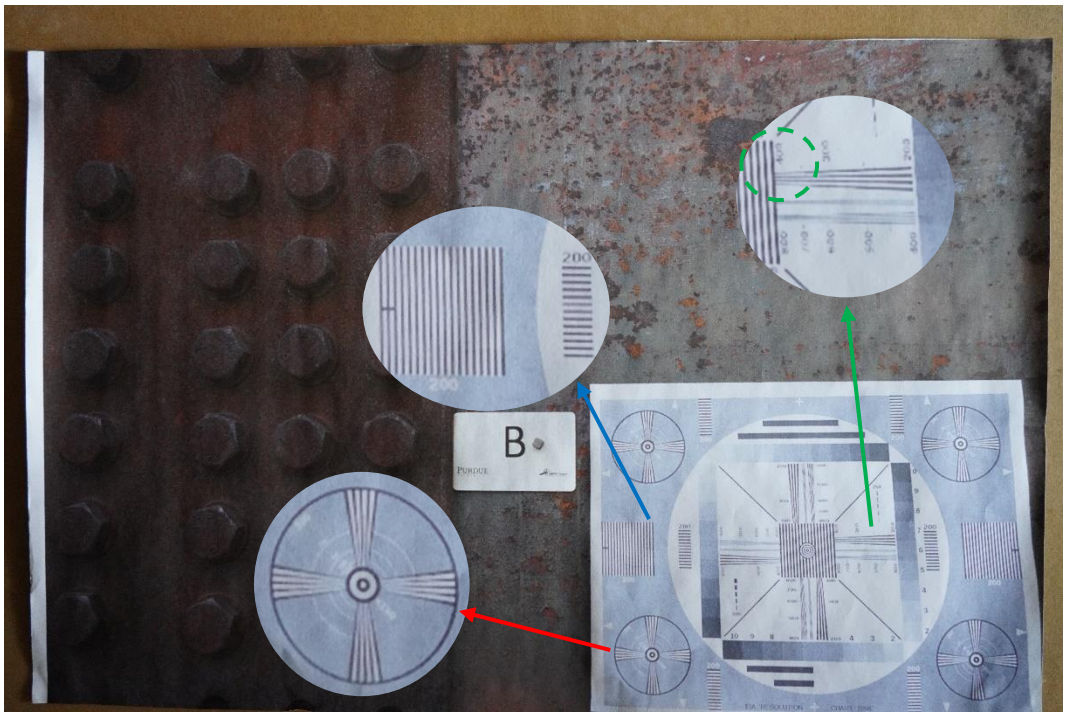

Figure 104 Exhibit 5735 with EIA Resolution Chart 1956 inside evaluation chamber.

5. DISCUSSION

In this research, the evaluation chamber that allows to provide a method for prequalification to a given UAS has be developed. The evaluation chamber presents 7 obstacles that represent different common components of bridge structures. In general, the obstacles represent tall, slender, long-span, and difficult to reach structures. The course also provides steel and concrete elements to test the ability of the UAS to identify and quantify defects on real structures. In addition, the use of simulated defects using images was explored and found to be a reasonable method to ensure a consistent testing environment is maintained when multiple test sites are developed.

Minimum requirements specified for the camera, battery life, and extra features help ensure data are collected in a format that allows the inspector to perform a reliable and continuous assessment of a structure during the test.

Through testing using real pilots and represented UAVs, this research has provided confidence that the concept of using a defined evaluation chamber is a reliable and effective way to test the following of a UAS:

- skills of the pilot,
- avoidance techniques of the pilot,
- navigation in enclosed environments,
- navigation in no-line-of-sight environments,
- evaluation of methods to gather visual information for inspection of civil engineering structures.

The skills of the pilot and their avoidance techniques were tested while maneuvering to each of the obstacles while gathering images of the elements to inspect. Navigation of enclosed environment was evaluated when no GPS signal was detected inside the evaluation chamber, either by deactivating it or when the UAV did not land itself for being inside a no-flight zone. Navigation in no-line-of-sight environments was tested as the line of sight varied from 100% line-of-sight to 0%. The quality of the data can also be evaluated as the line-of-sight is varied. Finally, the quality

of the images collected by the UAVs used was shown to be high when comparing them to the original images and finding that relevant defects were located inside the evaluation chamber. The quality was measure with resolution charts that determined a medium to high-quality in the images, in the quality of the camera and lenses used, and in effective lighting conditions inside the container.

The author believes that the proposed evaluation chamber provides a new assessment tool which can be used to evaluate and compare technologies and vendors when considering an inspection using UAVs. The evaluation chamber also provided data to gain a clearer understanding of all the phenomenon presented when UAVs approach structures. While previous research has focused on avoiding planar and tall structures, or in the analysis of the data gathered with high-cost specially designed technology, these results demonstrate that a common UAV can provide adequate visual inspection images, if all the parts involved in the UAS are trained and qualified.

6. CONCLUSIONS AND RECOMMENDATIONS

6.1 Conclusions

This research aimed to provide an obstacle avoidance course to be used to qualify an Unmanned Aerial System (UAS) in the inspection of structures such as bridges. Based on satisfactory flight results with images obtained during flight that are close to the actual images and elements presented inside the course, it can be concluded that the designed course can determine if an UAS is qualified to inspect a structure. The results indicate that for some UAVs, the pilot skills are needed the most compared to other UAVs. But in general, the resemblance of corners, circular elements, enclosed spaces, absence of GPS signal or IMUs, and the loss of line-of-sight inside the container, provides a measure to assess UAS capabilities in the inspection of structures.

By analyzing images provided by the UAS that are taken from a close distance with the appropriate angle and orientation, an inspector is able to identify defects that are not accessible by that person without the help of a heavy vehicle, ladder, or mounting equipment. Thus, the evaluation chamber portrays an environment that the pilot and inspector would have to encounter when inspecting difficult-to-reach structures.

The presence of real specimens inside the container provides a point of comparison with the images along the obstacles on the course. If taken several times, the UAS will be familiar with the test, but the possibility to change the provided images inside the course allows to provide a fair assessment of any UAS that takes this test.

The elements can be easily replicated in any place in the U.S. with simple materials and with the provided dimensions. Any steel specimen that presents a defect can be placed inside the course, and the images used in the faces of the obstacles can be printed in a plotter commonly available in any printing station following the recommendations of Chapter 3.

Based on these conclusions, inspectors should consider to apply this test to any UAS prior to inspection of bridges and other structures, and refrain to conduct an inspection if the UAS does not comply with the minimum requirements presented in this research work.

6.2 Recommendations

The proctor along with the pilot must check the status of the UAV, including propellers, body, and battery before starting the flight. If the UAS experiments issues inside the evaluation chamber and the test needs to be stopped, a complete assessment of the UAV must be performed to look for any damage in the propellers and the general body before attempting the evaluation chamber again.

If the test location is nearby or inside a no-flight zone, the UAS will only be authorized to fly inside the evaluation chamber. If calibration in an open environment is needed, the pilot must check any restrictions or request permission before flying.

A scoring system has not been provided for this test since it is not included in the scope of this research. However, several considerations are provided by the author that could lead to a final grading system:

- The author considers a classification system rather than a pass or fail system would be more beneficial to the parts involved in the UAS and the owners of the structures to be inspected, where the owners would be able to find an UAS capable of inspecting their specific type of structure.
- Several classifications would be provided based on their performance inside the evaluation chamber but also considering how they navigate around certain obstacles representing specific areas of a bridge and relating them to the actual structures. In that way, the more the UAS inspects correctly inside the evaluation chamber, the higher classification will be achieved.
- A higher level in the classification should be assigned to those UAS who successfully complete Obstacle 7 (with limited line-of-sight conditions), followed by Obstacle 4 (resembling underneath conditions), and Obstacle 5 (framing elements).

- An analysis must be performed to determine the number of years the grading achieved would be valid before expiring, if an expiration date is determined, and the additional procedures to renew the grading or improve the level achieved by the UAS.
- Experience could be considered in the classification based on hours of flight and the types of structures inspected by the UAS before attempting the test.

6.3 Future Work

This research clearly illustrates ideal flight conditions in the environment, but also raises the question of changes in the wind speed, temperature in the day of the inspection, battery life, rain, flying over water bodies, and so on, that need to be addressed in future works since outside sources such as: wind, rain, temperature, can affect flying conditions.

Future work will also need to include an analysis in the effect of battery life, camera capabilities, and data collection from a structure to be inspected. Flight time should be considered as well tied to battery life and how important is in terms of inspection times and completing a task in long span structures (spans greater than 140 feet).

Finally, the author acknowledges the existence and ongoing development of technologies intended to be used with UAS that allegedly improve inspection of structures, such as: thermal imaging, magnetometers, protective cages, LiDAR, and so on. Before introducing those technologies to the test presented in this research and most importantly to bridge inspection, a detailed study must be performed to assess their actual benefit and impact in the inspection of structures.

7. REFERENCES

Abdullah, Q. (2020). *Classification of the Unmanned Aerial Systems | GEOG 892: Unmanned Aerial Systems*. https://www.e-education.psu.edu/geog892/node/5

Albaker, B. M., & Rahim, N. A. (2010). Unmanned aircraft collision detection and resolution: Concept and survey. *2010 5th IEEE Conference on Industrial Electronics and Applications*, 248–253. https://doi.org/10.1109/ICIEA.2010.5516808

American Association of State Highway and Transportation Officials. (2019). *Manual for bridge element inspection*.

American Concrete Institute. (2013). *Report on nondestructive test methods for evaluation of concrete in structures*. American Concrete Institute.

Andert, F., Adolf, F.-M., Goormann, L., & Dittrich, J. S. (2010). Autonomous Vision-Based Helicopter Flights Through Obstacle Gates. *Journal of Intelligent and Robotic Systems*, *57*(1–4), 259–280. https://doi.org/10.1007/s10846-009-9357-3

ASTM. (2003). Standard test method for obtaining and testing drilled cores and sawed beams of concrete. *Annual Book of American Society of Testing and Materials*, *4*.

ASTM International. (n.d.). *Unmanned Aircraft Overview—ASTM International*. Retrieved April 3, 2021, from https://www.astm.org/industry/unmanned-aircraft-overview.html

Atkins, B. (2017). *Camera Lens Testing- Sharpness, Chromatic Aberration and Distortion—Bob Atkins Photography*. Lens Testing. http://www.bobatkins.com/photography/technical/lens_sharpness.html

Beale, J. (2011, October 1). *Resolution Test Patterns*. http://www.bealecorner.com/trv900/respat/#EIA1956

Bridge, J. A., & Ifju, P. G. (2018). *Use of Small Unmanned Aerial Vehicles (sUAV) for Structural Inspection* (p. 165). University of Florida, Civil and Coastal Engineering.

Campbell, J. (2018, July 18). *Public Roads—A New View for Bridge Inspectors , Summer 2018—FHWA-HRT-18-004*. https://www.fhwa.dot.gov/publications/publicroads/18summer/03.cfm

Carnathan, B. (n.d.). *About Enhanced ISO 12233 Resolution Chart Image Quality Data*. The-Digital-Picture.Com. Retrieved April 8, 2021, from https://www.the-digital-picture.com/Help/ISO-12233.aspx

Cawley, P. (2001). Non-destructive testing—Current capabilities and future directions. *Proceedings of the Institution of Mechanical Engineers, Part L: Journal of Materials: Design and Applications*, *215*(4), 213–223. https://doi.org/10.1177/146442070121500403

Chakravarthy, A., & Ghose, D. (1998). Obstacle avoidance in a dynamic environment: A collision cone approach. *IEEE Transactions on Systems, Man, and Cybernetics - Part A: Systems and Humans*, *28*(5), 562–574. https://doi.org/10.1109/3468.709600

Cheeseman, I., & Bennett, W. (1955). *The effect of the ground on a helicopter rotor in forward flight*.

Cheng, L., Wu, C.-D., Zhang, Y.-Z., & Wang, Y. (2012). An Indoor Localization Strategy for a Mini-UAV in the Presence of Obstacles. *International Journal of Advanced Robotic Systems*, *9*(4), 153. https://doi.org/10.5772/52754

Christ, R. D., & Wernli, R. L. (2014). Chapter 17—Navigational Sensors. In R. D. Christ & R. L. Wernli (Eds.), *The ROV Manual (Second Edition)* (pp. 453–475). Butterworth-Heinemann. https://doi.org/10.1016/B978-0-08-098288-5.00017-8

Dalamagkidis, K., Valavanis, K. P., & Piegl, L. A. (2011). *On integrating unmanned aircraft systems into the national airspace system: Issues, challenges, operational restrictions, certification, and recommendations* (Vol. 54). springer science & Business Media.

Dempsey, M. E., & Rasmussen, S. (2010). Eyes of the army–US Army roadmap for unmanned aircraft systems 2010–2035. *US Army UAS Center of Excellence, Ft. Rucker, Alabma*, *9*.

DJI. (2015, April). *Phantom 3 Professional Spec*. DJI Official. https://www.dji.com/phantom-3-pro

DJI. (2018, August 23). *Mavic 2 Pro—Spec*. DJI Official. https://www.dji.com/mavic-2/info

Dorafshan, S., Maguire, M., Hoffer, N., & Coopmans, C. (2017a). *Fatigue Crack Detection Using Unmanned Aerial Systems in Under-Bridge Inspection* (FHWA-ITD-17-256; p. 120).

Dorafshan, S., Maguire, M., Hoffer, N. V., & Coopmans, C. (2017b). Challenges in bridge inspection using small unmanned aerial systems: Results and lessons learned. *2017 International Conference on Unmanned Aircraft Systems (ICUAS)*, 1722–1730. https://doi.org/10.1109/ICUAS.2017.7991459

Dorafshan, S., Thomas, R. J., & Maguire, M. (2018). Fatigue Crack Detection Using Unmanned Aerial Systems in Fracture Critical Inspection of Steel Bridges. *Journal of Bridge Engineering*, *23*(10), 04018078. https://doi.org/10.1061/(ASCE)BE.1943-5592.0001291

Duque, L. (2017). *UAV-Based Bridge Inspection and Computational Simulations*. 169.

E54 Committee. (2017). *Standard Test Method for Determining Visual Acuity and Field of View of On-Board Video Systems for Teleoperation of Robots for Urban Search and Rescue Applications*. ASTM International. https://doi.org/10.1520/E2566-17A

E54 Committee. (2021a). *Standard Test Method for Evaluating Emergency Response Robot Capabilities: Radio Communication: Line-of-Sight Range*. ASTM International. https://doi.org/10.1520/E2854_E2854M-21

E54 Committee. (2021b). *Standard Test Method for Evaluating Emergency Response Robot Capabilities: Radio Communication: Non-Line-of-Sight Range*. ASTM International. https://doi.org/10.1520/E2855-12R21

Erdos, D., Erdos, A., & Watkins, S. E. (2013). An experimental UAV system for search and rescue challenge. *IEEE Aerospace and Electronic Systems Magazine*, *28*(5), 32–37. https://doi.org/10.1109/MAES.2013.6516147

F38 Committee. (2007). *Standard Specification for Design and Performance of an Airborne Sense-and-Avoid System*. ASTM International. https://doi.org/10.1520/F2411-07

Fahlstrom, P., & Gleason, T. (2012). *Introduction to UAV systems*. John Wiley & Sons.

Title 14 of the Code of Federal Regulations (CFR), Pub. L. No. 54 FR 34294, 91.113 Right-of-way rules: Except water operations. (1989).

Federal Aviation Administration. (2020a). *Processing of Unmanned Aircraft Systems Requests* (JO 7200.23B).

Federal Aviation Administration. (2020b, August 4). *Become a Drone Pilot* [Template]. https://www.faa.gov/uas/commercial_operators/become_a_drone_pilot/

Federal Aviation Administration. (2020c, October 26). *Certificated Remote Pilots including Commercial Operators* [Template]. https://www.faa.gov/uas/commercial_operators/

Federal Highway Administration. (2014). *MAP-21: Moving ahead for progress in the 21st century*.

Federal Highway Administration, Ryan, T., Mann, E., Chill, Z., & Ott, B. (2012). Bridge inspector's reference manual (BIRM). *Arlington, Virginia: Federal Highway Administration*.

Galkin, B., Kibilda, J., & DaSilva, L. A. (2019). UAVs as Mobile Infrastructure: Addressing Battery Lifetime. *IEEE Communications Magazine*, *57*(6), 132–137. https://doi.org/10.1109/MCOM.2019.1800545

Gillins, D. T., Parrish, C., Gillins, M. N., & Simpson, C. (2018). *Eyes in the sky: Bridge inspections with unmanned aerial vehicles*.

Gillins, M. N., Gillins, D. T., & Parrish, C. (2016). Cost-Effective Bridge Safety Inspections Using Unmanned Aircraft Systems (UAS). *Geotechnical and Structural Engineering Congress 2016*, 1931–1940. https://doi.org/10.1061/9780784479742.165

Gowda, M., Manweiler, J., Dhekne, A., Choudhury, R. R., & Weisz, J. D. (2016). Tracking drone orientation with multiple GPS receivers. *Proceedings of the 22nd Annual International Conference on Mobile Computing and Networking - MobiCom '16*, 280–293. https://doi.org/10.1145/2973750.2973768

Gucunski, N., National Research Council (U.S.), & Second Strategic Highway Research Program (U.S.) (Eds.). (2013). *Nondestructive testing to identify concrete bridge deck deterioration*. Transportation Research Board.

Hallermann, N., & Morgenthal, G. (2012, December 6). *The Application of Unmanned Aerial Vehicles for the Inspection of Structures*.

Hallermann, N., & Morgenthal, G. (2014). Visual inspection strategies for large bridges using Unmanned Aerial Vehicles (UAV). In A. Chen, D. Frangopol, & X. Ruan, *Bridge Maintenance, Safety, Management and Life Extension* (pp. 661–667). CRC Press. http://www.crcnetbase.com/doi/abs/10.1201/b17063-96

Hallermann, N., & Morgenthal, G. (2013). *Unmanned aerial vehicles (UAV) for the assessment of existing structures*. *101*. https://doi.org/10.2749/222137813808627172

Hayden, J. S. (1976). *The effect of the ground on helicopter hovering power required*. Proc. AHS 32nd Annual Forum.

Historic Bridge Foundation. (2021). *Bridgehunter.com: Historic Bridges of the United States*. http://bridgehunter.com/

Hooi, C. G., Lagor, F. D., & Paley, D. A. (2015). *Flow sensing for height estimation and control of a rotor in ground effect: Modeling and experimental results*. Proceedings of the AHS 71st Annual Forum.

Hottman, S. B., Hansen, K., & Berry, M. (2009). *Literature review on detect, sense, and avoid technology for unmanned aircraft systems*.

Inspectie Leefomgeving en Transport (ILT). (2020). *Pre-Defined Risk Assessment (PDRA)* (Remote UAS Operations PDRA-01-CAA-NL2020).

Johnson, G. M., & Fairchild, M. D. (2003). A top down description of S-CIELAB and CIEDE2000. *Color Research & Application*, *28*(6), 425–435. https://doi.org/10.1002/col.10195

Johnson, W. (2009). *NDARC NASA Design and Analysis of Rotorcraft*. National Aeronautics and Space Administration, Ames Research Center.

Jongerius, A. (2018). *The use of unmanned aerial vehicles to inspect bridges for Rijkswaterstaat.*

Keshmiri, S., Kim, A. R., Shukla, D., Blevins, A., & Ewing, M. (2018). Flight Test Validation of Collision and Obstacle Avoidance in Fixed-Wing UASs with High Speeds Using Morphing Potential Field. *2018 International Conference on Unmanned Aircraft Systems (ICUAS)*, 589–598. https://doi.org/10.1109/ICUAS.2018.8453299

Kopyt, A., & Żugaj, M. (2020). Analysis of Pilot Interaction with the Control Adapting System for UAV. *Journal of Aerospace Engineering*, *33*(4), 04020025. https://doi.org/10.1061/(ASCE)AS.1943-5525.0001109

Kundu, A., & Matis, T. I. (2017). A Delivery Time Reduction Heuristic using Drones under Windy Conditions. *IIE Annual Conference. Proceedings*, 1864–1869.

Kwak, J., & Sung, Y. (2018). Autonomous UAV Flight Control for GPS-Based Navigation. *IEEE Access*, *6*, 37947–37955. https://doi.org/10.1109/ACCESS.2018.2854712

Lei, B., Wang, N., Xu, P., & Song, G. (2018). New Crack Detection Method for Bridge Inspection Using UAV Incorporating Image Processing. *Journal of Aerospace Engineering*, *31*. https://doi.org/10.1061/(asce)as.1943-5525.0000879

Lin, Y.-C., Cheng, Y.-T., Zhou, T., Ravi, R., Hasheminasab, S. M., Flatt, J. E., Troy, C., & Habib, A. (2019). Evaluation of UAV LiDAR for Mapping Coastal Environments. *Remote Sensing*, *11*(24), 2893. https://doi.org/10.3390/rs11242893

Manweiler, J. G., Jain, P., & Roy Choudhury, R. (2012). *Satellites in our pockets: An object positioning system using smartphones*. 211–224.

Mariakakis, A. T., Sen, S., Lee, J., & Kim, K.-H. (2014). *Sail: Single access point-based indoor localization*. 315–328.

Mashaly, A. S., Wang, Y., & Liu, Q. (2016). Efficient sky segmentation approach for small UAV autonomous obstacles avoidance in cluttered environment. *2016 IEEE International Geoscience and Remote Sensing Symposium (IGARSS)*, 6710–6713. https://doi.org/10.1109/IGARSS.2016.7730752

Metni, N., & Hamel, T. (2007). A UAV for bridge inspection: Visual servoing control law with orientation limits. *Automation in Construction*, *17*(1), 3–10. https://doi.org/10.1016/j.autcon.2006.12.010

Mohan, A., & Poobal, S. (2018). Crack detection using image processing: A critical review and analysis. *Alexandria Engineering Journal*, *57*(2), 787–798. https://doi.org/10.1016/j.aej.2017.01.020

Mon, Y.-J. (2013). Vision-Based Obstacle Avoidance Controller Design for Mobile Robot by Using Single Camera. *International Journal of Computer Science Issues (IJCSI); Mahebourg*, *10*(2 Part 2), 248–250.

Morgenthal, G., & Hallermann, N. (2014). Quality Assessment of Unmanned Aerial Vehicle (UAV) Based Visual Inspection of Structures. *Advances in Structural Engineering*, *17*(3), 289–302. https://doi.org/10.1260/1369-4332.17.3.289

National Coordination Office for Space-Based Positioning, Navigation, and Timing. (2020, November 9). *GPS.gov: Other Global Navigation Satellite Systems (GNSS)*. https://www.gps.gov/systems/gnss/

Nikolic, J., Burri, M., Rehder, J., Leutenegger, S., Huerzeler, C., & Siegwart, R. (2013). *A UAV system for inspection of industrial facilities*. 1–8.

NOAA/NCEI. (2021). *Local Climatological Data from Lafayette Purdue University Airport, IN US Station*. National Oceanic & Atmospheric Administration / National Centers for Environmental Information.

Otero, L. D. (2015). *Proof of concept for using unmanned aerial vehicles for high mast pole and bridge inspections.* Florida. Dept. of Transportation. Research Center.

Parrot. (2019, May). *Parrot ANAFI Thermal—Spec*. https://www.parrot.com/us/drones/anafi-thermal

Pereira, F. C., & Pereira, C. E. (2015). Embedded Image Processing Systems for Automatic Recognition of Cracks using UAVs. *IFAC-PapersOnLine*, *48*(10), 16–21. https://doi.org/10.1016/j.ifacol.2015.08.101

Powers, C., Mellinger, D., Kushleyev, A., Kothmann, B., & Kumar, V. (2013). *Influence of aerodynamics and proximity effects in quadrotor flight*. 289–302.

Pratap, M., & Per, E. (2006). Global positioning system: Signals, measurements and performance. *Ganga-Jamuna Press, New York,*.

Purdue University. (2021). *S-BRITE - Bridge Component Gallery*. The Center for the Aging Infrastructure - Purdue University. https://engineering.purdue.edu/CAI/SBRITE/Facilities/BCGallery/BCG-home

Rai, A., Chintalapudi, K. K., Padmanabhan, V. N., & Sen, R. (2012). *Zee: Zero-effort crowdsourcing for indoor localization*. 293–304.

Ramon-Soria, P., Perez-Jimenez, M., Arrue, B. C., & Ollero, A. (2019). Planning System for Integrated Autonomous Infrastructure Inspection using UAVs. *2019 International Conference on Unmanned Aircraft Systems (ICUAS)*, 313–320. https://doi.org/10.1109/ICUAS.2019.8797874

Salaan, C. J. O., Okada, Y., Mizutani, S., Ishii, T., Koura, K., Ohno, K., & Tadokoro, S. (2018). Close visual bridge inspection using a UAV with a passive rotating spherical shell. *Journal of Field Robotics*, *35*(6), 850–867. https://doi.org/10.1002/rob.21781

Sanchez-Cuevas, P. J., Heredia, G., & Ollero, A. (2017). Multirotor UAS for bridge inspection by contact using the ceiling effect. *2017 International Conference on Unmanned Aircraft Systems (ICUAS)*, 767–774. https://doi.org/10.1109/ICUAS.2017.7991412

Scherer, S., Singh, S., Chamberlain, L. J., & Elgersma, M. (2007). *Flying Fast and Low Among Obstacles: Methodology and Experiments*. https://doi.org/10.1184/R1/6554927.v1

Seo, J., Duque, L., & Wacker, J. (2018). Drone-enabled bridge inspection methodology and application. *Automation in Construction*, *94*, 112–126. https://doi.org/10.1016/j.autcon.2018.06.006

Seo, J., Wacker, J., & Duque, L. (2018). *Evaluating the Use of Drones for Timber Bridge Inspection*. 152.

Shen, G., Chen, Z., Zhang, P., Moscibroda, T., & Zhang, Y. (2013). *Walkie-Markie: Indoor pathway mapping made easy*. 85–98.

Tanner, P. E., Overmeyer, A. D., Jenkins, L. N., Yao, C.-S., & Bartram, S. M. (2015). *Experimental investigation of rotorcraft outwash in ground effect*. 1–26.

Tenžera, D., Puž, G., & Radić, J. (2012). Visual inspection in evaluation of bridge condition. *Gradevinar*, *64*(9).

Thompson, P. D., & Shepard, R. W. (2000). *AASHTO Commonly-recognized bridge elements*. Materials for National Workshop on Commonly Recognized Measures for Maintenance, Scottsdale, Arizona.

Tomiczek, A. (2018). *Small Unmanned Aerial Vehicles (sUAV) for Structural Inspection*. University of Florida.

U.S. Department of Transportation. (2013). *N 8900.227—Unmanned Aircraft Systems (UAS) Operational Approval*. *8900*, 43.

U.S. Department of Transportation. (2019). *Status of the Nation's Highways, Bridges, and Transit Conditions & Performance* (Report to Congress 23rd Edition; p. 486). https://www.fhwa.dot.gov/policy/23cpr/pdfs/23cpr.pdf

Wang, H., Sen, S., Elgohary, A., Farid, M., Youssef, M., & Choudhury, R. R. (2012). *No need to war-drive: Unsupervised indoor localization*. 197–210.

Watanabe, Y., Calise, A., & Johnson, E. (2007, August 20). Vision-Based Obstacle Avoidance for UAVs. *AIAA Guidance, Navigation and Control Conference and Exhibit*. AIAA Guidance, Navigation and Control Conference and Exhibit, Hilton Head, South Carolina. https://doi.org/10.2514/6.2007-6829

Yamada, M., Nakao, M., Hada, Y., & Sawasaki, N. (2017). Development and field test of novel two-wheeled UAV for bridge inspections. *2017 International Conference on Unmanned Aircraft Systems (ICUAS)*, 1014–1021. https://doi.org/10.1109/ICUAS.2017.7991308

Zhang, Y., Yuan, X., Li, W., & Chen, S. (2017). Automatic power line inspection using UAV images. *Remote Sensing*, *9*(8), 824.

Zhou, P., Li, M., & Shen, G. (2014). *Use it free: Instantly knowing your phone attitude*. 605–616.

Zink, J., & Lovelace, B. (2015). *Unmanned Aerial Vehicle Bridge Inspection Demonstration Project* (MN/RC 2015-40; p. 214). http://www.lrrb.org/pdf/201540.pdf

Zoldi, D. (2020, November 9). In Search of the BVLOS Holy Grail. *Inside Unmanned Systems*. https://insideunmannedsystems.com/in-search-of-the-bvlos-holy-grail/

APPENDIX A. GALLERY OF IMAGES

Original images used in the obstacles inside the evaluation chamber are attached to this research work as JPG files.